

Towards the Quark Gluon Plasma via MHV Techniques

Tanjona Radonirina Rabemananjara

supervised by

Dr. W.A. Horowitz

A Thesis presented for the degree of
Master of Science



Theoretical Physics
Department of Physics
University of Cape Town

August 2018

The copyright of this thesis vests in the author. No quotation from it or information derived from it is to be published without full acknowledgement of the source. The thesis is to be used for private study or non-commercial research purposes only.

Published by the University of Cape Town (UCT) in terms of the non-exclusive license granted to UCT by the author.

Dedicated to
My Mother and Vahatra

Towards the Quark Gluon Plasma via MHV Techniques

Tanjona Radonirina Rabemananjara

Submitted for the degree of Master of Science

August 2018

Abstract

We study the multiple radiative gluon emission off a massless and highly energetic quark in the pQCD picture. We introduce the Maximally Helicity Violating (MHV) techniques to cope with the complexities in computing cross sections in multi-jet QCD. The multiphoton emission in QED is reviewed to emphasize the efficiency of the MHV approach. We show that the computation of the multiple photon emission current provides insight into the understanding of the multiple radiative gluon emission in QCD. We then compute the momentum distribution for one, two and three soft and collinear radiative gluons from a hard struck quark. Our MHV results exhibit non-Abelian information about the correlation of gluons. As a phenomenological analysis, we study the energy spectrum for emitting radiative gluons using our MHV results. By comparing the MHV and the standard Poisson approximation of uncorrelated multiple emission results, we see that there is significant difference between the two methods.

Declaration

I know the meaning of plagiarism and declare that all the work in this thesis entitled, "*Towards the Quark-Gluon Plasma (QGP) via MHV Techniques*", save for that which is properly acknowledged, is my own. This thesis has been submitted to the Turnitin module and I confirm that my supervisor has seen my report and any concerns revealed by such have been resolved with my supervisor.

Signed:

Signed by candidate

Date: July 31, 2018

Copyright © 2018 by Tanjona Radonirina Rabemananjara.

"The copyright of this thesis rests with the author. No quotations from it should be published without the author's prior written consent and information derived from it should be acknowledged".

Acknowledgements

My sincere gratitude goes to my supervisor Dr. W. A. Horowitz for his presence, guidance and close collaboration throughout my training. I am especially indebted to him for his inestimable help and suggestions. Thank you for always understanding me and for being such a wonderful supervisor. I will never forget all the advice and lessons that you told me both on the professional and personal level.

This work would not have been possible without the financial support of the Department of Physics of the University of Cape Town and the African Institute for Mathematical Sciences (AIMS). I would like also to express my deepest appreciation to the SA-CERN consortium and the National Research Foundation (NRF) for their invaluable support to attend conferences and workshops.

I am also grateful to all of those with whom I have had the pleasure to meet during this project, including Prof. Robert de Mello Koch, Prof. Jeff Murugan, Prof. Allan Cornell, Prof. Bruce Mellado and Dr. Andrianiaina Rasoanaivo. Thanks are extended to my officemates and friends Kevin, Ryan and Matthew for making the journey a wonderful experience.

Finally, I would like to express my sincere gratitude to my family and friends, Mom, Ando sy Ony ary Vahatra, Angela, Niry, Hasimbola, Avotra and Bernoulli, for their unconditional love and support.

Contents

Abstract	iii
Declaration	iv
Acknowledgements	v
1 Introduction	1
2 MHV Techniques	6
2.1 Spinor helicity formalism	7
2.1.1 Spinor variables	7
2.1.2 Vanishing condition of scattering amplitudes	11
2.1.3 Application to $2g \rightarrow 2g$ gluon scattering	12
2.2 Color structure of amplitudes	17
2.2.1 Insight from the $2g \rightarrow 2g$ process	17
2.2.2 Color-kinematic decomposition	19
2.3 Little group scaling	21
2.4 On-shell recursion relation	23
2.4.1 Complex shifts and Cauchy's theorem	23
2.4.2 Analytic study of the tree-level amplitude $\hat{A}_n(z)$	24
2.5 The BCFW on-shell recursion	26
2.5.1 BCFW deformation	26
2.5.2 The BCFW recursion relation	27
2.6 Summary	28
3 Review of the $qg \rightarrow qg$ calculation	30
3.1 Computation of the 3-point amplitude using the little group scaling	30

3.2	Decomposition of the four-point amplitude using BCFW formalism	31
3.3	Total differential cross section	33
3.4	Generalizing the MHV amplitudes	36
3.5	Summary	39
4	Radiative emission	40
4.1	Review of the photon bremsstrahlung in QED	41
4.2	Soft-collinear gluon radiation off a massless quark	44
4.2.1	One radiative gluon emission	44
4.2.2	Two radiative gluon emission	48
4.2.3	Three radiative gluon emission	54
4.3	Summary	62
5	Radiative Emission Phenomenology	63
5.1	Parametrization of the kinematics and approximations	63
5.2	One gluon emission case	65
5.3	Two gluon emission case	66
5.4	Three gluon emission case	69
5.5	Strong angular ordering	71
5.6	Probability density	73
5.7	Summary	75
6	Conclusions and discussions	77
	Appendix	82
A	Spinor Helicity Formalism	82
A.1	Conventions for 4D Spinor Helicity Formalism	82
A.2	Spinor variables	83
B	Spinor Identities	84
B.1	Momentum Conservation	84
B.2	Fierz rearrangement	84
B.3	Schouten identity	85
B.4	From spinors to Dirac Traces	85

C Color Structures	86
C.1 Definition and normalization	86
C.2 Color computation	86
C.3 Decomposition of product of T^a	87
D MHV/N^kMHV Amplitude Calculations	89
D.1 Two gluon emission	89
D.2 Three gluon emission	91
Bibliography	99

List of Figures

2.1	Diagrammatic illustration of how A_n partial amplitude is split into two subdiagrams each with a number of legs less than n via the general on-shell recursion. The summation is performed over all possible topological diagrams and the helicity. In the subdiagrams, $i_{\pm m}$ are shorthand for $(i \pm m)$.	25
2.2	Diagrammatic representation of how A_{n+2} partial amplitude with n external gluons and one pair of quark-antiquark is split into two subdiagrams each with a number of legs less than $(n + 2)$ via BCFW recursion. Again, the summation is performed over all possible topological diagrams and the helicity h_I .	28
3.1	BCFW diagrammatic representation of the decomposition of the four-point MHV amplitude into three-point subamplitudes via the $[k, l]$ -shift. Only two diagrams contribute to the full MHV partial amplitude $A_4(p^-, k^-, l^+, q^+)$.	32
3.2	Diagrammatic representation of the BCFW on-shell recursion for the general MHV amplitude with quark-antiquark line. The quark p and the gluon i are chosen to have negative helicities with a $[i, i_{+1}]$ -shift. \hat{P} and \hat{Q} are respectively the shorthand notations for $(\hat{p}_{i+1} + p_{i+2})$ and $(\hat{p}_i + p_{i-1})$.	37
4.1	Diagrammatic representation of the multiple photon Bremsstrahlung in QED in the process $q\gamma \rightarrow q + n\gamma$ where n represents the number of photon Bremsstrahlung. The soft photons have momentum s_i (i runs from 1 to n).	41
4.2	MHV diagrammatic representation of the single gluon emission in the $qgg\bar{q}$ -process. The soft radiative gluon s_1 ($s_1 \sim 0$) is assumed to be collinear to the high energetic quark which scatters with a single gluon.	44
4.3	MHV diagrammatic representation of the two gluon emission in the $qgg\bar{q}$ -process. The soft radiative gluons s_1 and s_2 ($s_1, s_2 \sim 0$) are assumed to be collinear to the high energetic quark which undergoes a single scattering.	48

- 4.4 BCFW diagrammatic representation of the NMHV amplitude for the two gluon emission. The helicity is chosen to be $(-, -, +, +)$ with the $[l, 1]$ -shift. Notice that the two internal lines \hat{P}_{kl} and \hat{P}_{12} are both on-shell. The two diagrams \mathcal{D}_1 and \mathcal{D}_2 are related by symmetry. 52
- 4.5 Independent emission of the two radiative gluons versus the case where the two radiative gluons can interact. 54
- 4.6 MHV diagrammatic representation of the three gluon emission in the $qgg\bar{q}$ -process. The soft radiative gluons s_1, s_2 and s_3 ($s_1, s_2, s_3 \sim 0$) are assumed to be collinear to the high energetic quark passing through the QGP medium. 55
- 4.7 Diagrammatic representation of the BCFW recursion for the computation of N^2 MHV amplitude with $[1, 2]$ -shift. The two hard gluons and one soft gluon have negative helicity, where the remaining soft gluons have positive helicity. 59
- 5.1 Energy spectrum for a single radiated gluon using Eq. (5.2.12) for different values of x_{min}, α_s and energy E which are represented by the different colors. As the energy of the initial quark increases, the probability of emitting a single radiated gluon decreases. 66
- 5.2 Energy spectrum for two gluon emission for different values of x_{min}, α_s and E . The dashed lines represent the Poisson Approximation and the solid lines represent the MHV result expressed by Eq. (5.3.19) and Eq. (5.3.20). The black, blue and red lines correspond respectively to $E = 100$ GeV (with $x_{min} = 0.001, \alpha_s = 0.1$), $E = 10$ GeV (with $x_{min} = 0.01, \alpha_s = 0.2$) and $E = 1$ GeV (with $x_{min} = 0.1, \alpha_s = 0.3$). In the calculation, m_π is taken to be 0.1 GeV/ c^2 68
- 5.3 Energy spectrum for three gluon emission for different values of x, α_s and E . The dashed lines represent the Poisson Approximation and the solid lines represent the MHV result expressed by Eq. (5.4.27). The black, blue and red lines correspond respectively to $E = 100$ GeV (with $x_{min} = 0.001, \alpha_s = 0.1$), $E = 10$ GeV (with $x_{min} = 0.01, \alpha_s = 0.2$) and $E = 1$ GeV (with $x_{min} = 0.1, \alpha_s = 0.3$). In the calculation, m_π is taken to be 0.1 GeV/ c^2 . . . 71

- 5.4 Comparison of the energy spectrum for emitting $n = 1, 2$ and 3 radiative gluons for an initial quark of energy $E = 100$ GeV, $x_{min} = 0.001$ and $\alpha_s = 0.1$. The different colors represent the number n of emitted radiative gluon. The solid lines represent the MHV results while the dashed lines represent the usual Poisson result for uncorrelated emission. The solid blue line correspond to the MHV results for three gluon emission represented by Eq. (5.4.27). In the calculation, the mass of the pion is taken to be $m_\pi = 0.1$ GeV/ c^2 72
- 5.5 Ratio between the MHV momentum distribution and the Poisson given by Eq. (5.5.31) and Eq. (5.5.32). The values of the angles θ_1 and ϕ_1 are fixed and taken to be respectively 0.05 rad and 0 rad. The solid lines represent the ratio function $f^{(2)}(\{\theta_i, \phi_i\})$ for different values of $\Delta\phi_{1,2}$. The red dashed line (horizontal line) represents the case where the MHV results is exactly similar to the Poisson. As the difference in angles between gets bigger, the MHV result converges into the Poisson. 73
- 5.6 Ratio between the MHV momentum distribution and the Poisson for the case of three radiated gluons. We fixed $\theta_1 = 0.05$ rad and $\phi_1 = 0$ rad. The different lines represent the ratio $f^{(3)}(\{\theta_i, \phi_i\})$. The solid lines represent the ratio for $\phi_3 = \pi/6$ while the dashed lines represent the ration for $\phi_3 = \pi/2$. Similarly, the red dashed line represents the case where the MHV result is exactly similar to the Poisson, which is the case where the angles are strongly ordered. The peaks show the region where $\theta_3 \approx \theta_1$ and/or $\theta_3 \approx \theta_2$. 74
- 5.7 Probability density of total fractional energy given by $\epsilon = \sum_i \omega_i/E$ for a quark jet with an initial energy $E = 100$ GeV up to a third order. We restricted ϵ to belong in the interval $[0, 1]$. The solid lines represent the probability density for the MHV case where the dashed lines represent the probability density for the usual Poisson. The red lines (both solid and dashed) represent the total probability density at third order (respectively for MHV and Poisson). The individual probability are shown in different colors. The probability for no radiation $p_0(\epsilon)$ (for the case $n = 0$) is not shown above. 75

List of Tables

2.1 Comparison of the number of diagrams that contributes to the full and partial-amplitudes. The first row indicates the number of particles involved in the process. The second and the third row compare the number of diagrams contributing respectively for the partial and full amplitude for n arbitrary external state particles. 21

Chapter 1

Introduction

One of the prominent features of the non-Abelian theory of the strong force or Quantum Chromodynamics (QCD) at low energy is *color confinement*. Color confinement is a property of QCD which basically states that isolated quarks and gluons cannot exist in nature [1]. In this energy regime, the non-Abelian nature of QCD makes the theory extremely hard to solve and it may even be impossible to analytically obtain a solution. Indeed, due to the strength of the coupling constant, the usual perturbative approach cannot be applied and one has to rely on numerical approaches such as Lattice QCD (LQCD) [2].

Unlike the quantum field theory of electrodynamics (QED), the coupling strength of QCD is weak at short distances, that is at high energy. The weakening of the coupling constant is known as *asymptotic freedom*. The property of asymptotic freedom was discovered by D. Gross and F. Wilczek [3] and independently by D. Politzer in 1973 [4]. This discovery leads to the prediction of the existence of a deconfined state made of free quarks and gluons [5,6]. The aim of heavy-ion experiments at the Relativistic Heavy Ion Collider (RHIC) at the Brookhaven National Laboratory (BNL) in the United States and the Large Hadron Collider (LHC) at the European Organization for Nuclear Research (CERN) in Switzerland is to collide heavy-ions so as to create immensely high energy densities which could produce a system of deconfined quarks and gluons [7,8].

In 2003, by making head-on collisions between gold-ions (Au-Au) at the center of mass energy of $\sqrt{s_{NN}} \sim 200$ GeV, scientists at RHIC for the first time produced an ultra-hot and dense soup made of asymptotically free strong-interacting quarks and gluons [9–12]. This new state of matter characterized by an equilibrium system composed of deconfined quarks and gluons is known as Quark-Gluon Plasma (QGP) [13,14]. Starting in 2010,

CERN extended the work at BNL to even higher energy and density by colliding lead-ions (Pb-Pb) [15–18]. Data collected from LHC have confirmed the existence of QGP. One of the most exciting results from experiments conducted both at CERN and RHIC is the depletion of high transverse momentum (p_{\perp}) hadrons [19–21] which is a signature of a color opaque medium, technically known as *jet quenching*. The term jet quenching refers to the modification of the evolution of a high energetic parton passing through the QGP due to its interaction with the medium [22]. Data collected at heavy-ion experiments (RHIC and LHC) suggested that jet quenching is a consequence of the energy loss of the primordial parton [23–26]. Jet quenching is important because it provides a valuable tool to probe the properties of quark gluon plasma produced in heavy-ion collisions [27].

The jet quenching phenomenon can be understood in the following way: the formation of a deconfined quark-gluon plasma at a very early stage of a relativistic heavy-ion collisions engenders the creation of high momentum partons (quarks or gluons). In high energy regimes (coupling constant $\alpha_s \ll 1$), the physics of the QGP-matter is governed by the weak-coupling physics of Quantum Chromodynamics (QCD) [28,29] which is in the domain of applicability of perturbative-QCD (pQCD). Indeed, due to the Asymptotic Freedom of QCD, quark and gluon interactions become very weak at very high momenta [3, 4, 30]. Thus, in the weakly-coupled regime one may use pQCD to study the physics of the QGP [31–33]. The interaction of these self-generated partons with the surrounding medium leads to an energy loss. The exact source of parton energy loss is directly tied to the balance between *collisional energy loss* and *radiative energy loss*. The collisional energy loss occurs when the self-generated parton loses energy via elastic collision with other particles composing the medium [34]. On the other hand, the inelastic scattering of a high energy parton and a thermal gluon can yield the emission of gluon radiations (Bremsstrahlung gluons) and the decrease of the energy [28, 35–37]. Data collected from ultrarelativistic heavy-ion experiments at LHC suggested that in the high energy regime ($E_T > 50$ GeV), jet modification appears to be dominated by the radiative energy loss [28, 38]. The evaluation of the amount of energy lost—via radiative process—during the interaction with the medium can provide insights into the dynamics of the constituent of QGP.

The study of the jet energy loss has stimulated the need to develop innovative many-body perturbative QCD approaches. All of the computation of the radiative energy loss formalisms were limited in the single gluon radiation [39,40]. The non-Abelian behavior of

QCD makes the calculation beyond the first order an extremely hard problem. However, in order to fully understand what is happening on the experimental side, a realistic energy loss model must include multiple gluon emission [27]. From the Quantum Electrodynamics (QED) perspective, the concept of multiple soft and collinear radiative photon emission is fully understood [41]. The probability distribution for emitting multiple radiative photons has been resummed and shown to follow a Poisson distribution

$$dN_\gamma^{(n)}(\{s_i\}) = \frac{1}{n!} \prod_{i=1}^n dN_\gamma^{(1)}(s_i), \quad (1.0.1)$$

where $dN_\gamma^{(1)}(s_i)$ represents the differential probability distribution for emitting a photon with soft momentum s_i . This suggests that each emission of radiative photons is independent. In some energy loss formalisms such as GLV (Gyulassy, Levai and Vitev) [22, 42, 43] and ASW (Armesto, Salgado and Wiedemann) [22], multiple gluon emission is computed using a similar assumption where the distribution follows the Poisson convolution of the single inclusive gluon distribution. However, a question remains as to whether the gluons are emitted independently (Poisson Ansatz) or not. The main difference between the theory of electrodynamic and the strong force lies in the fact that QCD is non-Abelian. Therefore, it is expected that the gluons are correlated and the distribution should exhibit a non-Poissonian nature.

The present thesis brings a new approach to the study of the radiative energy loss formalism in QGP using recent mathematical tools in the computation of scattering amplitudes. In Chapter 2, we lay the foundations for understanding the results accomplished in Chapter 3,4,5. For the sake of total pedagogical clarity, we briefly review some basic mathematical tools incorporated into the so-called Maximally Helicity Violating (MHV) techniques. First, we begin by introducing the spinor helicity formalism. In particular, we devote ourselves to its formulation for massless gauge theories¹. We show that written in terms of the spinor variables, most of the amplitudes contributing to a given physical process vanish and the non-vanishing ones possess a very simple analytical structure. In order to emphasize the simplicity of using spinor variables, we compute the well known two-to-two pure gluon process and compare the result to the expression found in literature. The presence of the color factors makes calculations in QCD extremely complicated. In order to reduce the color degrees of freedom in QCD processes, we introduce the color-

¹Despite the fact that the spinor helicity formalism was initially formulated for massless particles, generalization to include massive particles has been put forward in [44–47].

kinematic decomposition. Separating the kinematic components to the color factor makes the process of computing scattering amplitudes much easier. We then briefly move to the formulation of the little group scaling in the context of the spinor helicity formalism. Scattering amplitudes are objects that should remain invariant under little group transformation, and from this basic principle we show how to construct in a very simple way the expression of any amplitudes in Yang-Mills theory. At the end of the chapter, we introduce the famous BCFW (Britto-Cachazo-Feng-Witten) on-shell recursion relation [48, 49]. This kind of relation allows us to construct recursively any higher order amplitudes from the most basic and fundamental three-point amplitudes. This on-shell recursion will become important when we study the multiple radiative gluon emission in QCD. The BCFW exploits the hidden symmetries of the scattering amplitudes that are made manifest by the spinor helicity formalism.

In Chapter 3, we first review the calculation of the full cross section of the four-point QCD process ($qg \rightarrow qg$) by decomposing the amplitude into three-point subamplitudes using the BCFW on-shell recursion. The little group along with the spinor helicity formalism is then used to compute the three-point subamplitudes. We show that the simplicity and the power of the MHV techniques makes the computation of two-to-two scattering processes in QCD easier. From the computation of the $qg \rightarrow qg$ process, we construct the MHV formula for a process involving two gluons and one quark-antiquark pair. For the sake of generality, we compute in Section 3.4 the general formula for the full MHV and $\overline{\text{MHV}}$ (anti-MHV) amplitudes for any arbitrary number of gluons with one quark antiquark pair. This has been done by relying on the power of the BCFW on-shell recursion. The results from Chapter 3 will be crucial to the study of the radiative energy loss formalism in QGP. The calculation of the k^{th} -order Next-to-MHV ($N^k\text{MHV}$) amplitudes is presented in the next section.

Chapter 4 is devoted to the analytical study of the multiple radiative emission in QCD, which might provide a crucial insight towards the full understanding of radiative energy loss phenomena in QGP. We study the process in which a highly energetic quark interacts hardly with an energetic gluon—represented by the QCD process, $qg \rightarrow qg$ —leading to radiative emission. In particular, we study how the momentum distribution of emitting radiative gluons changes in the soft and collinear limit if we take into account the non-Abelian nature of QCD. The first section is a review of the multiple photon emission in QED as represented in Fig. 4.1. The main objective is to show, using the MHV

techniques, that the total momentum distribution is given by the product of each emission of a photon. The exponentiation of the final distribution gives the Poisson distribution. The next sections are dedicated to the calculation of the momentum distribution for the emission of one, two, and three radiative gluons. Using the soft-collinear approximation, we successfully derive the multiplicity distribution for multiple radiative gluon emission beyond the usual Poisson approximation. Our expressions differ from the usual Poisson approximation results by a correction term which comes from the correlation between the emitted gluons. This correction term represents the non-Abelian nature of the strong force.

In order to qualitatively assess the relevance of our results, we numerically compute in Chapter 5 different physical quantities. We first start by parameterizing the kinematics. We consider a configuration in which the primordial quark is significantly deflected by the medium such that the outgoing quark is perpendicular to the direction of the initial quark. As stated before, the radiative gluons are assumed to be emitted with a soft momentum ($s_i \rightarrow 0$) and a very small angle ($\theta_i \sim 0$) with respect to the outgoing quark. In fact, the radiative gluons are allowed to take only a very small fraction of energy x_i from the primordial quark. In Section 5.5, we test our results under the strong angular ordering limit. When the radiative gluons have strong angular ordering, interactions between the emitted gluons become small and the results follow the Poisson approximation, as they should. In Section 5.6, we compute the convoluted probability density of the total fractional energy given by $\epsilon = \sum_i \omega_i/E$ for a quark jet with an initial energy $E = 100$ GeV. We perform the numerical calculation of both the expected Poisson results and the MHV results for one, two and three gluon case and compare the results.

Conclusions are drawn in Chapter 6, with a summary of all the main results and a brief discussion. In addition, we also suggest further developments and outlooks of our current research. Technical details, such as the conventions for the spinor variables, the computations of the color factors, and the calculations of the Next-to-MHV amplitudes are shown in Appendices A, B, C, and D.

Chapter 2

MHV Techniques

The scattering amplitudes of on-shell particles are the most basic quantities in quantum field theory. They lie directly in the heart of high energy phenomenology physics providing a link between theoretical predictions and experimental data. In the weak coupling regime, scattering amplitudes in QCD are given as a perturbative expansion of a set of Feynman diagrams that encode the mathematical expressions that sum to the amplitude. The conventional method of computing scattering processes, however, has many drawbacks when it comes to computing QCD processes. Despite the complications arising by the Feynman diagram methods, the final results of scattering amplitudes can be rather simple and compact. For the last two decades, tremendous efforts have been devoted toward reformulating scattering amplitudes in a different way in order to expose the underlying structure responsible for the simplicity of the final results [50]. For massless theories in particular, there is a variety of methods that simplify the calculation of scattering amplitudes enormously, both at tree and loop levels. These techniques are collectively referred to as *on-shell* techniques or *Maximally Helicity Violating*¹ (MHV) techniques. At very high temperature and high densities, the masses of the quarks and the gluons are relatively small compared to the QCD scale (Λ_{QCD}), thus neglecting the masses of these particles are justified when studying QCD processes in high energy regime.

¹The Maximally Helicity Violating or in short MHV comes from studying $2 \rightarrow n$ scattering. By crossing symmetry, an incoming particle with positive (or respectively negative) helicity becomes an outgoing particle with negative (or respectively positive) helicity. Thus, considering all the momentum to be outgoing, the process $\mathcal{A}(1^+, \dots, \{i^-, j^-\}, \dots, n^+)$ crosses over $1^- 2^- \rightarrow 3^+ \dots \{i^-, j^-\} \dots n^+$; this is "Helicity Violating". We will see in the next sections that these kinds of amplitudes are the non-vanishing helicity violating amplitudes; that is the reason why we call them: Maximally Helicity Violating.

The first part of this chapter is devoted to the introduction of some preliminary backgrounds in computing scattering amplitudes in gauge theories using the MHV techniques. In particular, we discuss the spinor helicity formalism and the color structure of amplitudes. The implementation of these techniques is illustrated by the computation of a well known two-to-two process in QCD, $2g \rightarrow 2g$. For more details, computation of multiple external state gluon processes can be seen in [51, 52]. The second part is instead devoted to the construction of tree-level recursion relations between amplitudes with a different number of external legs. In particular, the BCFW on-shell recursion is analyzed and studied in depth. The technical backgrounds from this chapter will be then applied to the study of the radiative energy loss formalism in QGP.

2.1 Spinor helicity formalism

Perturbative QCD is primarily concerned with the interaction of quarks and gluons at momentum scales for which the masses of these particles can be ignored. It was realized that massless particles have remarkable properties when expressed in the helicity basis [50]. In fact, due to the symmetry obeyed by scattering amplitudes, most of the massless tree-level amplitudes turned out to vanish in this basis [47]. In addition, the non-vanishing amplitudes were found to possess simple structure depending on how much they violate the helicity conservation.

In this section, we review the spinor helicity formalism. This formalism was first introduced when physicists realized that the Lorentz group $SO(1, 3)$ in four dimensions is isomorphic to the group $SL(2) \times SL(2)$ and hence the finite-dimensional representations are classified as (m, n) , where m and n are integers or half-integers. As an illustration of the applicability of the spinor helicity formalism, we review the computation of the two-to-two gluon process in Section 2.1.3.

2.1.1 Spinor variables

This section is devoted to the introduction of the one of the most fundamental tools used throughout this thesis, the *spinor helicity formalism*. We see that massless particles have remarkable properties when expressed in the helicity basis. In point of fact, spinor helicity formalism renders the analytic expression of scattering amplitudes in a more compact and simple form compared to the standard formulation using momentum four-vectors [53, 54].

In principle, the spinor helicity formalism maps the components of a momentum four-vector p_μ into those of two-by-two matrices given by

$$p_{a\dot{a}} = p_\mu(\sigma^\mu)_{a\dot{a}} = \begin{pmatrix} p_0 - p_3 & -p_1 + ip_2 \\ -p_1 - ip_2 & p_0 + p_3 \end{pmatrix}. \quad (2.1.1)$$

where $\sigma^\mu = (\sigma^0, \vec{\sigma})$ are the usual Pauli matrices. Notice that in the above equation, the undotted index transforms as left-handed Weyl spinor and the dotted one as right-handed. One can in particular notice that the determinant of this two-by-two matrix is a Lorentz invariant quantity and is given by

$$\det(p_{a\dot{a}}) = p_\mu p^\mu = m^2. \quad (2.1.2)$$

In the high energy limit where particles are massless, this determinant vanishes, $\det(p_{a\dot{a}}) = p_\mu p^\mu = 0$. Thus, for a lightlike momentum p , we can write the momentum as a product of two vectors

$$p_{a\dot{a}} = \lambda_a \tilde{\lambda}_{\dot{a}}, \quad (2.1.3)$$

where λ_a and $\tilde{\lambda}_{\dot{a}}$ are respectively the left and right handed spinors with the spinor indices running from 1 to 2. Notice that λ_a and $\tilde{\lambda}_{\dot{a}}$ are often called *holomorphic* and *anti-holomorphic* spinors due to their transformation under the spinor representation of the Lorentz group. For real valued momenta, λ_a and $\tilde{\lambda}_{\dot{a}}$ are complex conjugate of each other ($\lambda_a = \tilde{\lambda}_{\dot{a}}^*$). In case of complex momentum, λ_a and $\tilde{\lambda}_{\dot{a}}$ are independent. We will see in the following sections that scattering amplitudes possess interesting properties when we require some of the momenta to be complex. For the moment, let us stick to the treatment of real-valued momenta.

Given two momentum p_i and p_j , their scalar product can be expressed in the helicity basis as follows

$$2(p_i p_j) = \varepsilon^{ab} \varepsilon^{\dot{a}\dot{b}} (p_i)_{a\dot{a}} (p_j)_{\dot{b}b}. \quad (2.1.4)$$

The antisymmetric tensors ε^{ab} and $\varepsilon^{\dot{a}\dot{b}}$ can be thought of as raising and lowering spinor indices, similar as $g^{\mu\nu}$ does for vector indices. Rewriting the momentum as $(p_i)_{a\dot{a}} = \lambda_a \tilde{\lambda}_{\dot{a}}$ and $(p_j)_{\dot{b}b} = \mu_b \tilde{\mu}_{\dot{b}}$, we can re-express the above product as follows

$$2(p_i p_j) = (\varepsilon^{ab} \lambda_a \mu_b) (\varepsilon^{\dot{a}\dot{b}} \tilde{\lambda}_{\dot{a}} \tilde{\mu}_{\dot{b}}) = \langle ij \rangle [ij], \quad (2.1.5)$$

where we have defined above the spinor products in terms of the angle and square brackets

notation. The angle and square representation of the spinors are defined as

$$\langle ij \rangle \equiv \varepsilon^{ab} \lambda_a \mu_b, \quad (2.1.6)$$

$$[ij] \equiv \varepsilon^{\dot{a}\dot{b}} \tilde{\lambda}_{\dot{a}} \tilde{\mu}_{\dot{b}}. \quad (2.1.7)$$

Here, $\langle ij \rangle$ and $[ij]$ are respectively the shorthand notations for $\langle p_i | p_j \rangle$ and $[p_i | p_j]$. For simplicity, we have omitted all the spinor indices. Since spinors are simple mathematical objects, they are subject to few algebraic manipulations. For instance, one can use the contraction conventions for left and right-handed spinors (see Appendix A) to show that the above definitions imply $\langle ii \rangle = [ii] = 0$ [50]. On the other hand, the correspondence between the angle ($\langle i |, | i \rangle$) and the square ($[i |, | i \rangle$) brackets and the Dirac spinors are explicitly expressed in [50]. As a result, all other product of angle and square spinors vanish, as an example $\langle ij \rangle = [ij] = 0$. Notice also that these spinor products are antisymmetric, which means that $\langle ij \rangle = -\langle ji \rangle$ and $[ij] = -[ji]$. Another useful relation which can be derived from Eq. (2.1.6) and Eq. (2.1.7) is that square and angle brackets are related to each other according to the relation $\langle ij \rangle^* = [ij]$.

As a consequence, the standard Lorentz invariant expression written in terms of a momentum four-vector as $s_{ij} = (p_i + p_j)^2$ can now be expressed in terms of the angle and square brackets as

$$s_{ij} = (p_i + p_j)^2 = \langle ij \rangle [ij]. \quad (2.1.8)$$

In particular, for two-to-two processes, the above expression correctly defines the Mandelstam variables s, t and u .

The real power of the spinor helicity formalism appears when one would like to deal with vector boson polarizations. In fact, for spin-1 bosons, one can also express the polarizations in term of a pair of massless spinors. In order to construct our expression of polarizations in terms of square and angle brackets, we must recall ourselves that physical polarizations satisfy the condition $\epsilon_\mu^*(p_i, k) \epsilon^\mu(p_i, k) = -1$ and the transverse condition ensures that $p_\mu \epsilon^\mu = 0$. Thus, the polarization can be expressed as [55, 56]:

$$\epsilon_\mu^-(p_i, k) = -\frac{1}{\sqrt{2}} \frac{[k | \gamma_\mu | i \rangle}{[ki]} \quad \text{and} \quad \epsilon_\mu^+(p_i, k) = \frac{1}{\sqrt{2}} \frac{\langle k | \gamma_\mu | i \rangle}{\langle ki \rangle}, \quad (2.1.9)$$

where k is a reference lightlike momentum that can be chosen arbitrary. This freedom in choosing the reference momentum reflects the gauge invariance as we will discuss soon. In fact, one can assign different reference spinors for each external spin-1 particles. However, the reference momentum k cannot be aligned to the momentum p_i since we do not want the product $\langle ik \rangle$ and/or $[ik]$ to vanish.

Let us briefly verify that the abovementioned conditions are satisfied for our expression of polarizations shown in Eq. (2.1.9). Since taking the complex conjugate of $\langle k|\gamma_\mu|i\rangle$ gives $[k|\gamma_\mu|i\rangle$ and vice versa, these polarization vectors of definite helicity satisfy $(\epsilon_\mu^\pm)^* = -\epsilon_\mu^\mp$. It follows straightforwardly that

$$[\epsilon_\mu^\pm(p_i, k)]^* [(\epsilon^\mu)^\pm(p_i, k)] = -\frac{1}{2} \frac{\langle k|\gamma^\mu|i\rangle [k|\gamma_\mu|i\rangle}{\langle ki\rangle [ki]}. \quad (2.1.10)$$

In order to get rid of the spinor representation of the gamma matrices, we need to apply the *Fierz rearrangement* which is defined by Eq. (B.2.5) in the Appendix B as

$$\langle i|\gamma^\mu|j\rangle [l|\gamma_\mu|k\rangle = 2\langle ik\rangle [lj]. \quad (2.1.11)$$

By virtue of this relation we can now compute Eq. (2.1.10),

$$[\epsilon_\mu^\mp(p_i, k)] [(\epsilon^\mu)^\pm(p_i, k)] = -\frac{\langle ki\rangle [ki]}{\langle ki\rangle [ki]} = -1. \quad (2.1.12)$$

The above equation shows that the condition $\epsilon_\mu^*(p_i, k)\epsilon^\mu(p_j, k) = -1$ is satisfied. In addition, since we have $\langle ii\rangle = [ii] = 0$ it follows straightforwardly that the transverse condition $p_\mu\epsilon^\mu = 0$ is also satisfied. Similarly, we can derive the following properties for the polarizations, $\epsilon_\mu^\pm(p_i, k)(\epsilon^\pm)^\mu(p_j, k) = 0$ and $\epsilon_\mu^+(p_i, k)(\epsilon^-)^\mu(k, r) = 0$.

Let us now check that two choices of reference spinors are related by gauge transformation. Let us consider two reference momenta k and k' and let us compute the following expression

$$\omega^-(k, k') = \epsilon_\mu^-(p_i, k) - \epsilon_\mu^-(p_i, k') \quad (2.1.13)$$

$$= \frac{1}{\sqrt{2}} \frac{[k'|\gamma_\mu|i\rangle}{[k'i]} - \frac{1}{\sqrt{2}} \frac{[k|\gamma_\mu|i\rangle}{[ki]} \quad (2.1.14)$$

$$= \frac{[k'|\gamma_\mu|i\rangle[ik] - [k|\gamma_\mu|i\rangle[ik']]}{\sqrt{2}[k'i][ik]} \quad (2.1.15)$$

$$= \frac{([k'k] - [kk'])}{\sqrt{2}[k'i][ik]} |i\rangle[i]. \quad (2.1.16)$$

From the first to the second line, we used the fact that $[k|\gamma_\mu|i\rangle = \langle i|\gamma_\mu|k\rangle$ as shown in Appendix B. Then, we just expanded the expression to go from the second to the third line. From the third to the last line, we evaluated the spinor products using the spinor representation of the gamma matrices, contracted the appropriate spinor indices, and factorized the terms related to p_i . Therefore, the two polarizations are related by

$$\epsilon_\mu^-(p_i, k) \longrightarrow \epsilon_\mu^-(p_i, k') + \omega^-(k, k')p_i, \quad \text{with} \quad \omega^-(k, k') = \sqrt{2} \frac{[k'k]}{[k'i][ik]}. \quad (2.1.17)$$

One can use similar approach to show that

$$\epsilon_\mu^+(p_i, k) \longrightarrow \epsilon_\mu^+(p_i, k') + \omega^+(k, k')p_i, \quad \text{with} \quad \omega^+(k, k') = \sqrt{2} \frac{\langle k' k \rangle}{\langle k' i \rangle \langle ik \rangle}. \quad (2.1.18)$$

Here, $\omega^\pm(k, k')$ is some scalar. We see that both Eq. (2.1.17) and Eq. (2.1.18) represent a gauge transformation. That is, the polarizations do change depending on the choice of reference spinor but in a way that leaves the full amplitude invariant under the Ward identity [50, 57]. In fact, when summing over all possible diagrams, the final answer of the amplitude is independent of the choice of reference momentum.

2.1.2 Vanishing condition of scattering amplitudes

In order to fully understand the behavior of the scattering amplitudes when expressed in terms of spinor variables, let us first devote ourselves to the study of the conditions that lead amplitudes to vanish. For this, let us consider the two-to-two gluon process—which the cross section will be computed in the next section.

At tree-level, the expression of the $2g \rightarrow 2g$ scattering process that we are going to denote \mathcal{A}_4 is composed of three contributions:

$$\mathcal{A}_4(1, 2, 3, 4) = \mathcal{A}_s(1, 2, 3, 4) + \mathcal{A}_t(1, 2, 3, 4) + \mathcal{A}_u(1, 2, 3, 4), \quad (2.1.19)$$

where s, t and u denotes the different channels and $1, 2, 3, 4$ labels the gluons. Here, the momenta are chosen to be *incoming*. Let us first focus our attention on the particular case of the s -channel process \mathcal{A}_s and consider the case where the helicity conservation is maximally violated, i.e we have $\mathcal{A}_s(1^{h_1}, 2^{h_2}, 3^{h_3}, 4^{h_4}) = \mathcal{A}_s(1^-, 2^-, 3^-, 4^-)$.

Recall that every term in \mathcal{A}_s has a factor $\epsilon_\mu^{h_i}(p_i, k)(\epsilon^{h_j})^\mu(p_j, k)$. As we have seen in the previous section, in terms of angle and square brackets, the polarizations are defined as

$$\epsilon_\mu^-(p_i, k) = -\frac{1}{\sqrt{2}} \frac{[k|\gamma_\mu|i]}{[ki]} \quad \text{and} \quad \epsilon_\mu^+(p_i, k) = \frac{1}{\sqrt{2}} \frac{\langle k|\gamma_\mu|i]}{\langle ki \rangle}. \quad (2.1.20)$$

Using the property of the polarizations, one can straightforwardly check that all the polarizations in $\mathcal{A}_s(1^-, 2^-, 3^-, 4^-)$ are orthogonal: $\epsilon_\mu^-(p_i, k)(\epsilon^-)^\mu(p_j, k) = 0$. Thus, we have $\mathcal{A}_s(1^\pm, 2^\pm, 3^\pm, 4^\pm) = 0$, and similarly one can verify that using the same argument both $\mathcal{A}_t(1^\pm, 2^\pm, 3^\pm, 4^\pm)$ and $\mathcal{A}_u(1^\pm, 2^\pm, 3^\pm, 4^\pm)$ are equal to zero. That is to say, amplitudes with all positive (or negative) helicities vanish at tree-level.

Now, let us choose the helicity of p_1 (the gluon labeled by 1 with momentum p_1) to be different from the rest. Choose the reference vector for $p_{i \neq 1}$ to be p_1 , thus we have the

following vanishing terms

$$\epsilon_\mu^\pm(p_i, p_1)(\epsilon^\mp)^\mu(p_1, k) = 0, \quad (i \neq 1) \quad (2.1.21)$$

$$\epsilon_\mu^\pm(p_i, p_1)(\epsilon^\pm)^\mu(p_j, p_1) = 0, \quad (i, j \neq 1) \quad (2.1.22)$$

We can deduce that $\mathcal{A}_s(1^\mp, 2^\pm, 3^\pm, 4^\pm)$, $\mathcal{A}_t(1^\mp, 2^\pm, 3^\pm, 4^\pm)$ and $\mathcal{A}_u(1^\mp, 2^\pm, 3^\pm, 4^\pm)$ all vanish. This tells us that amplitudes with all but one positive (or all but one negative) helicity also vanish at tree-levels.

Therefore, the leading non-vanishing amplitudes must have at least two negative or two positive helicities; such classes of amplitudes are known as the Maximally Helicity Violating (MHV) amplitudes or the anti-Maximally Helicity Violating ($\overline{\text{MHV}}$) amplitudes respectively. This generalizes to the notion of Next-to- k^{th} -order MHV ($N^k\text{MHV}$) amplitudes with $(k + 2)$ negative helicity particles.

2.1.3 Application to $2g \rightarrow 2g$ gluon scattering

In order to illustrate the efficiency of using spinor variables, let us compute the cross section of the $2g \rightarrow 2g$ QCD process. Consider all the momenta to be *incoming*, we already know that the first non-vanishing amplitudes are given by the MHV (or $\overline{\text{MHV}}$) amplitudes and let us choose the following configuration of helicity $(h_1, h_2, h_3, h_4) = (-, -, +, +)$. Since all the momenta are considered to be incoming, the corresponding Mandelstam variables considering all the gluons to be massless are given by $s = 2(p_1 p_2)$, $t = 2(p_1 p_4)$ and $u = 2(p_1 p_3)$, where s, t and u represent the different topologies of the Feynman diagrams.

With the above choice of helicity configuration, we can choose as reference momentum for the polarizations ϵ_1 and ϵ_2 to be the momentum p_4 , and choose as reference momentum for the polarizations ϵ_3 and ϵ_4 to be p_1 . In this case, only the contraction $(\epsilon_2 \epsilon_3)$ survives while all other contractions vanish.

The usual QCD Feynman rules [41] can now be applied to write down the expression of the scattering amplitudes of the s -channel diagram

$$i\mathcal{A}_s(1, 2, 3, 4) = \begin{array}{c} \epsilon_2; a_2 \\ \text{---} \\ p_2 \\ \text{---} \\ p_1 \\ \text{---} \\ \epsilon_1; a_1 \end{array} \begin{array}{c} \text{---} \\ e \\ \text{---} \\ p_3 \\ \text{---} \\ p_4 \\ \text{---} \\ \epsilon_4; a_4 \end{array} \begin{array}{c} \epsilon_3; a_3 \\ \text{---} \\ p_3 \\ \text{---} \\ p_4 \\ \text{---} \\ \epsilon_4; a_4 \end{array} = -ig_s^2 \tilde{f}^{a_1 a_2 e} \tilde{f}^{a_3 a_4 e} A_s(1, 2, 3, 4), \quad (2.1.23)$$

where $A_s(1, 2, 3, 4)$ is what we call *color-stripped* amplitude. Notice that $A_s(1, 2, 3, 4)$ is

color-free and depends only on the kinematics as defined as

$$A_s(1, 2, 3, 4) = \frac{1}{2(p_1 p_2)} \left\{ (\epsilon_1 \epsilon_2)(p_1 - p_2) + 2\epsilon_2(p_2 \epsilon_1) - 2\epsilon_1(p_1 \epsilon_2) \right\} \\ \times \left\{ (\epsilon_3 \epsilon_4)(p_3 - p_4) + 2\epsilon_4(p_4 \epsilon_3) - 2\epsilon_3(p_3 \epsilon_4) \right\}. \quad (2.1.24)$$

However, by virtue of our gauge choice the above equation simplifies to

$$A_s(1, 2, 3, 4) = \frac{2}{(p_1 p_2)} (\epsilon_2 \epsilon_4)(p_2 \epsilon_1)(p_3 \epsilon_4). \quad (2.1.25)$$

Translating into the spinor variables (angle and square brackets) and using the *Fierz rearrangement* for spinors we have the following results,

$$\epsilon_\mu^-(p_2, p_4)(\epsilon^+)^{\mu}(p_3, p_1) = -\frac{1}{2} \frac{\langle 1|\gamma_\mu|3\rangle [4|\gamma^\mu|2\rangle]}{[42] \langle 13\rangle} = -\frac{\langle 12\rangle [43]}{\langle 13\rangle [42]}, \quad (2.1.26)$$

$$p_2^\mu \epsilon_\mu^-(p_1, p_4) = -\frac{1}{\sqrt{2}} \frac{[4|\not{p}_2|1\rangle}{[41]} = -\frac{1}{\sqrt{2}} \frac{\langle 21\rangle [42]}{[41]}, \quad (2.1.27)$$

$$p_3^\mu \epsilon_\mu^+(p_4, p_1) = \frac{1}{\sqrt{2}} \frac{\langle 1|\not{p}_3|4\rangle}{\langle 14\rangle} = \frac{1}{\sqrt{2}} \frac{\langle 13\rangle [34]}{\langle 14\rangle}. \quad (2.1.28)$$

Combining all the results and doing some simplification, we get

$$A_s(1^-, 2^-, 3^+, 4^+) = -\frac{\langle 12\rangle [34]^2}{\langle 14\rangle [12][14]}. \quad (2.1.29)$$

In order to make this result compact, we can express A_s in terms of the angle brackets only. From the momentum conservation (see Section B.1 of Appendix B), we have $\langle 12\rangle [23] = -\langle 14\rangle [43]$, and from the relations $(p_1 + p_2)^2 = (p_3 + p_4)^2$ and $(p_1 + p_4)^2 = (p_2 + p_3)^2$ we obtain $\langle 12\rangle [12] = \langle 34\rangle [34]$ and $\langle 14\rangle [14] = \langle 23\rangle [23]$ respectively. Using these relations, we can simplify Eq. (2.1.29) to get the expression of the full s -channel amplitude

$$\mathcal{A}_s(1^-, 2^-, 3^+, 4^+) = g_s^2 \tilde{f}^{a_1 a_2 e} \tilde{f}^{a_3 a_4 e} A_s(1^-, 2^-, 3^+, 4^+), \quad (2.1.30)$$

$$\text{with } A_s(1^-, 2^-, 3^+, 4^+) = \frac{\langle 12\rangle^4}{\langle 12\rangle \langle 23\rangle \langle 34\rangle \langle 41\rangle}. \quad (2.1.31)$$

Similarly, by writing the mathematical expression of the u channel diagram using the Feynman rules and then re-writing the expression in terms of the spinor variables, we can derive a compact expression of the full u -channel diagram. Let us start with

$$i\mathcal{A}_u(1, 2, 3, 4) = \begin{array}{c} \epsilon_2; a_2 \\ \text{wavy line} \\ p_2 \\ \text{wavy line} \\ \epsilon_3; a_3 \\ p_4 \\ \text{wavy line} \\ e \\ \text{wavy line} \\ p_1 \\ \text{wavy line} \\ \epsilon_4; a_4 \\ p_3 \\ \text{wavy line} \\ \epsilon_1; a_1 \end{array} = -ig_s^2 \tilde{f}^{a_1 a_3 e} \tilde{f}^{a_2 a_4 e} A_u(1, 2, 3, 4), \quad (2.1.32)$$

where the expression of the u -channel color-stripped amplitude is given by:

$$A_u(1, 2, 3, 4) = \frac{1}{2(p_1 p_3)} \{ (\epsilon_1 \epsilon_3)(p_1 - p_3) + 2\epsilon_3(p_3 \epsilon_1) - 2\epsilon_1(p_1 \epsilon_3) \} \\ \times \{ (\epsilon_2 \epsilon_4)(p_2 - p_4) + 2\epsilon_4(p_4 \epsilon_2) - 2\epsilon_2(p_2 \epsilon_4) \}. \quad (2.1.33)$$

According to our choice of gauge, all the contractions of polarizations vanish except $(\epsilon_2 \epsilon_3)$, thus the above amplitude can be written as

$$A_u(1, 2, 3, 4) = \frac{2}{(p_1 p_3)} (\epsilon_2 \epsilon_3)(p_3 \epsilon_1)(p_2 \epsilon_4). \quad (2.1.34)$$

And due to our initial choice of helicity configuration, we have

$$p_2^\mu \epsilon_\mu^+(p_4, p_1) = \frac{1}{\sqrt{2}} \frac{\langle 1 | \not{p}_2 | 4 \rangle}{\langle 14 \rangle} = \frac{1}{\sqrt{2}} \frac{\langle 12 \rangle [24]}{\langle 14 \rangle}, \quad (2.1.35)$$

$$p_3^\mu \epsilon_\mu^-(p_1, p_4) = -\frac{1}{\sqrt{2}} \frac{[4 | \not{p}_3 | 1 \rangle}{[41]} = -\frac{1}{\sqrt{2}} \frac{\langle 31 \rangle [43]}{[41]}. \quad (2.1.36)$$

With the above contractions, we can now write down the expression of the u -channel color-stripped amplitude

$$A_u(1^-, 2^-, 3^+, 4^+) = \frac{\langle 12 \rangle^2 [34]^2}{\langle 13 \rangle \langle 14 \rangle [13] [41]}. \quad (2.1.37)$$

Again, we can express this amplitude in terms of the angle brackets only. For the u -channel diagram, the momentum conservation implies that $\langle 12 \rangle [23] = -\langle 14 \rangle [43]$ and $[31] \langle 12 \rangle = -[34] \langle 42 \rangle$, and in addition, from the relation $(p_1 + p_4)^2 = (p_2 + p_3)^2$ we have $\langle 14 \rangle [14] = \langle 23 \rangle [23]$. Therefore, the full u -channel amplitude can be written as

$$\mathcal{A}_u(1^-, 2^-, 3^+, 4^+) = g_s^2 \tilde{f}^{a_1 a_2 e} \tilde{f}^{a_3 a_4 e} A_u(1^-, 2^-, 3^+, 4^+), \quad (2.1.38)$$

$$\text{with } A_u(1^-, 2^-, 3^+, 4^+) = \frac{\langle 12 \rangle^4}{\langle 13 \rangle \langle 32 \rangle \langle 24 \rangle \langle 14 \rangle}. \quad (2.1.39)$$

Finally, one can show that due to our choice of gauge the t -channel diagram does not contribute in the full expression of the $2g \rightarrow 2g$ amplitude. Using the Feynman rules, the t -channel diagram can be expressed as

$$i\mathcal{A}_t(1, 2, 3, 4) = \begin{array}{c} \epsilon_2; a_2 \\ \text{wavy line} \\ p_2 \\ \text{wavy line} \\ \epsilon_3; a_3 \\ p_3 \\ \text{wavy line} \\ e \\ \text{wavy line} \\ p_1 \\ \text{wavy line} \\ \epsilon_1; a_1 \\ \text{wavy line} \\ p_4 \\ \text{wavy line} \\ \epsilon_4; a_4 \end{array} = -ig_s^2 \tilde{f}^{a_1 a_4 e} \tilde{f}^{a_3 a_2 e} A_t(1, 2, 3, 4), \quad (2.1.40)$$

with

$$A_t(1, 2, 3, 4) = \frac{1}{2(p_1 p_4)} \{ (\epsilon_1 \epsilon_4)(p_1 - p_4) + 2\epsilon_4(p_4 \epsilon_1) - 2\epsilon_1(p_1 \epsilon_4) \} \\ \times \{ (\epsilon_3 \epsilon_2)(p_3 - p_2) + 2\epsilon_2(p_2 \epsilon_3) - 2\epsilon_3(p_3 \epsilon_2) \}. \quad (2.1.41)$$

Considering our choice of helicity and polarization, all the contractions in the above expression vanish and we get $\mathcal{A}_t(1^-, 2^-, 3^+, 4^+) = 0$. Thus, the contribution to the full amplitude of the $2g \rightarrow 2g$ gluon scattering for our particular choice of helicity configuration comes from the s and u -channel. Thus, we have

$$\mathcal{A}(1^-, 2^-, 3^+, 4^+) = g_s^2 \left(\mathcal{C}_s \frac{\langle 12 \rangle^4}{\langle 12 \rangle \langle 23 \rangle \langle 34 \rangle \langle 41 \rangle} + \mathcal{C}_u \frac{\langle 12 \rangle^4}{\langle 13 \rangle \langle 32 \rangle \langle 24 \rangle \langle 14 \rangle} \right), \quad (2.1.42)$$

where the color factors \mathcal{C}_s and \mathcal{C}_u are respectively given by $\tilde{f}^{a_1 a_2 e} \tilde{f}^{a_3 a_4 e}$ and $\tilde{f}^{a_1 a_2 e} \tilde{f}^{a_3 a_4 e}$. In order to get the expression of the final cross section of the process, we need to calculate the square of Eq. (2.1.42) and sum over the colors. Using the definition of the Mandelstam variables, squaring the matrix elements is straightforward,

$$\left| \frac{\langle 12 \rangle^4}{\langle 12 \rangle \langle 23 \rangle \langle 34 \rangle \langle 41 \rangle} \right|^2 = \left(\frac{\langle 12 \rangle^4}{\langle 12 \rangle \langle 23 \rangle \langle 34 \rangle \langle 41 \rangle} \right) \left(\frac{[12]^2}{[12][23][34][41]} \right) = \frac{s^2}{t^2}, \quad (2.1.43)$$

$$\left| \frac{\langle 12 \rangle^4}{\langle 13 \rangle \langle 32 \rangle \langle 24 \rangle \langle 14 \rangle} \right|^2 = \left(\frac{\langle 12 \rangle^2}{\langle 13 \rangle \langle 32 \rangle \langle 24 \rangle \langle 14 \rangle} \right) \left(\frac{[12]^4}{[13][32][24][14]} \right) = \frac{s^4}{u^2 t^2}, \quad (2.1.44)$$

On the other hand, the computation of the crossed terms are trickier. While summing all the crossed terms, we get an expression which cannot be directly expressed in terms of the Mandelstam variables,

$$A_s^* A_u + A_s A_u^* = -\frac{s^4}{2t^2} \left(\frac{1}{\langle 12431 \rangle} + \frac{1}{[12431]} \right). \quad (2.1.45)$$

Notice that if spinors appear in a physical quantity, then it must terminate, i.e. it has the form $\langle i_1 i_2 \rangle [i_2 i_3] \cdots [i_n i_1]$. In the above expression, we have introduced the shorthand notation $\langle i_1 i_2 \cdots i_n i_1 \rangle$ for this product as shown in Appendix B.4. Notice that such quantity can be evaluated by performing Dirac traces as follows

$$\langle ij \rangle [jk] \langle kl \rangle [li] = \frac{1}{2} \left[\text{Tr} (1 - \gamma_5) \not{p}_i \not{p}_j \not{p}_k \not{p}_l \right] \\ = \frac{1}{2} [s_{ij} s_{kl} + s_{il} s_{jk} - s_{ik} s_{jl} - 4i \varepsilon(i, j, k, l)], \quad (2.1.46)$$

where $\varepsilon(i, j, k, l) = \varepsilon_{\mu\nu\rho\sigma} p_i^\mu p_j^\nu p_k^\rho p_l^\sigma$ and $\varepsilon_{\mu\nu\rho\sigma}$ is the completely antisymmetric tensor. This implies that $\langle 12431 \rangle$ and $[12431]$ are complex conjugate of each other. Using this, the sum

of the crossed terms in the expression of the amplitude squared is given by

$$A_s^* A_u + A_s A_u^* = -\frac{s^4}{2t^2} \frac{\text{Tr}(\not{p}_1 \not{p}_2 \not{p}_4 \not{p}_3)}{|\langle 12431 \rangle|^2} \quad (2.1.47)$$

$$= -\frac{s^4}{2t^2} \frac{(p_1 p_2)(p_3 p_4) + (p_1 p_3)(p_2 p_4) - (p_1 p_4)(p_2 p_3)}{4(p_1 p_2)(p_1 p_3)(p_2 p_4)(p_3 p_4)} \quad (2.1.48)$$

$$= -\frac{s^4}{2t^2} \frac{(s^2 + u^2 - t^2)}{s^2 u^2}. \quad (2.1.49)$$

From the first to the second line, we just expanded the trace term and the angle-square brackets Lorentz invariant product in the denominator. From the second to the last line, we translated the scalar product into the Mandelstam variables. One can simplify the last equation further by recalling that the Mandelstam variables satisfy $s + t + u = 0$. The later implies that $(s^2 + u^2) = t^2 - 2us$. Thus, we have the extremely simple expression

$$A_s^* A_u + A_s A_u^* = \frac{s^3}{t^2 u}. \quad (2.1.50)$$

On the other hand, we can compute the expression of the color factors using the properties of the structure constants. One can straightforwardly check that we have the following expressions

$$\mathcal{C}_s \mathcal{C}_s^\dagger = \mathcal{C}_u \mathcal{C}_u^\dagger = (\tilde{f}^{a_1 a_2 e} \tilde{f}^{a_3 a_4 e})^2 = 4N^2(N^2 - 1), \quad (2.1.51)$$

$$\mathcal{C}_s \mathcal{C}_u^\dagger = \mathcal{C}_s^\dagger \mathcal{C}_u = (\tilde{f}^{a_1 a_2 e} \tilde{f}^{a_3 a_4 e})(\tilde{f}^{a_1 a_3 d} \tilde{f}^{a_2 a_4 d}) = 2N^2(N^2 - 1). \quad (2.1.52)$$

Notice that it is because of Eq. (2.1.52) that we managed to combine the crossed kinematic terms in Eq. (2.1.45). Combining all the results and making some simplifications, we can write down the expression of the amplitude squared averaged over the colors for our specific MHV helicity configuration

$$|\bar{\mathcal{A}}(1^-, 2^-, 3^+, 4^+)|^2 = 4g_s^2 N^2 (N^2 - 1) \left(\frac{s^4}{t^2 u^2} - \frac{s^2}{tu} \right). \quad (2.1.53)$$

In order to get full expression of the amplitude, one has to do the summation over all possible helicity configurations. For our two-to-two process, one can check that there are in total four possible helicity configurations for non-vanishing MHV amplitudes. However, one can check that all the remaining MHV amplitudes are related to Eq.(2.1.53) by crossing symmetry. This is because flipping the helicity flips the labels. For instance, in order to go from $|\bar{\mathcal{A}}(1^-, 2^-, 3^+, 4^+)|^2$ to $|\bar{\mathcal{A}}(1^-, 2^+, 3^-, 4^+)|^2$ one has just to swap s and u . Therefore, the non-vanishing cases are given by the six permutation of the Mandelstam variables s, t and u . So, we have

$$|\bar{\mathcal{A}}(gg \rightarrow gg)|^2 = 4g_s^2 N^2 (N^2 - 1) \sum_{\mathcal{P}_3(s,t,u)} \left(\frac{s^4}{t^2 u^2} - \frac{s^2}{tu} \right). \quad (2.1.54)$$

To get the final expression of the differential cross section, we need to average over the initial states which is given by $4(N^2 - 1)^2$ possibilities for the spins and the colors. Taking $N = 3$ and doing some fair amount of simplification using the Mandelstam properties, we get the standard expression as shown in Eq. (2.1.55). One can verify that this result is consistent with [58].

$$\frac{1}{256} |\bar{\mathcal{A}}(gg \rightarrow gg)|^2 = \frac{9}{2} g_s^4 \left(3 - \frac{ut}{s^2} - \frac{us}{t^2} - \frac{st}{u^2} \right). \quad (2.1.55)$$

2.2 Color structure of amplitudes

QCD can be thought as an expanded version of the quantum version of the theory of electrodynamics or in short QED. Whereas in QED there is just one kind of charge, QCD comes with three different kinds of charges, labeled by colors [1]. Thus, scattering amplitudes in QCD are functions of momenta, helicities and color charges. The presence of color charges—which manifests by the non-Abelian nature of the force—makes the calculations in QCD extremely complicated. So in order to simplify calculations, it is useful to separate the color charges apart from the kinematics. Works based on dividing systematically the computation of scattering amplitudes into gauge invariant components have been reviewed in [59, 60]. There was found that one can nicely organize the color degrees of freedom in order to separate the kinematic part. This approach to disentangle the color factors and the kinematics is referred to as *color-kinematic decomposition*. In this section, we describe some conventions for organizing the color structure of gauge theory amplitudes in Yang-Mills theory. In particular, we will introduce the notion of *color-ordered partial amplitudes* which emerges from the trace-based color-decomposition.

2.2.1 Insight from the $2g \rightarrow 2g$ process

To get an intuition of how the color factors can be stripped off from the kinematics, let us consider again the $2g \rightarrow 2g$ scattering of gluons and choose all the momenta to be *incoming*. As we have already shown in the previous section, at tree-level, the full amplitude is given by $\mathcal{A} = \mathcal{A}_s + \mathcal{A}_t + \mathcal{A}_u$, where s, t and u represent the different channels.

Let us first focus on the color-stripped amplitude $A_s(1, 2, 3, 4)$ of the s -channel. We can see from Eq. (2.2.56) that $A_s(1, 2, 3, 4)$ is *antisymmetric* under swap of $1 \rightarrow 2$ or $3 \rightarrow 4$ and *symmetric* under simultaneous interchange of both $1 \rightarrow 2$ and $3 \rightarrow 4$. Thus, we have

the following equalities for the color-stripped amplitudes:

$$A_s(1, 2, 3, 4) = A_s(2, 1, 4, 3) = -A_s(2, 1, 3, 4) = -A_s(1, 2, 4, 3). \quad (2.2.56)$$

On the other hand, by eliminating the color structures \tilde{f}^{abc} in favor of the generator matrices T^a , the color structure for the s -channel diagram can be written as:

$$\tilde{f}^{a_1 a_2 e} \tilde{f}^{a_3 a_4 e} = -Tr([T^{a_1}, T^{a_2}][T^{a_3}, T^{a_4}]) \quad (2.2.57)$$

$$\begin{aligned} &= -Tr(T^{a_1} T^{a_2} T^{a_3} T^{a_4}) + Tr(T^{a_2} T^{a_1} T^{a_3} T^{a_4}) \\ &\quad + Tr(T^{a_1} T^{a_2} T^{a_4} T^{a_3}) - Tr(T^{a_2} T^{a_1} T^{a_4} T^{a_3}). \end{aligned} \quad (2.2.58)$$

One can notice that the color factor of the s -channel amplitude is also a sum of four terms that is *antisymmetric* under the swap of $1 \rightarrow 2$ or $3 \rightarrow 4$. Therefore, the full s -channel amplitude can be written as a sum of terms that have gluons ordered the same in the color-stripped amplitudes and the color traces:

$$\begin{aligned} \mathcal{A}_s(1, 2, 3, 4) &= g_s^2 \{ Tr(T^{a_1} T^{a_2} T^{a_3} T^{a_4}) A_s(1, 2, 3, 4) + Tr(T^{a_2} T^{a_1} T^{a_3} T^{a_4}) A_s(2, 1, 3, 4) \\ &\quad + Tr(T^{a_1} T^{a_2} T^{a_4} T^{a_3}) A_s(1, 2, 4, 3) + Tr(T^{a_2} T^{a_1} T^{a_4} T^{a_3}) A_s(2, 1, 4, 3) \}. \end{aligned} \quad (2.2.59)$$

The above equation shows that the full s -channel amplitude can be written as a sum of single traces and color-stripped amplitudes. Notice that the t - and s -channel color-stripped amplitude are just a $2 \leftrightarrow 4$ ($A_t(1, 2, 3, 4) = A_s(1, 4, 3, 2)$) and $2 \leftrightarrow 3$ ($A_u(1, 2, 3, 4) = A_s(1, 3, 2, 4)$)-cross of the s -channel one. Thus, the full $2g \rightarrow 2g$ scattering amplitude $\mathcal{A} = \mathcal{A}_s + \mathcal{A}_t + \mathcal{A}_u$ is composed of twelve terms, all of which can be written as a product of a trace and color-stripped amplitude $Tr(\dots)A_s(\dots)$. However, one can simplify further the expression by pairing-up terms using the cyclic property of the trace. For instance,

$$Tr(T^{a_1} T^{a_2} T^{a_3} T^{a_4}) \{ A_s(1, 2, 3, 4) + A_t(1, 4, 3, 2) \} = Tr(T^{a_1} T^{a_2} T^{a_3} T^{a_4}) A_4(1, 2, 3, 4)$$

where the color-stripped amplitude $A(1, 2, 3, 4)$ is given by

$$A_4(1, 2, 3, 4) = \begin{array}{c} \begin{array}{ccc} \begin{array}{c} 2 \\ \text{wavy} \\ \diagdown \\ 1 \end{array} & \begin{array}{c} \text{wavy} \\ \text{---} \\ \text{wavy} \\ \diagup \\ 4 \end{array} & \begin{array}{c} 3 \\ \text{wavy} \\ \diagup \\ 3 \end{array} \\ \begin{array}{c} 1 \\ \text{wavy} \\ \diagup \\ 1 \end{array} & \begin{array}{c} \text{wavy} \\ \text{---} \\ \text{wavy} \\ \diagdown \\ 4 \end{array} & \begin{array}{c} 4 \\ \text{wavy} \\ \diagdown \\ 4 \end{array} \end{array} + \begin{array}{c} \begin{array}{ccc} \begin{array}{c} 2 \\ \text{wavy} \\ \diagdown \\ 1 \end{array} & \begin{array}{c} \text{wavy} \\ \text{---} \\ \text{wavy} \\ \diagup \\ 4 \end{array} & \begin{array}{c} 3 \\ \text{wavy} \\ \diagup \\ 3 \end{array} \\ \begin{array}{c} 1 \\ \text{wavy} \\ \diagup \\ 1 \end{array} & \begin{array}{c} \text{wavy} \\ \text{---} \\ \text{wavy} \\ \diagdown \\ 4 \end{array} & \begin{array}{c} 4 \\ \text{wavy} \\ \diagdown \\ 4 \end{array} \end{array} \end{array} = \begin{array}{c} \begin{array}{ccc} \begin{array}{c} 2 \\ \text{wavy} \\ \diagdown \\ 1 \end{array} & \begin{array}{c} \text{wavy} \\ \text{---} \\ \text{wavy} \\ \diagup \\ 4 \end{array} & \begin{array}{c} 3 \\ \text{wavy} \\ \diagup \\ 3 \end{array} \\ \begin{array}{c} 1 \\ \text{wavy} \\ \diagup \\ 1 \end{array} & \begin{array}{c} \text{wavy} \\ \text{---} \\ \text{wavy} \\ \diagdown \\ 4 \end{array} & \begin{array}{c} 4 \\ \text{wavy} \\ \diagdown \\ 4 \end{array} \end{array} \end{array}. \quad (2.2.60)$$

By doing repeatedly this process, we can nicely write the expression of the full amplitude for the four-gluon scattering process. In fact, one will end up to the following expression

$$\mathcal{A}_4(1, 2, 3, 4) = g_s^2 \sum_{\mathcal{P}_4/Z_4} Tr(T^{a_1} T^{a_2} T^{a_3} T^{a_4}) A_4(1, 2, 3, 4), \quad (2.2.61)$$

where the summation is performed over the non-cyclic permutation of the four gluons. In the next section, we see how this generalizes into the case where we have n gluons and a presence of a pair of quark-antiquark.

2.2.2 Color-kinematic decomposition

Although the gauge group of QCD is $SU(3)$, for generalization let us consider consider a Yang-Mills theory with gauge group $SU(N)$. For the external state particles, we consider two different $SU(N)$ representations: (i) the adjoint representation where the color indices labeled by a run over $1, 2, \dots, N^2 - 1$ for the gluons, and (ii) the fundamental representation N , with its conjugate representation \bar{N} , for quarks and antiquarks respectively. For the fundamental representation the color indices are labeled by $i \in \{1, 2, \dots, N\}$ while anti-fundamental indices are denoted by $j \in \{1, 2, \dots, N\}$. The generator matrices of $SU(N)$ in the fundamental representation are traceless hermitian $N \times N$ matrices, denoted by $(T^a)_{ij}$. Throughout the calculations, the generators T^a are normalized such that $\text{Tr}(T^a T^b) = \delta^{ab}$ and $[T^a, T^b] = i\tilde{f}^{abc}T^c$ where the constant structure is defined as $\tilde{f}^{abc} = \sqrt{2}f^{abc}$. Thus, for a generic Feynman diagram the color factor contain a factor of $(T^a)_{ij}$ for each gluon-quark-antiquark vertex, a factor of \tilde{f}^{abc} for each pure three-gluon vertex, and a contracted pair of structure constants $\tilde{f}^{abc}\tilde{f}^{cde}$ for each pure four-gluon vertex. These are the only vertices we will encounter in our computations.

To expose and identify all different types of color structures that can appear in a given scattering amplitude, we first eliminate the structure constant \tilde{f}^{abc} in favor of the generator T^a (as we saw in the previous section) using the relation

$$i\tilde{f}^{abc} = \text{Tr}(T^a T^b T^c) - \text{Tr}(T^a T^c T^b), \quad (2.2.62)$$

which follows from the definition of the structure constants. Thus, for a typical pure-gluon Feynman diagram one can apply such transformation repeatedly in order to obtain a large number of traces of the generic form $\text{Tr}(\dots T^a \dots) \dots \text{Tr}(\dots)$. In addition, if we have a presence of external quarks-antiquarks pair, then there will be also strings of T^a 's terminated by fundamental and anti-fundamental indices, of the form $(T^a \dots T^b)_{ij}$, one for each external quark-antiquark pair. In order to reduce the number of traces, the following relation can be repeatedly used

$$(T^a)_{ij}(T^b)_{kl} = \delta_{il}\delta_{kj} - \frac{1}{N}\delta_{ij}\delta_{kl}. \quad (2.2.63)$$

The above relation is known as the *Fierz identity* and the term proportional to $(1/N)$ reflects the fact the generator matrices T^a are hermitian and traceless.

In the particular case of tree-level amplitudes with external states in the adjoint representation, such as pure n -gluon amplitudes, we can always reduce the color factors to end up with a single trace $\text{Tr}(T^{a_1} \dots T^{a_n})$ where a_i here denotes the color index and the label i represents the gluons (which runs from 1 to n). Thus, for n -gluon tree amplitudes this reduction leads to a trace-based decomposition as follows

$$\mathcal{A}_n(\{p_i, h_i, a_i\}) = g_s^{n-2} \sum_{\mathcal{P}_n/Z_n} \text{Tr}(T^{a_1} \dots T^{a_n}) A_n(1^{h_1}, \dots, n^{h_n}), \quad (2.2.64)$$

where the sum is performed over the non-cyclic permutation of the gluons due to the cyclic property of the trace. In the above expression, \mathcal{A}_n denotes the full amplitude which depends on the external momenta of the gluons p_i , the helicity h_i and the adjoint indices a_i (for $i = 1, \dots, n$). $A_n(1^{h_1}, \dots, n^{h_n})$ is called *color-ordered partial amplitudes* which have all the color factors removed, but hold the information about the kinematics. In literature, various name have been given to this gauge invariant component, such as color-ordered amplitude and dual amplitudes [50, 61, 62]. It was shown that amplitudes with color factor stripped off are much easier to compute and that the average number of amplitudes that must be evaluated is much smaller compared to the full amplitude [49, 59]. It is worth emphasizing that each partial amplitude corresponds to a particular color flow, which can be naively thought as the ordering in which the gluons are emitted.

The color-kinematic decomposition provides a good organization of the colors in the expression of scattering amplitudes [61] and leaves apart the computation of partial amplitudes. It turns out that these gauge invariant amplitudes possess a lots of properties making their computations easy. In particular, it was shown in [63] that the average number of partial amplitudes, for the scattering of n gluons, that must be evaluated is much smaller compared to the full amplitudes (see Table 2.1).

Similarly, we can extend the above factorization to decompose tree-level amplitudes that involve n -gluons and one pair of quark-antiquark. In presence of external quarks and antiquarks, amplitudes can be reduced to single strings of the generator matrices T^a :

$$\mathcal{A}_{n+2}(p, \{k_i, h_i, a_i\}, q) = g_s^n \sum_{\mathcal{P}_n} (T^{a_1} \dots T^{a_n})_{ij} A_{n+2}(p^{h_p}, \{k_i, h_i\}, q^{h_q}). \quad (2.2.65)$$

In Eq. (2.2.65) the summation is performed over all possible permutation of n gluons. The quark and the antiquark are denoted by p and q respectively, and the gluons are

# Particles	4	5	6	7	8	9	10
# Diagrams Partial amplitude	3	10	36	133	501	1991	7335
# Diagrams Full amplitude	4	25	220	2485	343000	559405	10525900

Table 2.1: Comparison of the number of diagrams that contributes to the full and partial-amplitudes. The first row indicates the number of particles involved in the process. The second and the third row compare the number of diagrams contributing respectively for the partial and full amplitude for n arbitrary external state particles.

labeled by i which runs from 1 to n . Notice that in this color basis, the indices of the quark and the antiquark are fixed and do not participate in the permutation. We say that the colors flow from the quark, pass through the gluons and end up to the antiquark.

One might worry that the color-kinematic decomposition will lead to a fair amount of proliferation in the number of partial amplitudes that have to be computed. However, the power of such decomposition lies in the fact that partial amplitudes exhibit interesting properties that make manifest the analytical symmetry of scattering amplitudes. One can straightforwardly check that partial amplitudes satisfy the following properties:

- (i) Charge conjugation: $A(p, 1, \dots, n, q) = -A(q, 1, \dots, n, p)$. This is because flipping the charges on a quark-antiquark line gives rise to a minus sign.
- (ii) Color-ordered identity: $A(1, 2, \dots, n-1, n) = (-1)^n A(n, n-1, \dots, 2, 1)$. This property directly follows from the antisymmetry of color-ordered partial amplitudes.
- (iii) Cyclic in the sense that $A(1, 2, \dots, n-1, n) = A(n, 1, 2, \dots, n-1)$. This property is an immediate consequence of the color-ordered amplitudes.
- (iv) Parity under change of $h_i \rightarrow -h_i$: $|A(\{p_i, h_i, a_i\})|^2 = |A^*(\{p_i, -h_i, a_i\})|^2$. This is because changing the helicity of the particles into the opposite sign changes all angle brackets into square brackets and vice-versa. We will have a particular look at this property when computing the $2g \rightarrow 2g$ and $qg \rightarrow qg$ -process.

2.3 Little group scaling

Spinor helicity variables possess certain aesthetic elegance. Their utility resides from the fact that they make manifest the symmetry obeyed by the scattering amplitudes. These symmetries are the Lorentz invariance and the so-called little group. In this section, we

introduce the little group scaling in the context of the spinor helicity formalism. Recall that in terms of the angle and square brackets, the momentum of a particle is given by $p_i = |i\rangle[i]$ (we have suppressed the spinor indices). The little group is the group of transformation that leaves invariant the momentum of an on-shell particle [64]. Thus, the little group transformation is the scaling:

$$|i\rangle \longrightarrow t|i\rangle \quad \text{and} \quad |i] \longrightarrow t^{-1}|i]. \quad (2.3.66)$$

By virtue of this rescaling, one can setup some ground rules for the external fermions and spin-1 bosons:

(i) Spinors for fermion scale as t^{-2h} , where h denotes the helicity of the fermion ($h = \pm 1/2$) as already shown above.

(ii) Polarization vectors for spin-1 bosons scale as t^{-2h} for $h = \pm 1$. By rescaling the spinors $|i\rangle$ and $|i]$, one can indeed check in the expression of the polarization in Eq. (2.1.20) that this rule is true. So, we have:

$$\epsilon_\mu^- \rightarrow t^2 \epsilon_\mu^- = -\frac{t^2}{\sqrt{2}} \frac{[k|\gamma_\mu|i\rangle}{[ki]} \quad \text{and} \quad \epsilon_\mu^+ \rightarrow t^{-2} \epsilon_\mu^+ = \frac{t^{-2}}{\sqrt{2}} \frac{\langle k|\gamma_\mu|i] \rangle}{\langle ki \rangle}, \quad (2.3.67)$$

Hence, the little group scaling of each polarization encodes its associated helicity. A scattering amplitude with multiple external state particles will be then multi linear in the corresponding polarizations,

$$A(1^{h_1}, \dots, n^{h_n}) = \epsilon_{\mu_1}^{h_1} \dots \epsilon_{\mu_n}^{h_n} A^{\mu_1 \dots \mu_n}(1, \dots, n). \quad (2.3.68)$$

Recall that the tensorial object on the right-hand side of the above equation is the usual amplitude computed from Feynman diagrams in the standard approach, and the object on the left-hand side represent a set of functions corresponding to different helicity configurations. These objects are known as the true scattering amplitudes in the sense that they are gauge invariant. Therefore, for on-shell amplitudes, the scaling of a particle labeled by i gives rise to a weight $(-2h_i)$ where h_i labels the helicity of the particle i ,

$$A(\dots, \{t_i|i\rangle, t_i^{-1}|i]\}, \dots) = t^{-2h_i} A(\dots, \{|i\rangle, |i]\}, \dots). \quad (2.3.69)$$

From this expression, one can easily compute all three-point amplitudes in QCD. An example of such computation will be shown in the next chapter.

2.4 On-shell recursion relation

Despite the fact that the spinor helicity formalism and the color-kinematic decomposition provide an efficient way to compute MHV amplitudes, the computation of the k^{th} -order NMHV amplitudes remain a challenge. However, in order to understand processes with multiple external states in QCD, N^k MHV amplitudes have to be computed. To overcome that challenge, one can rely on on-shell relations to construct recursively higher order amplitudes [65] from lower order amplitudes. The most well known on-shell recursion is referred to as BCFW on-shell recursion relations formulated by Britto-Cachazo-Feng-Witten [48]. The idea behind recursion relations is to exploit the analytic structure of the amplitude in order to reduce the calculation of higher-point amplitudes into the computation of subamplitudes with lower order.

This section focuses on the properties of scattering amplitudes in Yang-Mills theory. By studying amplitudes on a complex plane, we develop recursion relations, namely the BCFW on-shell recursion. We see that the astonishing power of the on-shell recursion allows us to construct the generalization for any higher order QCD processes.

2.4.1 Complex shifts and Cauchy's theorem

An on-shell partial amplitude A_n is basically defined by the momenta of the external state particles (which are reals) and their respective helicity. The idea behind the complexification of momenta is to transform A_n into a meromorphic function $\hat{A}_n(z)$, where $z \in \mathbb{C}$. However, by shifting the momentum, we must assure that it preserves the momentum conservation and the on-shell condition.

Let us consider the following transformation:

$$p_i \longrightarrow \hat{p}_i = p_i + z r_i, \quad \text{with } z \in \mathbb{C}. \quad (2.4.70)$$

The above transformation is linear in z and has to satisfy the following conditions:

- (i) In order for the momentum conservation to be satisfied, $\sum_i \hat{p}_i = 0$, we require that the momentum r_i to satisfy $\sum_i r_i = 0$.
- (ii) In order to preserve the on-shell condition, $\hat{p}_i^2 = 0 \forall i \in \{1, n\}$, we require that $r_i r_j = 0 \forall i, j \in \{1, n\}$ (in particular $r_i^2 = 0$) and $r_i p_i = 0$.

2.4.2 Analytic study of the tree-level amplitude $\hat{A}_n(z)$

At tree-level, the complex partial amplitude $\hat{A}_n(z)$ does not have any branch cuts, its analytical structures are captured by its singularities, and the only possible singularities at tree-level arise from the propagators [50]. This can be seen from the perspective of a Feynman diagram. The only place where we can get poles is from the propagator $1/\hat{P}_i$ where \hat{P}_i here represents an arbitrary propagator containing shifted momenta. An interesting property which can be inferred from the definitions in Section 2.4.1 is that \hat{P}_i^2 is also linear in z .

To see that, let us start by defining a subset of generic momenta $\{p_i\}_{i \in I}$ and define $\hat{P}_i = \sum_{i \in I} \hat{p}_i$. According to the definitions in Section 2.4.1 we have

$$\hat{P}_i^2 = \left(\sum_{i \in I} p_i \right)^2 + 2z \left(\sum_{i \in I} p_i \right) \left(\sum_{i \in I} r_i \right) + z^2 \left(\sum_{i \in I} r_i \right)^2, \quad (2.4.71)$$

$$= P_I^2 + 2z P_I R_I. \quad (2.4.72)$$

When the singularity occurs at the pole $\hat{P}_i^2 = 0$, we can derive from the last line of the above equalities the expression

$$z_I = -\frac{P_I^2}{2R_I P_I}, \quad (2.4.73)$$

from which we can rewrite Eq. (2.4.72) to have an expression of \hat{P}_i^2 as a function of the complex number z_I ,

$$\hat{P}_i^2 = -\frac{P_I^2}{z_I}(z - z_I). \quad (2.4.74)$$

From this last equation, we can see that $1/\hat{P}_i^2$ only gives pole at $z_I = -P_I^2/(2P_I R_I)$ and for generic momenta $z_I \neq 0$. For the leading order tree-level diagrams, no diagram can have more than one power of $1/\hat{P}_i^2$. This tells us that the complex tree-level partial amplitude $\hat{A}_n(z)$ only has simple poles and they are all located away from the origin.

We can now study the behavior of $\hat{A}_n(z)$ in the complex plane. Let us consider the following contour integral

$$\mathcal{I} = -\frac{i}{2\pi} \oint_{\mathcal{C}} dz \frac{\hat{A}_n(z)}{z}, \quad (2.4.75)$$

where the contour \mathcal{C} is big enough to include all infinite poles and defined to be

$$\mathcal{C} = \lim_{R \rightarrow \infty} \mathcal{C}_R, \quad \mathcal{C}_R = \{z \in \mathbb{C} | z = R e^{i\theta}, 0 \leq \theta \leq 2\pi\}. \quad (2.4.76)$$

By deforming the contour \mathcal{C} to surround all the possible poles, Cauchy's theorem tells us that the evaluation of \mathcal{I} is equivalent to calculating poles and residues of $\hat{A}_n(z)/z$,

$$\mathcal{B}_n = \sum_{z_I} \text{Res} \left[\frac{\hat{A}_n(z)}{z}, z_I \right]. \quad (2.4.77)$$

Notice that the complex function $\hat{A}_n(z)/z$ has three different kinds of poles: (i) at $z = 0$ with residue $\hat{A}_n(z=0) = A_n$, (ii) at $z = z_I$ with residue $\text{Res} \left[\hat{A}_n(z)/z, z_I \right]$, and (iii) at $z = \infty$ with residue \mathcal{B}_n . Thus, we have the following expression

$$\mathcal{B}_n = A_n + \sum_{z_I \neq 0} \text{Res} \left[\frac{\hat{A}_n(z)}{z}, z_I \right]. \quad (2.4.78)$$

In order to understand how $\hat{A}_n(z)$ behaves at poles z_I , we need to understand how $\hat{A}_n(z)$ behaves as $z \rightarrow z_I$, i.e. when $\hat{P}_I \rightarrow 0$. Consider a partial amplitude, only diagrams with internal propagator \hat{P}_I contribute to the limit $\hat{P}_I \rightarrow 0$, which allows us to factorize the amplitude into two subamplitudes and the propagator connecting the two subamplitudes has momentum P_I . We thus have the following factorization property:

$$\text{Res} \left[\frac{\hat{A}_n(z)}{z}, z_I \right]_{z_I \neq 0} = -\hat{A}_L(z_I) \frac{1}{P_I^2} \hat{A}_R(z_I). \quad (2.4.79)$$

Notice that both the two subamplitudes are on-shell in the limit $\hat{P}_I \rightarrow 0$. As a final result, we have

$$A_n = \sum_{I, h_I} \hat{A}_L(z_I) \frac{1}{P_I^2} \hat{A}_R(z_I), \quad (2.4.80)$$

where the summation is performed over both all possible diagrams giving non-trivial subset of I and all possible on-shell particle states that can be exchanged on the internal line. Represented diagrammatically, the above mathematical expression can be represented as shown in Fig. 2.1.

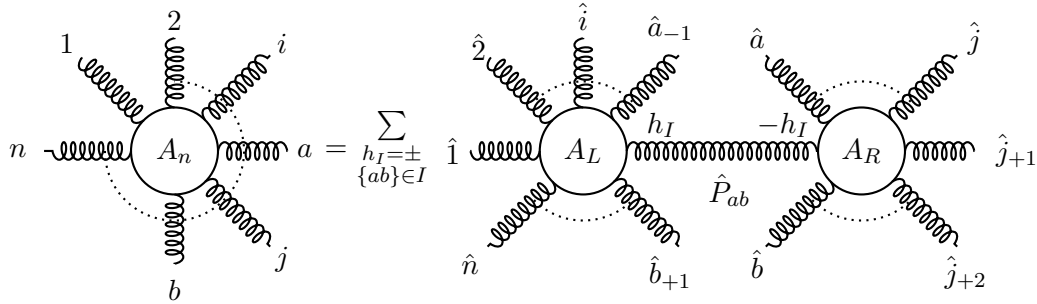


Figure 2.1: Diagrammatic illustration of how A_n partial amplitude is split into two subdiagrams each with a number of legs less than n via the general on-shell recursion. The summation is performed over all possible topological diagrams and the helicity. In the subdiagrams, $i_{\pm m}$ are shorthand for $(i \pm m)$.

Recall that in this particular recursion we shifted all external gluon lines. As illustrated by Fig. 2.1, this particular all-line shift produces recursion relations that could allow us

to construct all MHV and non-MHV amplitudes from lower-point subamplitudes. This construction of amplitudes can be extended to the notion of MHV vertex expansion or CSW (Cachazo-Svrcek-Witten) expansion [66]. Notice that the all-line shift is not the only transformation that can be performed. We see in Section 2.5.2 how to construct recursion relations with only two shifted momenta with a presence of fermion lines.

2.5 The BCFW on-shell recursion

Recursion relations have been developed by Berends and Giele in 1988 in order to construct n -point parton amplitudes from the most building block—three-point—amplitudes with one leg off-shell [67]. They found that this off-shell recursion method remains useful as an algorithm for efficient numerical calculations of scattering amplitudes. The newer and most known on-shell recursion methods, referred to as BCFW recursion relations were formulated in 2005 [48, 49], whose building blocks are themselves on-shell subamplitudes. These on-shell recursions are elegant and beautiful as they use as input gauge invariant objects which make manifest the hidden symmetry of the scattering amplitudes.

In this section, we describe the construction of tree amplitudes via the Britto-Cachazo-Feng-Witten (BCFW) on-shell recursion which is a particular case of the general on-shell recursion. As alluded in the previous section, the BCFW recursion is based on introducing a complex parameter-shift of the external massless spinors. The general on-shell recursion in Section 2.4 does not define a specific choice of shift-vectors r_i while the BCFW deformation does. In addition, the dimension of the BCFW recursion is specified to $d = 4$ while the dimension is not specified for the general recursion. Undoubtedly, the main feature of the BCFW is the fact that it only shifts two of the external legs. We see in the next chapter how to compute the general formula of MHV amplitudes using the BCFW for a process involving an arbitrary number of gluons and one pair of quark-antiquark.

2.5.1 BCFW deformation

Start by choosing two external legs labeled i and j with momentum p_i and p_j respectively and shift by a vector q multiplied by the complex number z , so we have the following linear transformations

$$p_i \longrightarrow \hat{p}_i = p_i + zq, \quad (2.5.81)$$

$$p_j \longrightarrow \hat{p}_j = p_j - zq, \quad (2.5.82)$$

where $q = |i\rangle\langle j|$. One can straightforwardly check that the overall momentum is conserved since $\hat{p}_i + \hat{p}_j = p_i + p_j$, and the on-shell condition is satisfied, $\hat{p}_i^2 = \hat{p}_j^2 = q^2 = 0$.

Thus, expressing the above transformations in terms of the square and angle brackets we have the following equations

$$|\hat{i}\rangle\langle\hat{i}| = |i\rangle\langle i| + z|i\rangle\langle j|, \quad (2.5.83)$$

$$|\hat{j}\rangle\langle\hat{j}| = |j\rangle\langle j| - z|i\rangle\langle j|. \quad (2.5.84)$$

By doing a simple identification, we can arrive at the following results

$$\begin{cases} |\hat{i}\rangle = |i\rangle + z|j\rangle \\ |\hat{i}\rangle = |i\rangle \end{cases}, \text{ and } \begin{cases} |\hat{j}\rangle = |j\rangle \\ |\hat{j}\rangle = |j\rangle - z|i\rangle \end{cases}. \quad (2.5.85)$$

Such deformations are called $[i, j]$ -shift. Indeed, it only affect the two external legs i and j . One can straightforwardly verify that any spinor products of the form $\langle k\hat{i}$ and $[k\hat{j}]$ are linear in z (where k is an arbitrary momentum) while the other quantities such as $\langle\hat{i}\hat{j}\rangle$, $[\hat{i}\hat{j}]$, $\langle j\hat{i}\rangle$ and $[\hat{i}\hat{j}]$ remain unshifted. One has the freedom to choose the helicity (h_i, h_j) , however, a good choice of helicity will lead to a maximum vanishing diagrams and therefore simplifies the calculation. One should be aware that the validity of the BCFW recursion relations requires that the residue of $\hat{A}_n(z)$ at $z = \infty$ vanishes. Argument based on background field methods in pure Yang-Mills theory establishes that the following types of helicity configurations $(-, -)$, $(-, +)$ and $(+, +)$ give valid BCFW recursion relations at large z -behavior.

2.5.2 The BCFW recursion relation

Initially, the BCFW on-shell recursion relation was first constructed for pure gluon processes. However, it can be naturally extended to include quarks with some exceptions. Identically, one chooses two external legs to take as reference lines, either gluons or quarks, then deforms the momentum exactly in the same way as shown in Eq. (2.5.85), and finally combines the two subamplitudes as expressed by Fig. 2.1. However, in order to not running into inconsistencies and preserving the vanishing condition of $\hat{A}_n(z)$ at $z = \infty$, one can neither shift two adjacent quark lines of different types with the same helicity, nor two adjacent quark lines of different types with different helicity, nor a quark and an adjacent gluon with the same helicity. To illustrate this, let us consider the QCD process involving n external gluons and one pair of quark-antiquark. By choosing a $[i, j]$ -shift, we can represent diagrammatically the recursion relations as follows

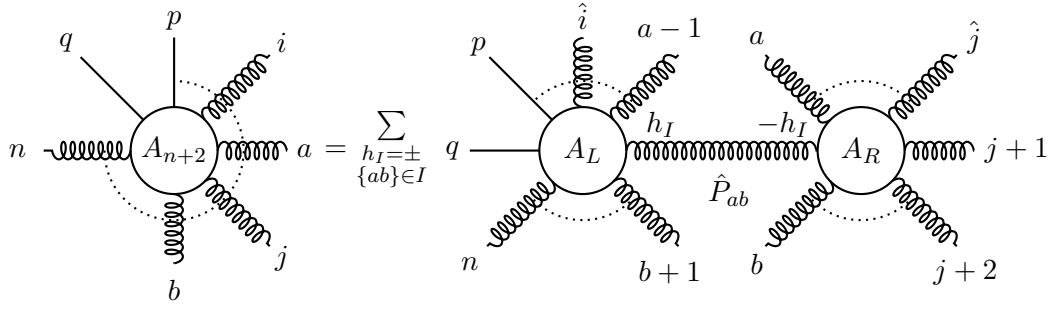


Figure 2.2: Diagrammatic representation of how A_{n+2} partial amplitude with n external gluons and one pair of quark-antiquark is split into two subdiagrams each with a number of legs less than $(n+2)$ via BCFW recursion. Again, the summation is performed over all possible topological diagrams and the helicity h_I .

The above diagrams can be mathematically expressed as

$$A_{n+2} = \sum_{h_I, \mathcal{O}} A_L \left(1, \dots, \hat{i}, \dots, a-1, \hat{P}_{ab}^{h_I}, b+1, \dots, n \right) \frac{1}{P_{ab}^2} A_R \left(-\hat{P}_I^{-h_I}, a, \dots, \hat{j}, \dots, b \right), \quad (2.5.86)$$

where $\mathcal{O} = \{\{ab\} | i \notin \{ab\} \wedge j \in \{ab\}\}$. Note that \hat{i} and \hat{j} cannot belong to the same subdiagram. To see that, let us consider an internal propagator P_I . The shifted legs \hat{i} and \hat{j} cannot belong to the same subdiagram because in that case $\hat{P}_I = P_I$. This is due to the fact that $\hat{p}_i + \hat{p}_j = p_i + p_j$. As expressed in Fig. 2.2, the internal shifted propagator now writes as $\hat{P}_I = P_I + zq$ (with $P_I = \sum_{i \in I} p_i$) and the poles are now at $z_I = -P_I/(2q)$. Of course, we can now have diagrams with quarks as an internal line. However, their propagators are the same as for the gluons. This case appears when the quark and the antiquark each belongs to different subdiagram.

2.6 Summary

In this Chapter, we first introduced in Section 2.1 the notion of spinor helicity variables using the square and angle bracket notations. As illustrated by the computation of the pure four-gluon process, the calculation of individual Feynman diagram becomes extremely simple when expressed in terms of their helicity. We introduced in Section 2.2 the concept of color-kinematic duality. We emphasized the simplicity of computing scattering amplitudes by separating the color factors from the color-ordered partial amplitudes. Section 2.4 focused on the development of on-shell recursion relations. We showed that the on-shell recursion relations allow us to construct recursively all higher order amplitudes from

the most basic three-point amplitudes. In particular, we focused on the most well known recursion relation, that is the BCFW. We will see in the next section the application of the BCFW recursion relation.

Chapter 3

Review of the $qg \longrightarrow qg$ calculation

In this Chapter, we try to achieve two main goals. The first is to re-derive the expression of the full cross section of the QCD process $qg \rightarrow qg$ using the mathematical tools introduced in the previous chapters. In particular, we use the BCFW on-shell recursion relations to decompose the amplitude into a product of three-point ones. We then use the little group scaling along with the color-kinematic decomposition and the spinor helicity formalism to compute those three-point subamplitudes. The second is to construct a general formula for any order MHV amplitudes (again) using the BCFW formalism. This will be extremely useful when we compute the multiple radiative emission in Chapter 4 and Chapter 5 for the study of the radiative energy loss phenomena.

3.1 Computation of the 3-point amplitude using the little group scaling

It has been shown in the previous sections that in Yang-Mills theory, all higher-point amplitudes can be constructed from the basic three-point amplitudes. In this section, we see how three-point amplitudes can be trivially computed using the little group scaling and the spinor helicity formalism.

Recall that in order for three-point amplitudes to not vanish, they can only depend either on the angle or square brackets. To see that, let us consider a three-point amplitude where the momentum of the particles are labeled by p_1, p_2 and p_3 . Considering all the momentum to be incoming, the momentum conservation writes as $p_1 + p_2 + p_3 = 0$, which implies that $(p_1 + p_2)^2 = p_3^2 = \langle 12 \rangle [12] = 0$. This tells us that either $\langle 12 \rangle$ or $[12]$ must be equal to zero. Let us first suppose that $\langle 12 \rangle$ does not vanish, then we have

$\langle 12 \rangle [23] = \langle 1 | p_2 | 3 \rangle = -\langle 1 | (p_1 + p_3) | 3 \rangle = 0$ and similarly $\langle 12 \rangle [13] = \langle 2 | (p_2 + p_3) | 3 \rangle = 0$ since $\langle ii \rangle = [ii] = 0$. This clearly demonstrates that $[12], [13]$ and $[23]$ vanish while $\langle 12 \rangle \neq 0$. Using similar approach, one can straightforwardly show that $\langle 13 \rangle$ and $\langle 23 \rangle$ vanish if we consider the case where $\langle 12 \rangle$ vanish while $[12]$ does not. Therefore, a non-vanishing three-point amplitude has to be a function of either square or angle brackets.

Let us now compute the partial three-point amplitude $A_3(p, k, q)$ where p and q denote the quark and the antiquark with the helicity $(-1/2)$ and $(1/2)$ respectively. Let us choose the gluon k to have a negative helicity in order to have an MHV amplitude. The partial amplitude $A_3(p, k, q)$ can be therefore expressed in terms of angle brackets as follows

$$A_3(h_p, h_k, h_q) = \langle pk \rangle^x \langle pq \rangle^y \langle kq \rangle^z. \quad (3.1.1)$$

The value of x, y and z are fixed by the little group scaling via the following equations

$$x + y = -2h_p, \quad (3.1.2)$$

$$x + z = -2h_k, \quad (3.1.3)$$

$$y + z = -2h_q. \quad (3.1.4)$$

Recalling that the helicities are given by $h_p = -1/2, h_q = 1/2$ and $h_k = -1$, the above system can be straightforwardly solved to find that, $x = 2, y = -1$ and $z = 0$. Thus, the three-point partial amplitude with the above choice of helicity can be expressed as

$$A_3(p^-, k^-, q^+) = \frac{\langle pk \rangle^3 \langle qk \rangle}{\langle pk \rangle \langle kq \rangle \langle qp \rangle}. \quad (3.1.5)$$

For an $\overline{\text{MHV}}$ three-point amplitude, one can take similar approach to show that

$$A_3(p^+, k^+, q^-) = \frac{[pk]^3 [qk]}{[pk] [kq] [qp]}. \quad (3.1.6)$$

One can notice that the expression of the three-point amplitudes are simple and compact. We will see in the next section that the general expression of MHV amplitudes involving a pair of quark-antiquark and an arbitrary number of gluons can be constructed in a very simple form using these three-point amplitudes.

3.2 Decomposition of the four-point amplitude using BCFW formalism

In order to compute the cross section of the QCD process $qg \rightarrow qg$, one can of course use the Feynman rules to express each tree-level diagram contributing to the process and then

rewrite the expression in terms of the spinor variables before squaring the full amplitude. This approach, however, seems complicated and rather tedious. In this section, we see how the BCFW on-shell recursion can be applied to compute efficiently QCD processes.

Considering all the momenta to be incoming, we end up computing the amplitude $\mathcal{A}_4(qgg\bar{q})$ where one of the quark has to become an antiquark. This can be restored later on using crossing symmetry. In this case, the only non-vanishing amplitude appears when two of the external state particles have negative helicity. Let us denote by p and q the momenta of the incoming quark and antiquark with the helicity $(-1/2)$ and $(1/2)$ respectively. In the same way, denote by k and l the momenta of the two gluons with the respective helicity (-1) and (1) . We can make a $[k, l]$ -shift which linearly transforms the momenta of the two gluons to get the following equations

$$|k\rangle \longrightarrow |\hat{k}\rangle = |k\rangle + z|l\rangle \quad \text{and} \quad |l\rangle \longrightarrow |\hat{l}\rangle = |l\rangle - z|k\rangle. \quad (3.2.7)$$

By virtue of these transformations, we can decompose the partial amplitude $A_4(p, k, l, q)$ into three-point subamplitudes. According to our initial choice of helicity configuration, there are two possible BCFW diagrams as shown in Fig. 3.1. One can notice that the

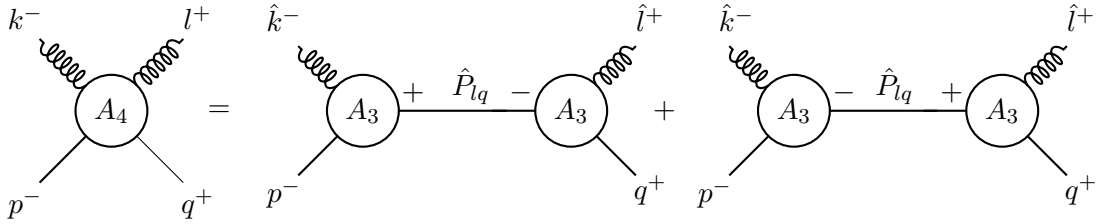


Figure 3.1: BCFW diagrammatic representation of the decomposition of the four-point MHV amplitude into three-point subamplitudes via the $[k, l]$ -shift. Only two diagrams contribute to the full MHV partial amplitude $A_4(p^-, k^-, l^+, q^+)$.

second diagram in Fig. 3.1 vanishes and does not contribute to the general expression of the scattering amplitude since $A_3(-, -, -)$ and $A_3(+, +, +)$ are both equal to zero. Thus, the four-point partial amplitude expresses as

$$A_4(p^-, k^-, l^+, q^+) = A_3(p^-, \hat{k}^-, \hat{P}_{lq}^+) \frac{1}{P_{lq}^2} A_3(-\hat{P}_{lq}^-, \hat{l}^+, q^+) \quad (3.2.8)$$

$$= \frac{\langle p\hat{k}\rangle^3 \langle \hat{P}_{lq}\hat{k}\rangle}{\langle p\hat{k}\rangle \langle \hat{k}\hat{P}_{lq}\rangle \langle \hat{P}_{lq}p\rangle} \frac{1}{\langle lq\rangle [lq]} \frac{[q\hat{l}]^3 [\hat{P}_{lq}\hat{l}]}{[\hat{P}_{lq}\hat{l}] [\hat{l}q] [q\hat{P}_{lq}]}. \quad (3.2.9)$$

The first line is just the application of the BCFW formula while from the first to the second line we used the Eq. (3.1.5) and Eq. (3.1.6). Notice that the above expressions still

a function of the shifted momentum. To get rid of the shifted momentum, one should recall the on-shell condition of the internal line ($\hat{P}_{lq}^2 = 0$), the shift equation and the momentum conservation. The on-shell condition implies that $\langle \hat{l}q \rangle [\hat{l}q] = 0$, which tells us that $\langle \hat{l}q \rangle$ must vanish since $[\hat{l}q] = [lq]$ is not equal to zero. This means that $|\hat{l}\rangle$ and $|q\rangle$ are collinear and we can write $|\hat{l}\rangle = x|q\rangle$. Moreover, using the shift equations in Eq. (3.2.7) and taking into account that $\langle \hat{l}q \rangle = 0$, we can find the value of the complex parameter $z = \langle lq \rangle \langle kq \rangle^{-1}$. Thus, the shift equations now become

$$|\hat{k}\rangle = |k\rangle + \frac{\langle kl \rangle}{\langle kq \rangle} |l\rangle \quad \text{and} \quad |\hat{l}\rangle = |l\rangle - \frac{\langle kl \rangle}{\langle kq \rangle} |k\rangle. \quad (3.2.10)$$

By virtue of these equations and the fact that $|\hat{l}\rangle = x|q\rangle$, it naturally follows that

$$|l\rangle - \frac{\langle kl \rangle}{\langle kq \rangle} |k\rangle = x|q\rangle. \quad (3.2.11)$$

We can easily solve the above equation by multiplying each side by $\langle l|$ to find $x = \langle kl \rangle \langle kq \rangle^{-1}$. On the other hand, recall that the internal momentum writes as $\hat{P}_{lq} = |\hat{P}_{lq}\rangle [\hat{P}_{lq}]$ which from the momentum conservation can also be rewritten as the sum of \hat{l} and q , $\hat{P}_{lq} = |\hat{l}\rangle [\hat{l}] + |q\rangle [q]$. Developing this last expression will give us the value of the square and angle component of \hat{P}_{lq} ,

$$\hat{P}_{lq} = |q\rangle \left(\frac{\langle kl \rangle}{\langle kq \rangle} [l] + [q] \right) \implies |\hat{P}_{lq}\rangle = |q\rangle \quad \text{and} \quad [\hat{P}_{lq}] = \left(\frac{\langle kl \rangle}{\langle kq \rangle} [l] + [q] \right). \quad (3.2.12)$$

We now have the explicit values of $|\hat{k}\rangle, |\hat{l}\rangle, |\hat{P}_{lq}\rangle$ and $[\hat{P}_{lq}]$, and recall that the other momentum remain unchanged. Putting these expressions back in Eq. (3.2.9), rearranging the terms and doing some simplifications we get the expression of the partial amplitude $A_4(p^-, k^-, l^+, q^+)$ given as follows

$$A_4(p^-, k^-, l^+, q^+) = \frac{\langle pk \rangle^3 \langle qk \rangle}{\langle pk \rangle \langle kl \rangle \langle lq \rangle \langle qp \rangle}. \quad (3.2.13)$$

The above expression represents the MHV partial amplitude for the case of one pair of quark-antiquark and two external gluons. This formula can be generalized to include n external gluons using the BCFW on-shell recursion as we will show in Section 3.4.

3.3 Total differential cross section

Let us now compute the full MHV amplitude $\mathcal{A}_4(p^-, k^-, l^+, q^+)$. From the color-kinematic decomposition, one can decompose the amplitude as follows

$$\mathcal{A}_4(p^-, k^-, l^+, q^+) = g_s^2 (T^{a_k} T^{a_l}) A_4(p^-, k^-, l^+, q^+) + g_s^2 (T^{a_l} T^{a_k}) A_4(p^-, l^+, k^-, q^+), \quad (3.3.14)$$

where the partial amplitudes are given by

$$A_4(p^-, k^-, l^+, q^+) = \frac{\langle pk \rangle^3 \langle qk \rangle}{\langle pk \rangle \langle kl \rangle \langle lq \rangle \langle qp \rangle}, \quad A_4(p^-, l^+, k^-, q^+) = \frac{\langle pk \rangle^3 \langle qk \rangle}{\langle pl \rangle \langle lk \rangle \langle kq \rangle \langle qp \rangle}. \quad (3.3.15)$$

From $A_4(p^-, k^-, l^+, q^+)$ to $A_4(p^-, l^+, k^-, q^+)$ one has just to interchange the k and l in the denominator. In order to compute the differential cross section we have to take the square of Eq. (3.3.14), sum over the colors and all the possible helicities. One can of course directly compute the amplitude squared. However, a much better way to do the calculation is to compute the square with respect to the color basis. We will see the necessity of such approach when we compute the square of the multiple radiative emission current. Therefore, the MHV amplitude squared, traced over the colors can be expressed as follows

$$|\overline{\mathcal{A}}_4(p^-, k^-, l^+, q^+)|^2 = g_s^2 \mathcal{C}_s(k, l) K_s(k, l) + g_s^2 \mathcal{C}_a(k, l) K_a(k, l), \quad (3.3.16)$$

where the color factors expressed as a function of the Casimir factors are given by

$$\mathcal{C}_s(k, l) = Tr(T^{a_k} T^{a_l} T^{a_l} T^{a_k}) = C_A C_F^2, \quad (3.3.17)$$

$$\mathcal{C}_a(k, l) = Tr(T^{a_k} T^{a_l} T^{a_k} T^{a_l}) = -C_F. \quad (3.3.18)$$

Recall that the ordering of the kinematics follows exactly the ordering of the colors. Thus, the two kinematic terms are also function of the symmetric and the antisymmetric product of the permutation of the two gluons expressed as

$$\begin{aligned} K_s(k, l) &= |A_4(p^-, k^-, l^+, q^+)|^2 + |A_4(p^-, l^+, k^-, q^+)|^2 \\ &= \frac{4(pk)^3(qk)}{(qp)^2} \sum_{\mathcal{P}_2(k, l)} \frac{\langle pq \rangle}{\langle pk \rangle \langle kl \rangle \langle lq \rangle} \frac{[pq]}{[pk][kl][lq]}, \end{aligned} \quad (3.3.19)$$

and on the other hand, we have

$$\begin{aligned} K_a(k, l) &= A_4(p^-, k^-, l^+, q^+) A_4^*(p^-, l^+, k^-, q^+) + A_4^*(p^-, k^-, l^+, q^+) A_4(p^-, l^+, k^-, q^+) \\ &= \frac{4(pk)^3(qk)}{(qp)^2} \sum_{\mathcal{P}_2(k, l)} \frac{\langle pq \rangle}{\langle pk \rangle \langle kl \rangle \langle lq \rangle} \frac{[pq]}{[pl][lk][kq]}. \end{aligned} \quad (3.3.20)$$

Therein, the terms with parentheses represent the usual dot product. Rearranging the colors and the kinematics so we can recover the full permutation, the amplitude squared simplifies as

$$|\overline{\mathcal{A}}_4(p^-, k^-, l^+, q^+)|^2 = g_s^2 C_A C_F^2 (K_s(k, l) + K_a(k, l)) - (C_F + C_A C_F^2) K_a(k, l). \quad (3.3.21)$$

We are now left with the evaluation of the kinematics. Using the Schouten identity, one can straightforwardly check that

$$\sum_{\mathcal{P}_2(k,l)} \frac{\langle pq \rangle}{\langle pk \rangle \langle kl \rangle \langle lq \rangle} = \prod_{i=k,l} \frac{\langle pq \rangle}{\langle pi \rangle \langle iq \rangle}. \quad (3.3.22)$$

The above relation is also satisfied for square brackets. Using the Lorentz invariant product, the first kinematic in Eq. (3.3.21) can be simplified as

$$K_s(k, l) + K_a(k, l) = \frac{(pk)^3(qk)}{(pk)(kq)(pl)(lq)}. \quad (3.3.23)$$

For the second term in Eq. (3.3.21), we can use the shorthand notation introduced in Section 2.1.3 and remark that $\langle pkqlp \rangle$ and $\langle plqkp \rangle$ are complex conjugate of each other. Therefore, $K_a(k, l)$ can be evaluated by performing Dirac traces which implies that

$$K_a(k, l) = -\frac{4(pk)^3(qk)}{(kl)(qp)} \frac{\text{Tr}(\not{p}\not{k}\not{q}\not{l})}{|\langle pkqlp \rangle|^2} \quad (3.3.24)$$

$$= \frac{(pk)^3(qk)}{(kl)(qp)} \left(\frac{1}{(pk)(lq)} + \frac{1}{(pl)(kq)} - \frac{(pq)(kl)}{\prod(p_i)(i_q)} \right). \quad (3.3.25)$$

We can now translate the variables into the Mandelstam variables appropriate for the process $qg \rightarrow qg$. After rearranging the terms and making some simplifications, the amplitude squared for our specific choice of helicity can be written as

$$|\bar{\mathcal{A}}_4(p^-, k^-, l^+, q^+)|^2 = g_s^4 C_A C_F^2 \left(\frac{9u}{4s} - \frac{s^2}{t^2} \right). \quad (3.3.26)$$

To complete the calculation, we need to sum the amplitude squared over all the possible helicities configuration. For our two-to-two process, only 4 possible configuration of helicity gives non-vanishing amplitudes: $(-, -, +, +)$, $(-, +, -, +)$, $(+, -, +, -)$ and $(+, +, -, -)$. However, due to the parity of the partial amplitudes,

$$|\bar{\mathcal{A}}_4(p^-, k^-, l^+, q^+)|^2 = |\bar{\mathcal{A}}_4(p^+, k^+, l^-, q^-)|^2 \quad (3.3.27)$$

$$|\bar{\mathcal{A}}_4(p^-, k^+, l^-, q^+)|^2 = |\bar{\mathcal{A}}_4(p^+, k^-, l^+, q^-)|^2 \quad (3.3.28)$$

This implies that we only have to compute the amplitude squared for two configurations: (i) $|\bar{\mathcal{A}}_4(p^-, k^-, l^+, q^+)|^2$ which we have already computed (ii) $|\bar{\mathcal{A}}_4(p^-, k^+, l^-, q^+)|^2$ which is related to (i) by flipping the helicity of the two gluons. That is to say, we do not have to take into consideration the helicity of the (anti-)quark while doing the average. Flipping the helicity of the gluons is equivalent to swapping the momentum of the k and l . In terms of Mandelstam variables, this is equivalent to the interchange of u and s . Physically, this swap of momentum represents the case where the two gluons are interchanged. Taking

into account the factors for averaging over the colors and helicities, we get the final cross section of our process

$$\frac{d\sigma}{d\cos\theta}(qg \rightarrow qg) = \frac{2}{9} \frac{\pi\alpha_s^2}{s} \left(\frac{9}{4} \frac{u^2 + s^2}{us} - \frac{s^2 + u^2}{t^2} \right) \quad (3.3.29)$$

where we rewrite the coupling constant as $g_s^2 = 4\pi\alpha_s$, s is the square of the center of mass energy and θ is the scattering angle. One can compare this result to [58] and check that it is consistent.

3.4 Generalizing the MHV amplitudes

Having established the BCFW on-shell recursion and applied it to the calculation of the $qg \rightarrow qg$ scattering process, we now give a simple yet non-trivial derivation of the general MHV formula for $(n+2)$ -point amplitudes which involves n arbitrary gluons and a pair of quark-antiquark. Let us take an inductive approach, which means that we assume that the MHV formula in Eq. (3.4.30) is true at the order $(n+1)$ and show that it is still true at order $(n+2)$.

$$A(p^-, 1^+, \dots, i^-, \dots, (n-1)^+, q^+) = \frac{\langle pi \rangle^3 \langle qi \rangle}{\langle p1 \rangle \langle 12 \rangle \dots \langle (n-1)q \rangle \langle qp \rangle}. \quad (3.4.30)$$

For simplicity, but without loss of generality, let us assume that the negative helicity gluon is at position i , and the remaining gluons have positive helicity. According to the previous discussion, we will obtain a valid BCFW recursion without boundary term if we consider the $[i, i_{+1}]$ -shift. Thus, we have the following shift equations:

$$\begin{cases} |\hat{i}\rangle = |i\rangle + z|i_{+1}\rangle, & |\hat{i}\rangle = |i\rangle \\ |\hat{i}_{+1}\rangle = |i_{+1}\rangle - z|i\rangle, & |\hat{i}_{+1}\rangle = |i_{+1}\rangle. \end{cases} \quad (3.4.31)$$

With our choice of helicity and momentum shift, one can check that only two diagrams contribute to the full MHV amplitude as shown by the diagrammatic representation in Fig. 3.2. Each subdiagram is either an MHV or $\overline{\text{MHV}}$ -subamplitude which we can translate into its mathematical expression.

We can now write the respective mathematical expressions for the different diagrams using the square and angle bracket notations. In particular, the expression of the first diagram \mathcal{D}_1 is given by

$$\mathcal{D}_1 = A_L(p^-, \dots, \hat{i}^-, \hat{P}^+, i_{+3}^+, \dots, n, q) \frac{1}{\langle \hat{i}_{+1} i_{+2} \rangle [i_{+1} i_{+2}]} A_R(-\hat{P}^-, \hat{i}_{+1}^+, i_{+2}^+) \quad (3.4.32)$$

$$= \frac{\langle p\hat{i} \rangle^3 \langle q\hat{i} \rangle}{\langle p1 \rangle \dots \langle \hat{i}\hat{P} \rangle \langle \hat{P}i_{+3} \rangle \dots \langle nq \rangle \langle qp \rangle} \frac{1}{\langle i_{+1} i_{+2} \rangle [i_{+1} i_{+2}]} \frac{[\hat{i}_{+1} i_{+2}]^4}{[\hat{P}\hat{i}_{+1}] [\hat{i}_{+1} i_{+2}] [i_{+2} \hat{P}]}, \quad (3.4.33)$$

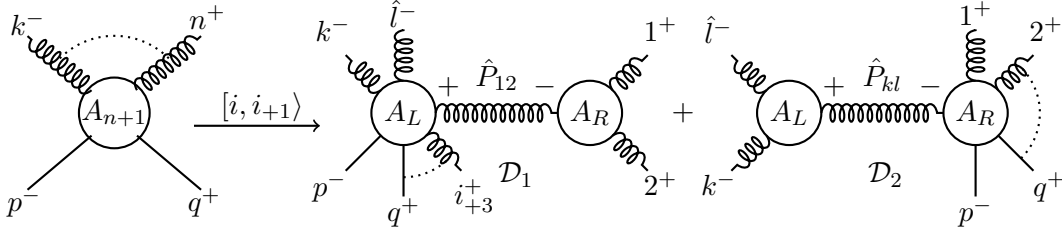


Figure 3.2: Diagrammatic representation of the BCFW on-shell recursion for the general MHV amplitude with quark-antiquark line. The quark p and the gluon i are chosen to have negative helicities with a $[i, i+1]$ -shift. \hat{P} and \hat{Q} are respectively the shorthand notations for $(\hat{p}_{i+1} + p_{i+2})$ and $(\hat{p}_i + p_{i-1})$.

where we used the following conventions for the analytic continuation: $|- \hat{P}\rangle = -|\hat{P}\rangle$ and $|- \hat{P}] = |\hat{P}]$. The on-shell condition tells us that $\hat{P}^2 = \langle \hat{i}_{+1} i_{+2} \rangle [\hat{i}_{+1} i_{+2}] = 0$. Since $[\hat{i}_{+1} i_{+2}] = [i_{+1} i_{+2}] \neq 0$ we have $\langle \hat{i}_{+1} i_{+2} \rangle = 0$. This implies that $|\hat{i}_{+1}\rangle$ and $|i_{+2}\rangle$ are collinear so we can write $|\hat{i}\rangle = x|i_{+2}\rangle$. Thus, using the shift equation for $|\hat{i}_{+1}\rangle$ we have the following expression for $|\hat{i}_{+1}\rangle$,

$$|\hat{i}_{+1}\rangle = |i_{+1}\rangle - z|i\rangle = x|i_{+2}\rangle. \quad (3.4.34)$$

We can solve the above equation for x by multiplying each side by $\langle i|$ in order to eliminate z . So, we have $x = \langle ii_{+1} \rangle / \langle ii_{+2} \rangle$. On the other hand, we can find the value of the complex parameter z by considering the on-shell condition:

$$\langle \hat{i}_{+1} i_{+2} \rangle = \langle i_{+1} i_{+2} \rangle - z \langle ii_{+2} \rangle = 0 \implies z = \frac{\langle i_{+1} i_{+2} \rangle}{\langle ii_{+2} \rangle}. \quad (3.4.35)$$

Furthermore, the internal in the first diagram can be expressed in terms of the spinor representation of the two external legs as $\hat{P} = |\hat{P}\rangle[\hat{P}] = |\hat{i}_{+1}\rangle[i_{+1}] + |i_{+2}\rangle[i_{+2}]$. It follows from this expression that

$$\hat{P} = |i_{+2}\rangle \left(\frac{\langle ii_{+1} \rangle}{\langle ii_{+2} \rangle} [i_{+1}] + [i_{+2}] \right). \quad (3.4.36)$$

With the above expressions, we can now get rid of the shifted momentum in Eq. (3.4.33).

One can straightforwardly check that we have the following

$$|\hat{P}\rangle = |i_{+2}\rangle, \quad |\hat{P}] = \frac{\langle ii_{+1} \rangle}{\langle ii_{+2} \rangle} [i_{+1}] + [i_{+2}], \quad (3.4.37)$$

$$|\hat{i}\rangle = |i\rangle + \frac{\langle i_{+1} i_{+2} \rangle}{\langle ii_{+2} \rangle} |i_{+1}\rangle, \quad \hat{i}_{+2} = |i_{+1}\rangle - \frac{\langle i_{+1} i_{+2} \rangle}{\langle ii_{+2} \rangle} |i\rangle. \quad (3.4.38)$$

Notice that all the other momentum remain unshifted. Plugging back the above expressions in Eq. (3.4.33), rearranging the terms and doing some simplifications, we get the final

expression for the first diagram in Fig. 3.2

$$\mathcal{D}_1 = \frac{\langle pi \rangle^3 \langle qi \rangle}{\langle p1 \rangle \langle 12 \rangle \cdots \langle nq \rangle \langle qp \rangle}. \quad (3.4.39)$$

On the other hand, by taking similar approach we can write down the mathematical expression of the second diagram \mathcal{D}_2 in Fig. 3.2

$$\mathcal{D}_2 = A_L(i_{-1}^+, \hat{i}^-, \hat{Q}^+) \frac{1}{\langle i_{-1} \hat{i} \rangle [i_{-1} \hat{i}]} A_R(-\hat{Q}^-, \hat{i}_{+1}^+, \cdots, n^+, q^+, p^-, \cdots) \quad (3.4.40)$$

$$= \frac{[i_{-1} \hat{Q}]^3}{[i_{-1} \hat{i}] [\hat{Q} \hat{i}]} \frac{1}{\langle i_{-1} \hat{i} \rangle [i_{-1} \hat{i}]} \frac{\langle p \hat{Q} \rangle^3 \langle q \hat{Q} \rangle}{\langle p1 \rangle \cdots \langle i_{-3} \hat{Q} \rangle \langle \hat{Q} \hat{i}_{+1} \rangle \langle \hat{i}_{+1} i_{+2} \rangle \cdots \langle nq \rangle \langle qp \rangle}, \quad (3.4.41)$$

where again for analytic continuation we used the conventions $|- \hat{Q} \rangle = -|\hat{Q} \rangle$ and $|- \hat{Q}] = |\hat{Q}]$. We can show that the above amplitude vanish. Recall that the on-shell condition requires that $\hat{Q}^2 = (p_{i_{-1}} + \hat{p}_i)^2 = 0$. This implies that $\langle i_{-1} \hat{i} \rangle [i_{-1} \hat{i}] = 0$. For generic momenta, $\langle i_{-1} \hat{i} \rangle = \langle i_{-1} i \rangle \neq 0$, so $[i_{-1} \hat{i}] = 0$. In addition, as

$$|\hat{Q} \rangle [\hat{Q} i_{-1}] = \hat{Q} |i_{-1}] = (p_{i_{-1}} + \hat{p}_i) |i_{-1}] = p_i |i_{-1}] = |\hat{i} \rangle [\hat{i} i_{-1}] = 0, \quad (3.4.42)$$

so we have $[\hat{Q} i_{-1}] = 0$. Thus, all spinor products in the first part of Eq. (3.4.41) vanish, with the three powers in the numerator versus the two in the denominator, we conclude that the second diagram \mathcal{D}_2 in Fig. 3.2 vanishes.

Combining all these results, we can finally write down the general MHV formula for amplitudes with n arbitrary number of gluons with a presence of a pair of quark-antiquark,

$$A_{n+2}^{\text{MHV}}(p^-, 1^+, \cdots, i^-, \cdots, n^+, q^+) = \frac{\langle pi \rangle^3 \langle qi \rangle}{\langle p1 \rangle \langle 12 \rangle \cdots \langle nq \rangle \langle qp \rangle}. \quad (3.4.43)$$

The above expression agrees with previous results in the literature, such as the five-point case in [59]. One can exactly take similar approach using the BCFW on-shell recursion relations to show that the general formula for $\overline{\text{MHV}}$ amplitudes is given by

$$A_{n+2}^{\overline{\text{MHV}}}(p^+, 1^-, \cdots, i^+, \cdots, n^-, q^-) = \frac{[pi]^3 [qi]}{[p1][12] \cdots [nq][qp]}. \quad (3.4.44)$$

By adding the appropriate color factors and the coupling constant, we can write down the general formula for both the full MHV and $\overline{\text{MHV}}$ amplitudes. Taking into account the ordering of the kinematics, the expressions are given as follows

$$A_{n+2}^{\text{MHV}}(p^-, \cdots, i^-, \cdots, q^+) = g_s^n \langle pi \rangle^3 \langle qi \rangle \sum_{\mathcal{P}_n} \frac{(T^{a_1} T^{a_2} \cdots T^{a_n})}{\langle p1 \rangle \langle 12 \rangle \cdots \langle nq \rangle \langle qp \rangle}, \quad (3.4.45)$$

and

$$A_{n+2}^{\overline{\text{MHV}}}(p^+, \cdots, i^+, \cdots, q^-) = g_s^n [pi]^3 [qi] \sum_{\mathcal{P}_n} \frac{(T^{a_1} T^{a_2} \cdots T^{a_n})}{[p1][12] \cdots [nq][qp]}. \quad (3.4.46)$$

Notice that all next-to Maximally Helicity Violating amplitudes can be derived from these expressions using the BCFW on-shell recursion relations. In fact, we will see an illustration of such computation in the next sections.

3.5 Summary

In this Chapter, we reviewed the calculation of the cross section of the QCD process $qg \rightarrow qg$. We showed that this particular two-to-two scattering process can be computed in a very efficient and elegant way using the BCFW on-shell recursion relations and the little group scaling. In particular, we derived the expression of the four-point amplitude from three-point amplitudes using the BCFW on-shell recursion. We then used the BCFW on-shell recursion to compute the general expression of the MHV and $\overline{\text{MHV}}$ partial ordered amplitudes. The generalization formulas, represented by Eq. (3.4.43) and Eq. (3.4.44), will be used in the next section when computing the momentum distribution of emitting multiple radiative gluons.

Chapter 4

Radiative emission

Over the past decades, various signatures have been proposed to study the hot QCD matter formed at RHIC and LHC. A potential pQCD model to study the physics of the QGP is to consider a process in which a self-generated parton (quark or gluon) interacts with a gluon coming from the medium and induces final state radiative gluons. Such picture has been first pioneered by Bjorken in 1982 [34] from which one can compute the multiplicity distribution for emitting Bremsstrahlung gluons.

On the QED side, the emission of Bremsstrahlung photons is fully understood. Indeed, the probability distribution for emitting multiple photon Bremsstrahlung has been trivially resummed and shown to follow the Poisson distribution [41]. Such result implies that each emission of Bremsstrahlung photon is independent. On the QCD side, however, the calculations are much more complicated due to the non-Abelian nature of the strong force and it seems that conventional method of pQCD fails to cope with the complexities of computing multiple radiative processes.

In the past few years, tremendous efforts have been put forward to address the question how the evolution of jet is altered by the presence of the QGP medium formed at RHIC and LHC. Alas, the current existing energy loss formalisms have a number of weaknesses which may have a large quantitative impact on the result. At the present day, the generalization of the parton energy loss for multiple radiative gluon emission is not known and all current calculations are based on the convolution of the single inclusive gluon. In some radiative energy loss formalisms such as GLV (Gyulassy, Levai, and Vitev) [42] and ASW (Armesto, Salgado, and Wiedemann) [22], multiple gluon emission is computed using the Poisson Ansatz which assumes that each emission of radiative gluon is independent. However, multiple gluon emission cannot assumed to be independent since as we know gluons can

interact with themselves.

In this section, we first review the simplest picture of multiple radiative particles emission given by a QED process. The study of the photon Bremsstrahlung in QED under the MHV scheme could be an important way forward towards the study of the radiative energy loss in QGP. Indeed, understanding the momentum distribution of multiple radiative photon emission can give us some insights on how the non-Abelian nature of QCD affects the distribution of the radiative gluon emission. Then, we move to the calculation of the momentum distribution of emitting up to three radiative gluons using both soft and collinear approximation.

4.1 Review of the photon bremsstrahlung in QED

The study of the photon Bremsstrahlung in QED is an important way forward towards the study of the radiative energy loss in QGP. Understanding the momentum distribution of the multiple radiative photon emission can give us some clue to understand how the non-Abelian nature of the QCD changes the multiplicity distribution of emitting multiple radiative gluons. Consider the process where a highly energetic quark is tickled by a photon and then emits radiations (see Fig.4.1). Similar calculation using the MHV techniques has been initially introduced in [68]. However, our main interest here is to prove Eq. (4.1.11).

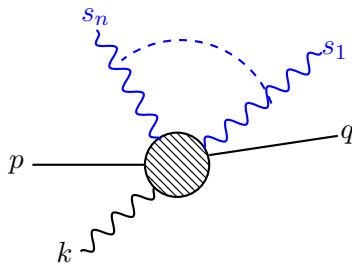


Figure 4.1: Diagrammatic representation of the multiple photon Bremsstrahlung in QED in the process $q\gamma \rightarrow q + n\gamma$ where n represents the number of photon Bremsstrahlung. The soft photons have momentum s_i (i runs from 1 to n).

Let us consider the case where we have an $\overline{\text{MHV}}$ amplitudes. Choose the incoming quark and the tickling photon to have positive helicity and all the remaining particles to have negative helicity. Going from the general formula for the $\overline{\text{MHV}}$ amplitudes, we change generator matrices T^a to 1 and coupling constant to \tilde{e} . Thus, the expression of the

amplitude for our QED process is given by

$$\mathcal{A}_{n+3}^{\overline{\text{MHV}}}(\{p_i, \gamma_i\}) = \frac{[pk]^3[qk]}{[qp]} \sum_{\mathcal{P}_{n+1}} \frac{\tilde{e}^{n+1}}{[pk][k1][12] \cdots [nq]}, \quad (4.1.1)$$

where the sum is performed over the permutation of the photons. We can factorize out the photon with momentum k from the soft photons. In that case, we reduce the sum over permutation \mathcal{P}_{n+1} into a sum over the permutation \mathcal{P}_n . So, we have

$$\mathcal{A}_{n+3}^{\overline{\text{MHV}}} = \frac{[pk]^3[qk]}{[qp]} \sum_{\mathcal{P}_n} \frac{\tilde{e}^n}{[p1] \cdots [nq]} \left(\frac{[p1]}{[pk][k1]} + \frac{[12]}{[1k][k2]} + \cdots + \frac{[nq]}{[nk][kq]} \right) \times \tilde{e}, \quad (4.1.2)$$

Applying the Schouten identity, the terms inside the parentheses simplifies into one term that is independent of the momentum of the soft photons,

$$\mathcal{A}_{n+3}^{\overline{\text{MHV}}} = \frac{[pk]^3[qk]}{[qp]} \frac{[pq]}{[pk][kq]} \sum_{\mathcal{P}_n} \frac{1}{[p1][12] \cdots [nq]}. \quad (4.1.3)$$

Here, the summation is performed over the permutation of the soft photons. We can rearrange this expression in order to separate completely the soft part from the hard scattering. Thus, we get the following expression

$$\mathcal{A}_{n+3}^{\overline{\text{MHV}}}(\{p_i, \gamma_i\}) = \left(\tilde{e} \frac{[pk]^3[qk]}{[pk][kq][qp]} \right) \times \tilde{e}^n \left(\sum_{\mathcal{P}_n} \frac{[pq]}{[p1][12] \cdots [nq]} \right) \quad (4.1.4)$$

From the above equation, one can isolate the emission current that contains the information about the Bremsstrahlung photons. Therefore, for the Abelian theory of the quantum electrodynamics the emission current is given by

$$J_{\text{QED}}^{(n)}(1, \cdots, n) = \tilde{e}^n \sum_{\mathcal{P}_n} \frac{[pq]}{[p1][12] \cdots [nq]}. \quad (4.1.5)$$

Let us now show that the emission of radiative photons are independent. This is equivalent to saying that the total emission current is given by the product of independent emission of each photon

$$J_{\text{QED}}^{(n)}(1, \cdots, n) = \tilde{e}^n \sum_{\mathcal{P}_n} \frac{[pq]}{[p1][12] \cdots [nq]} = \tilde{e}^n \prod_{i=1}^n \frac{[pq]}{[pi][iq]}. \quad (4.1.6)$$

As a direct consequence of the Schouten identity, this relation is certainly true for $n = 2$ (ignoring the coupling). Let us now check if this relation still holds for $n = 3$. We have,

$$\sum_{\mathcal{P}_3} \frac{[pq]}{[p1][12][23][3q]} = \sum_{\mathcal{P}_2} \frac{[pq]}{[p1][12][2q]} \left(\frac{[p1]}{[p3][31]} + \frac{[12]}{[13][32]} + \frac{[2q]}{[23][3q]} \right) \quad (4.1.7)$$

$$= \frac{[pq]}{[p3][3q]} \sum_{\mathcal{P}_2} \frac{[pq]}{[p1][12][2q]} \quad (4.1.8)$$

$$= \prod_{i=1}^3 \frac{[pq]}{[pi][iq]} \quad (4.1.9)$$

We used the Schouten identity to go from the first to the second line. From the second to the third line, we just use the fact the identity (4.1.6) is true for $n = 2$. Let us approach the problem by induction assuming that the identity is true for any arbitrary number n of radiative photons and show that it is still true for $(n + 1)$ number of Bremsstrahlung photons. We can always write

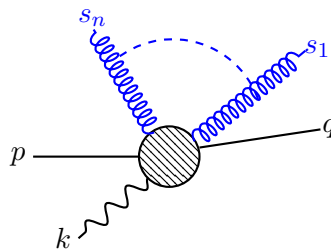
$$\sum_{\mathcal{P}_{n+1}} \frac{[pq]}{[p1][12] \cdots [(n+1)q]} = \sum_{\mathcal{P}_n} \frac{[pq]}{[p1][12] \cdots [nq]} \left\{ \frac{[pq]}{[p(n+1)][(n+1)q]} + \cdots + \frac{[nq]}{[n(n+1)][(n+1)q]} \right\}. \quad (4.1.10)$$

Again, one can see here that the term inside the parentheses simplifies to one term and depends only on the momentum of the quarks and the $(n + 1)$ th radiative photons. On the other hand, the summation over the permutation of photons becomes a product of the independent emission

$$\sum_{\mathcal{P}_{n+1}} \frac{[pq]}{[p1][12] \cdots [(n+1)q]} = \prod_{i=1}^{n+1} \frac{[pq]}{[p^i][iq]}. \quad (4.1.11)$$

This result shows that the identity in Eq. (4.1.6) is indeed true and each emission of photon is independent. As a result, the distribution of Bremsstrahlung photons follows the Poisson distribution.

Replacing the Bremsstrahlung photons by Bremsstrahlung gluons, it is straightforward to show that the emission current is given by Eq. (4.1.12). The difference is that gluons can carry color charges and two Bremsstrahlung gluons can be emitted from one gluon decay. Mathematically speaking, the difficulty in the calculation lies in the fact the generator matrices T^{a_i} do not commute. Therefore, one can naively expect that the momentum distribution of emitting Bremsstrahlung gluons does not follow the Poisson distribution. In fact, one would expect that the emission current for multiple gluon emission is given by $J_{\text{QCD}} = J_{\text{QED}} + J_{\text{NA}}$, where second term comes from the non-Abelian nature proper to the strong force.



$$\Rightarrow \mathcal{J}_g^{(n)} = g_s^2 [pq] \sum_{\mathcal{P}_n} \frac{(T^{a_1} \cdots T^{a_n})}{[p1][12] \cdots [nq]}. \quad (4.1.12)$$

4.2 Soft-collinear gluon radiation off a massless quark

In this section, we compute the $qg \rightarrow qg$ process with emission of one soft and collinear gluon with respect to the outgoing quark. At the tree level, for soft-collinear emission, we expect the leading term in the momentum expansion of the amplitude to be controlled by the *soft-collinear factor*. This section both reviews and improves the work done in [69] for the computation of one and two radiative gluon emission. We aim to compute the amplitude $|\bar{\mathcal{A}}(qg \rightarrow qg + ng)|^2$, where $n = 1, 2, 3$ represents the number of the radiative gluons. In addition to the soft-collinear approximation, we consider the case where we have a hard scattering, that is the direction of the outgoing quark is perpendicular to the direction of the primordial quark.

4.2.1 One radiative gluon emission

Let us now start by computing the momentum distribution of emitting a single radiative gluon. Label the momentum of the soft gluon to be s_1 , the remaining momenta are labeled in the same way as in Chapter 3 (see Fig. 4.2).

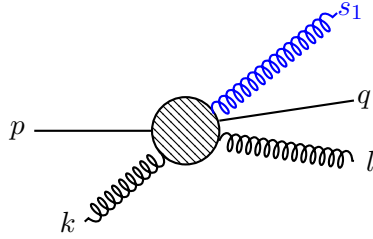


Figure 4.2: MHV diagrammatic representation of the single gluon emission in the $qgg\bar{q}$ -process. The soft radiative gluon s_1 ($s_1 \sim 0$) is assumed to be collinear to the high energetic quark which scatters with a single gluon.

According to the color-kinematic decomposition, the full amplitude for this process can be expressed as

$$\mathcal{A}_5(\{p_i, h_i, a_i\}) = g_s^3 \sum_{\mathcal{P}_3} (T^{a_k} T^{a_l} T^{a_1}) A_5(p, k, l, 1, q), \quad (4.2.13)$$

where the sum is performed over the permutation of the three gluons $k, l, 1$. It was shown in Chapter 3 that we do not have to worry about the helicities of p and q as soon as they have different helicities. That is to say, once fixed the amplitude for the whole process does not depend on the helicities of the pair of quark-antiquark. Let us first impose the

helicity of the first gluon to be negative, and the helicity of the soft and the second gluon to be positive $(h_k, h_l, h_1) = (-, +, +)$. With our choice of helicity, we can write down the expression of the MHV partial amplitude in Eq. (4.2.13),

$$\mathcal{A}_5(-, +, +) = g_s^3 \frac{\langle pk \rangle^3 \langle qk \rangle}{\langle qp \rangle} \sum_{\mathcal{P}_3(k,l,1)} \frac{(T^{a_k} T^{a_l} T^{a_1})}{\langle pk \rangle \langle kl \rangle \langle l1 \rangle \langle 1q \rangle}. \quad (4.2.14)$$

From this expression, we can factorize out the expression of the partial amplitudes of the what we call the parent process, $qg\bar{q}$. In that case, we can break up the sum over the permutation \mathcal{P}_3 into a sum over the permutation \mathcal{P}_2 which gives us the following result:

$$\mathcal{A}_5(-, +, +) = g_s^3 \sum_{\mathcal{P}_2(k,l)} \left(\frac{T^{a_1} T^{a_k} T^{a_l} \langle pk \rangle}{\langle p1 \rangle \langle 1k \rangle} + \frac{T^{a_k} T^{a_1} T^{a_l} \langle kl \rangle}{\langle k1 \rangle \langle 1l \rangle} + \frac{T^{a_k} T^{a_l} T^{a_1} \langle lq \rangle}{\langle l1 \rangle \langle 1q \rangle} \right) A_4(k, l), \quad (4.2.15)$$

where the partial amplitudes A_4 are given by the following expressions

$$A(k, l) = \frac{\langle pk \rangle^3 \langle qk \rangle}{\langle pk \rangle \langle kl \rangle \langle lq \rangle \langle qp \rangle} \quad \text{and} \quad A(l, k) = \frac{\langle pk \rangle^3 \langle qk \rangle}{\langle pl \rangle \langle lk \rangle \langle kq \rangle \langle qp \rangle} \quad (4.2.16)$$

In order to completely recover the full expression of the parent process, we have to deal with the color factors. Notice that product of generator matrices can always be written in terms of commutators. The idea is to regroup the color terms for the parent amplitude in such a way that we can factorize them out of the color term of the radiative process. Thus, using the decomposition shown in Appendix C.3 we have

$$\begin{aligned} \mathcal{A}_5(-, +, +) &= g_s^3 \sum_{\mathcal{P}_2(k,l)} T^{a_k} T^{a_l} T^{a_1} \left(\frac{\langle pk \rangle}{\langle p1 \rangle \langle 1k \rangle} + \frac{\langle kl \rangle}{\langle k1 \rangle \langle 1l \rangle} + \frac{\langle lq \rangle}{\langle l1 \rangle \langle 1q \rangle} \right) A_4(k, l) \\ &+ g_s^3 \sum_{\mathcal{P}_2(k,l)} \left([T^{a_1}, T^{a_k} T^{a_l}] \frac{\langle pk \rangle}{\langle p1 \rangle \langle 1k \rangle} + T^{a_k} [T^{a_1}, T^{a_l}] \frac{\langle kl \rangle}{\langle k1 \rangle \langle 1l \rangle} \right) A_4(k, l). \end{aligned} \quad (4.2.17)$$

The first term in this expression is what we call $\mathcal{A}_5(\text{parent})$ since it can be explicitly written as a function of the full amplitude \mathcal{A}_4 of the parent amplitude. Indeed, the sum over the permutation \mathcal{P}_2 is independent of the momentum of the radiative gluon s_1 , thus we can extract T^{a_1} from the summation, and thanks to the Schouten identity (Appendix B.3.10) the expression of the kinematics simplifies as,

$$\frac{\langle pk \rangle}{\langle p1 \rangle \langle 1k \rangle} + \frac{\langle kl \rangle}{\langle k1 \rangle \langle 1l \rangle} + \frac{\langle lq \rangle}{\langle l1 \rangle \langle 1q \rangle} = \frac{\langle pq \rangle}{\langle p1 \rangle \langle 1q \rangle}. \quad (4.2.18)$$

This expression is interesting in two ways, (i) it is invariant under scaling of $\langle p| \rightarrow a\langle p|$ and $|q\rangle \rightarrow b|q\rangle$, (ii) it does not depends explicitly on the momentum of the two hard

gluons k and l . Thus, after rearranging the terms and doing some simplifications, the MHV amplitude expressed in Eq. (4.2.17) simplifies as

$$\begin{aligned} \mathcal{A}_5(-, +, +) &= g_s^3 \left(\sum_{\mathcal{P}_2(k,l)} T^{a_k} T^{a_l} A_4(k, l) \right) T^{a_1} \frac{\langle pq \rangle}{\langle p1 \rangle \langle 1q \rangle} + \\ &g_s^3 \sum_{\mathcal{P}_2(k,l)} \left([T^{a_1}, T^{a_k} T^{a_l}] \frac{\langle pk \rangle}{\langle p1 \rangle \langle 1k \rangle} + T^{a_k} [T^{a_1}, T^{a_l}] \frac{\langle kl \rangle}{\langle k1 \rangle \langle 1l \rangle} \right) A_4(k, l). \end{aligned} \quad (4.2.19)$$

Recall that we are here interested in the case where the soft gluon is assumed to be emitted with a very small angle with respect to the outgoing quark while the direction of the outgoing quark is considered to be perpendicular to the direction of the primordial quark (large scattering angle). These conditions imply that the spinor product $\langle 1q \rangle$ goes to zero. The leading contribution in Eq. (4.2.19) is therefore dominated by term $\mathcal{A}_5(\text{parent})$. As a result for our first MHV amplitude, the expression is given by the following

$$\mathcal{A}_5(-, +, +) \approx \mathcal{A}_4(-, +) \times \mathcal{J}_g^{(1)}(1), \quad (4.2.20)$$

where the *single emission current* $\mathcal{J}_g^{(1)}(1)$ is defined as

$$\mathcal{J}_g^{(1)}(1) = g_s \frac{T^{a_1} \langle pq \rangle}{\langle p1 \rangle \langle 1q \rangle}. \quad (4.2.21)$$

We can now compute the square of the amplitude in Eq. (4.2.20) and sum over the colors for our particular MHV helicity configuration. By multiplying the expression in Eq. (4.2.20) by its conjugate, taking the trace and using the cyclic property of the trace one can show that we get the following expression

$$\sum_{\text{col.}} |\mathcal{A}_5(-, +, +)|^2 \approx \text{Tr} \left(|\mathcal{J}_g^{(1)}(s_1)|^2 \times |\mathcal{A}_4(-, +)|^2 \right). \quad (4.2.22)$$

One can verify that while extracting the expression of the amplitude squared and summed over the colors for the parent process, the above expression leads to

$$\sum_{\text{col.}} |\mathcal{A}_5(-, +, +)|^2 \approx \frac{1}{C_A} \text{Tr} \left(|\mathcal{J}_g^{(1)}(s_1)|^2 \right) \times \sum_{\text{col.}} |\mathcal{A}_4(-, +)|^2. \quad (4.2.23)$$

In order to simplify the notation, let us write $|\bar{\mathcal{J}}_g^{(1)}(1)|^2 = \text{Tr} (|\mathcal{J}_1(1)|^2)$. Now, the computation of the soft-collinear current squared is straight forward,

$$|\bar{\mathcal{J}}_g^{(1)}(1)|^2 = g_s^2 \text{Tr} (T^{a_1} T^{a_1}) \left| \frac{\langle pq \rangle}{\langle p1 \rangle \langle 1q \rangle} \right|^2. \quad (4.2.24)$$

Translating the product of square and angle brackets into a dot product and evaluating the trace in terms of the Casimir operator, it follows that

$$\sum_{\text{col.}} |\mathcal{A}_5(-, +, +)|^2 \approx g_s^2 \frac{C_F}{2} \frac{(pq)}{(ps_1)(s_1q)} \sum_{\text{col.}} |\mathcal{A}_4(-, +)|^2. \quad (4.2.25)$$

In order to get the final expression of the momentum distribution, we have to sum the above expression of amplitude over all possible helicity configurations. Let us recall that from the properties of partial amplitudes, we have $\mathcal{A}_5(h_k, h_l, h_1) = \mathcal{A}_5^*(-h_k, -h_l, -h_1)$. This implies that $|\mathcal{A}_5(h_k, h_l, h_1)|^2 = |\mathcal{A}_5^*(-h_k, -h_l, -h_1)|^2$. With this property, it is straight forward to see that one has to compute three different MHV amplitudes associated, each associated with a particular helicity configuration. They are given by $\mathcal{A}_5(-, +, +)$, $\mathcal{A}_5(+, -, +)$ and $\mathcal{A}_5(+, +, -)$. Since we have already computed the case where $(h_k, h_l, h_1) = (-, +, +)$, we can straightforwardly derive the expression of the other MHV helicity configurations. Indeed, one can check that two of the MHV amplitudes are given by

$$\mathcal{A}_5(+, -, +) = g_s^3 \frac{\langle pl \rangle^3 \langle ql \rangle}{\langle qp \rangle} \sum_{\mathcal{P}_3} \frac{T^{a_k} T^{a_l} T^{a_1}}{\langle pk \rangle \langle kl \rangle \langle l1 \rangle \langle 1q \rangle}, \quad (4.2.26)$$

$$\mathcal{A}_5(+, +, -) = g_s^3 \frac{\langle p1 \rangle^3 \langle q1 \rangle}{\langle qp \rangle} \sum_{\mathcal{P}_3} \frac{T^{a_k} T^{a_l} T^{a_1}}{\langle pk \rangle \langle kl \rangle \langle l1 \rangle \langle 1q \rangle}. \quad (4.2.27)$$

The contribution from the case where the soft radiative gluon has the minus helicity is negligibly small due to the fact that both $\langle p1 \rangle \langle q1 \rangle$ go to zero in the soft and collinear approximation. We can therefore neglect $\mathcal{A}_5(+, +, -)$ and only consider the case where the helicity of the gluons k and l are different. Recall that flipping the helicity of the two gluons involved in the hard scattering is equivalent to swapping the two gluons, that is to say interchanging k and l . Furthermore, by taking the same approach as before it is straight forward to show that the amplitude squared, summed over the colors is given by

$$\sum_{\text{col.}} |\mathcal{A}_5(+, -, +)|^2 \approx g_s^2 \frac{C_F}{2} \frac{(pq)}{(ps_1)(s_1q)} \sum_{\text{col.}} |\mathcal{A}_4(+, -)|^2. \quad (4.2.28)$$

Therefore, the full amplitude squared–summed over the colors and all possible helicities–for the process with emission of single radiative gluon can be expressed as

$$|\bar{\mathcal{A}}_5(qg \rightarrow qg + 1g)|^2 \approx g_s^2 \frac{C_F}{2} \frac{(pq)}{(ps_1)(s_1q)} |\bar{\mathcal{A}}_4(qg \rightarrow qg)|^2. \quad (4.2.29)$$

With this result, one can write down the full expression of the single emission current $|\bar{\mathcal{J}}_g^{(1)}(1)|^2$ that is given by the following expression

$$|\bar{\mathcal{J}}_g^{(1)}(1)|^2 = g_s^2 \frac{C_F}{2} \frac{(pq)}{(ps_1)(s_1q)}. \quad (4.2.30)$$

From this expression, one can deduce the expression of the single gluon multiplicity distribution $dN_g^{(1)}(x) = |\bar{\mathcal{J}}_g^{(1)}(1)|^2 d^3 s_1 / (2\pi)^3 2\omega_1$ that a single radiated gluon is emitted with a very small angle with respect to the outgoing quark. One can check that the expression of the multiplicity distribution exhibits two divergences: (i) *soft divergence* when $s_1 \rightarrow 0$, (ii) *collinear divergence* when the scalar product (s_1q) goes to zero.

4.2.2 Two radiative gluon emission

In the previous section, we computed the probability distribution that the soft radiative gluon can be emitted from a highly energetic quark with an eikonal trajectory. We found that at the leading approximation, the distribution tends to follow the Poisson distribution. In this section, we compute the case where we have two emission of soft radiative gluons. We now have to divide our calculation into two main parts. First, we compute the contribution from the MHV helicity configuration and then compute the case where we have an NMHV amplitudes. We show that in the soft-collinear limit, the contribution from the NMHV amplitudes are small and therefore can be neglected.

Let us now label the momentum of the second radiative gluon to be s_2 as represented in Fig. 4.3. From the color kinematic decomposition, the general expression for the process with emission of two soft radiative gluons is given by

$$\mathcal{A}_6(\{p_i, h_i, a_i\}) = g_s^4 \sum_{\mathcal{P}_4} (T^{a_k} T^{a_l} T^{a_1} T^{a_2}) A_6(p, k, l, 1, 2, q), \quad (4.2.31)$$

In Eq. (4.2.31), the summation is performed over the permutation of the four gluons. This means that the expansion of Eq. (4.2.31) will give rise to $4! = 24$ terms. A generic helicity configuration is denoted by (h_k, h_l, h_1, h_2) where again we do not have into account the helicity of the quark and the antiquark.

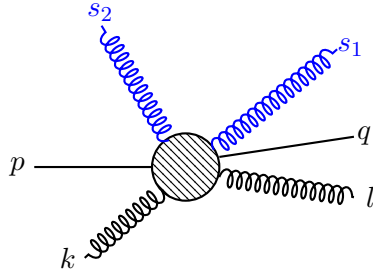


Figure 4.3: MHV diagrammatic representation of the two gluon emission in the $qgg\bar{q}$ -process. The soft radiative gluons s_1 and s_2 ($s_1, s_2 \sim 0$) are assumed to be collinear to the high energetic quark which undergoes a single scattering.

MHV amplitudes

Let us first consider the following configuration of helicity, $\mathcal{H}_1 = (-, +, +, +)$. All the gluons have positive helicities except the gluon with momentum k . We argued in the computation of the single gluon emission that all other configuration of helicities lead to a

vanishing amplitudes except for $\mathcal{H}_2 = (+, -, +, +)$. This is due to the fact that the spinor products $\langle 1q \rangle$ and $\langle 2q \rangle$ tend to zero in the collinear limit. For the helicity \mathcal{H}_1 , the MHV amplitude is given by the following expression

$$\mathcal{A}_6(\mathcal{H}_1) = g_s^4 \frac{\langle pk \rangle^3 \langle qk \rangle}{\langle qp \rangle} \sum_{\mathcal{P}_4} \frac{(T^{a_k} T^{a_l} T^{a_1} T^{a_2})}{\langle pk \rangle \langle kl \rangle \langle l1 \rangle \langle 12 \rangle \langle 2q \rangle}. \quad (4.2.32)$$

Similarly to the calculation of the single gluon emission, we can factorize out the partial amplitudes for the parent process. This allows us to break the summation over the permutation $\mathcal{P}_4(k, l, 1, 2)$ into two summations over the permutation $\mathcal{P}_2(k, l)$ and $\mathcal{P}'_2(1, 2)$. This can be expressed mathematically as

$$\begin{aligned} \mathcal{A}_6(\mathcal{H}_1) = g_s^4 \sum_{\mathcal{P}_2} \sum_{\mathcal{P}'_2} & \left(\frac{(T^{a_k} T^{a_l} T^{a_1} T^{a_2}) \langle l2 \rangle \langle kq \rangle}{\langle l1 \rangle \langle 12 \rangle \langle k2 \rangle \langle 2q \rangle} + \frac{(T^{a_k} T^{a_l} T^{a_1} T^{a_2}) \langle kl \rangle \langle lq \rangle}{\langle k1 \rangle \langle 1l \rangle \langle l2 \rangle \langle 2q \rangle} \right. \\ & + \frac{(T^{a_1} T^{a_k} T^{a_l} T^{a_2}) \langle pk \rangle \langle lq \rangle}{\langle p1 \rangle \langle 1k \rangle \langle l2 \rangle \langle 2q \rangle} + \frac{(T^{a_1} T^{a_2} T^{a_k} T^{a_l}) \langle pk \rangle \langle 1k \rangle}{\langle p1 \rangle \langle 1k \rangle \langle 12 \rangle \langle 2q \rangle} \\ & \left. + \frac{(T^{a_1} T^{a_k} T^{a_2} T^{a_l}) \langle pk \rangle \langle kl \rangle}{\langle p1 \rangle \langle 1k \rangle \langle k2 \rangle \langle 2l \rangle} + \frac{(T^{a_k} T^{a_l} T^{a_2} T^{a_1}) \langle k2 \rangle \langle kl \rangle}{\langle k1 \rangle \langle 12 \rangle \langle k2 \rangle \langle 2l \rangle} \right) A_4(k, l). \quad (4.2.33) \end{aligned}$$

By decomposing the color factors as shown in the Appendix C.3, we can decompose the amplitude above as $\mathcal{A}_6(\mathcal{H}_1) = \mathcal{A}_6(\text{parent}) + \mathcal{A}_6(\text{extra})$. The amplitude $\mathcal{A}_6(\text{parent})$ has a well ordered color factor and depends explicitly on the amplitude of the parent process that contains the information about the hard scattering. On the other hand, the amplitude $\mathcal{A}_6(\text{extra})$ contains all the extra-terms coming from the re-ordering of the colors. The full expression of $\mathcal{A}_6(\text{extra})$ is shown in the Appendix C. Using the soft and collinear approximation, we can show that $\mathcal{A}_6(\text{extra})$ is small compared to $\mathcal{A}_6(\text{parent})$ and therefore can be neglected. The details of such calculation is shown in Appendix D.1. Thus, the expression of the amplitude $\mathcal{A}_6(\mathcal{H}_1)$ is approximatively equivalent to the amplitude $\mathcal{A}_6(\text{parent})$ as follows

$$\mathcal{A}_6(\mathcal{H}_1) \approx g_s^4 \sum_{\mathcal{P}_2} \sum_{\mathcal{P}'_2} (T^{a_k} T^{a_l} T^{a_1} T^{a_2}) J(k, l, 1, 2) A_4(k, l). \quad (4.2.34)$$

Here, $J(k, l, 1, 2)$ can be thought as a partial current that contains the information about the kinematics of the soft scattering. The partial current $J(k, l, 1, 2)$ can be simplified using the Schouten identity. The full calculation is shown in Appendix D.1. The result turns out to be an expression independent of the momentum of the two gluons involved in the hard scattering. Thus, we can nicely write down the expression of the full amplitude

for our MHV helicity configuration as

$$\mathcal{A}_6(\mathcal{H}_1) \approx g_s^4 \left(\sum_{\mathcal{P}_2} (T^{a_k} T^{a_l}) A_4(k, l) \right) \left(\sum_{\mathcal{P}'_2} (T^{a_1} T^{a_2}) \frac{\langle pq \rangle}{\langle p1 \rangle \langle 12 \rangle \langle 2q \rangle} \right). \quad (4.2.35)$$

By separating the soft from the hard scattering, we can introduce the two gluon emission current denoted $\mathcal{J}_g^{(2)}(1, 2)$. Thus, for the two possible MHV helicity configurations we get the following expressions

$$\mathcal{A}_6(\mathcal{H}_1) \approx \mathcal{A}_4(-, +) \times \mathcal{J}_g^{(2)}(1, 2), \quad (4.2.36)$$

$$\mathcal{A}_6(\mathcal{H}_2) \approx \mathcal{A}_4(+, -) \times \mathcal{J}_g^{(2)}(1, 2). \quad (4.2.37)$$

Similarly to the calculation of the single gluon emission, squaring the above amplitudes, summing over the possible MHV configurations and taking the trace leads to the following expression

$$\sum_{\text{MHV}} |\mathcal{A}_6(\mathcal{H}_{1/2})|^2 \approx \frac{1}{C_A} |\bar{\mathcal{J}}_g^{(2)}(1, 2)|^2 \sum_{\text{MHV}} |\mathcal{A}_4(\mp, \pm)|^2. \quad (4.2.38)$$

Computing directly $|\bar{\mathcal{J}}_g^{(2)}(1, 2)|^2$ will be extremely complicated because of the color dependence. Indeed, while taking the square of the current the color components will be mixed. We can bypass such computation by computing the current square in the basis of the colors. We could then write $|\bar{\mathcal{J}}_g^{(2)}(1, 2)|^2$ as follows

$$|\bar{\mathcal{J}}_g^{(2)}(1, 2)|^2 = g_s^4 C_s(1, 2) K_s(1, 2) + g_s^4 C_a(1, 2) K_a(1, 2), \quad (4.2.39)$$

where the different color configurations are given by $C_s(1, 2)$ and $C_a(1, 2)$ (see Eq. 4.2.40, 4.2.41). Once evaluated, we can write the result in terms of the Casimir operators C_A, C_F (refer to Appendix C.2). On the other hand, the information about the kinematics are carried by $K_s(1, 2)$ and $K_a(1, 2)$ (see Eq. 4.2.42, 4.2.43).

$$C_s(1, 2) = \text{Tr}(T^{a_1} T^{a_2} T^{a_2} T^{a_1}) = C_A C_F^2, \quad (4.2.40)$$

$$C_a(1, 2) = \text{Tr}(T^{a_1} T^{a_2} T^{a_1} T^{a_2}) = C_A C_F^2 - \frac{1}{2} C_A^2 C_F, \quad (4.2.41)$$

$$K_s(1, 2) = \sum_{\mathcal{P}'_2} \frac{\langle pq \rangle}{\langle p1 \rangle \langle 12 \rangle \langle 2q \rangle} \frac{[pq]}{[p1][12][2q]}, \quad (4.2.42)$$

$$K_a(1, 2) = \sum_{\mathcal{P}'_2} \frac{\langle pq \rangle}{\langle p1 \rangle \langle 12 \rangle \langle 2q \rangle} \frac{[pq]}{[p2][21][1q]}. \quad (4.2.43)$$

We can simplify further the expression of the current squared using the expression of the color factors. So, we have

$$|\bar{\mathcal{J}}_g^{(2)}(1, 2)|^2 = g_s^4 C_A C_F^2 (K_s(1, 2) + K_a(1, 2)) - \frac{g_s^4}{2} C_A^2 C_F K_a(1, 2). \quad (4.2.44)$$

We can now straightforwardly compute the kinematic terms. One can in particular notice that the color stripped kinematic in the first term contains all the set of permutation similar to the QED case of two Bremsstrahlung photons emission. Let us call this term J_{QED} and is evaluated as,

$$J_{\text{QED}}(1, 2) = \left(\sum_{\mathcal{P}'_2} \frac{\langle pq \rangle}{\langle p1 \rangle \langle 12 \rangle \langle 2q \rangle} \right) \left(\sum_{\mathcal{P}'_2} \frac{[pq]}{[p1][12][2q]} \right) \quad (4.2.45)$$

$$= \left(\prod_{i=1}^2 \frac{\langle pq \rangle}{\langle pi \rangle \langle iq \rangle} \right) \left(\prod_{i=1}^2 \frac{[pq]}{[pi][iq]} \right) \quad (4.2.46)$$

$$= \frac{1}{2^2} \prod_{i=1}^2 \frac{(pq)}{(ps_i)(s_iq)}. \quad (4.2.47)$$

This result looks exactly similar to the emission current squared for the case of two Bremsstrahlung photon emission in QED (see Section 4.1). As a difference, the fact that gluons carry color charges appears in the color factor. However, because of the non-Abelian nature of the strong force we have an extra term which also contributes to the expression of the total emission current squared. In Eq. (4.2.44), this information is contained in $J_{\text{NA}} = K_a$, where NA stands for Non-Abelian.

$$J_{\text{NA}}(1, 2) = -\frac{(pq)}{(s_1 s_2)} \left(\frac{1}{\langle p1 \rangle \langle 2q \rangle [p2][1q]} + \frac{1}{\langle p2 \rangle \langle 1q \rangle [p1][2q]} \right) \quad (4.2.48)$$

$$= -\frac{(pq)}{(s_1 s_2)} \left(\frac{1}{\langle p1q2p \rangle} + \frac{1}{\langle p2q1p \rangle} \right) \quad (4.2.49)$$

$$= -\frac{(pq)}{(s_1 s_2)} \frac{\text{Tr}(\not{p}\not{s}_1\not{q}\not{s}_2)}{2^4 \prod_i (ps_i)(s_iq)}. \quad (4.2.50)$$

From the first to the second line, we just used the shorthand notation introduced in Section 2.1.3 to re-write the terms in the denominators. From the second to the third line, we evaluated the spinor quantities by performing Dirac traces. Notice that the denominator in Eq. (4.2.50) is a direct consequence of the fact that $\langle p1q2p \rangle$ and $\langle p2q1p \rangle$ are complex conjugate of each other.

Combining all these results, summing over all possible MHV helicity configurations, the amplitude in Eq. (4.2.38) finally becomes

$$|\overline{\mathcal{J}}_g(1, 2)|^2 = g_s^4 \left[\frac{C_F^2}{2^2} \prod_{i=1}^2 \frac{(pq)}{(ps_i)(s_iq)} + \frac{C_A C_F}{2} \frac{(pq)}{(s_1 s_2)} \frac{\text{Tr}(\not{p}\not{s}_1\not{q}\not{s}_2)}{2^4 \prod_i (ps_i)(s_iq)} \right]. \quad (4.2.51)$$

In order to do the summation over all the possible helicity configurations, we are required to compute the N^HMV amplitudes for the case of two gluon emission. However, we will show that the contribution from the N^MHV amplitudes are too small and therefore the radiative process is dominated by the MHV amplitudes.

NMHV amplitudes

The summation over the helicities for the case of two gluon emission requires the computation of the N^k MHV amplitudes at the first order ($k = 1$). In particular, in the case where we have to worry about the helicities of the 4 gluons, two of the gluons have to have a negative helicity in order to form an NMHV amplitude. As we have seen in the previous computation, flipping the helicity of two gluons is equivalent to flipping the labels. For instance, going from $(-, -, +, +)$ to $(-, +, -, +)$ we swap k and l in the expression of scattering amplitude. As a result, we are only required to compute one configuration of helicity for the NMHV amplitude. That is said, let us show that the contribution from the NMHV amplitude can be neglected as it was previously claimed.

Let us first choose the following configuration of helicity $\mathcal{H}_3 = (-, -, +, +)$. At this point, we have only seen to compute MHV amplitudes. Thanks to the BCFW on-shell recursion relation, we can reduce the computation of NMHV amplitudes into the computation of two MHV-amplitudes. In the BCFW on-shell recursion formalism, the shifted momentum can be chosen arbitrarily. However, with a good choice of helicity and shift we can reduce enormously the number of diagrams that we have to compute. One can notice that choosing the momentum l and s_1 to be the reference line, only two diagrams contribute to the expression of the NMHV amplitude. The equation for the $[l, 1]$ -shift can be written as follows,

$$|l\rangle \longrightarrow |\hat{l}\rangle = |l\rangle + z|1\rangle, \quad |1\rangle \longrightarrow |\hat{1}\rangle = |1\rangle - z|l\rangle. \quad (4.2.52)$$

Recall that in the $[l, 1]$ -shift, the spinors $|l\rangle$ and $|1\rangle$ remain unchanged.

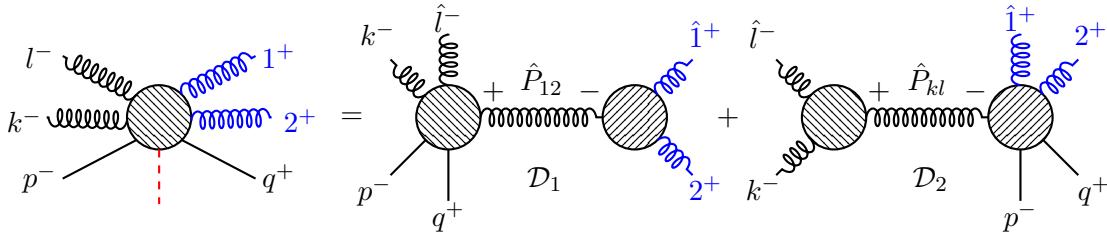


Figure 4.4: BCFW diagrammatic representation of the NMHV amplitude for the two gluon emission. The helicity is chosen to be $(-, -, +, +)$ with the $[l, 1]$ -shift. Notice that the two internal lines \hat{P}_{kl} and \hat{P}_{12} are both on-shell. The two diagrams \mathcal{D}_1 and \mathcal{D}_2 are related by symmetry.

Let us first focus on the first diagram \mathcal{D}_1 in the Fig. 4.4. One can notice that both the

two subdiagrams are $\overline{\text{MHV}}$. By taking into account the contribution from the internal line \hat{P}_{12} , we can therefore write down the expression of the amplitude for the first diagram

$$\mathcal{D}_1 = \frac{[p\hat{P}_{12}][q\hat{P}_{12}]^3}{[pk][k\hat{l}][\hat{l}\hat{P}_{12}][\hat{P}_{12}q][qp]} \frac{1}{\langle 12 \rangle [12]} \frac{[\hat{1}2]^4}{[\hat{P}_{12}\hat{1}][\hat{1}2][2\hat{P}_{12}]}. \quad (4.2.53)$$

As we can see, the amplitude shown above still depends on the shifted momenta. In order to get a physical scattering amplitude, we have to get rid of these shifted momenta. Fortunately, the shifted momenta in Eq. (4.2.53) are only in terms of the square brackets. By taking into account the momentum conservation and using the shift equation in Eq. (4.2.52) we can easily get rid of $|\hat{P}_{12}\rangle$ and $|\hat{1}\rangle$ (as shown in the Eq. (4.2.54)). The detailed calculations are shown in Appendix D.1.

$$|\hat{P}_{12}\rangle = \frac{\langle l1 \rangle}{\langle l2 \rangle} |1\rangle + |2\rangle, \quad |\hat{l}\rangle = |l\rangle + \frac{\langle 12 \rangle}{\langle l2 \rangle} |2\rangle. \quad (4.2.54)$$

With these two equations, we can now get rid of the shifted momenta in Eq. (4.2.53). After rearranging terms and doing some fair amount of simplifications, we get the final expression of the first diagram that contributes to the total NMHV amplitudes

$$\mathcal{D}_1 = \frac{1}{s_{l12}} \frac{\langle l|1+2|p\rangle\langle l|1+2|q\rangle^2}{\langle l1 \rangle \langle 12 \rangle [qp][pk]\langle 2l+1|k\rangle}, \quad (4.2.55)$$

where $s_{l12} = \langle l1 \rangle [l1] + \langle 12 \rangle [12] + \langle 2l \rangle [2l]$. In order to evaluate the contribution from the second diagram \mathcal{D}_2 , we do not have to do the whole computation. In fact, the two diagrams \mathcal{D}_1 and \mathcal{D}_2 are related by symmetry with all the helicities flipped. In particular, we can notice that in contrast to the diagram \mathcal{D}_1 , \mathcal{D}_2 is composed of two MHV subdiagrams. Thus, in order to get the right expression for \mathcal{D}_2 , we swap $k \leftrightarrow 2$, $l \leftrightarrow 1$ and $p \leftrightarrow q$ in the expression of \mathcal{D}_1 . In addition, due to the flip of helicities, all the square brackets become angle brackets and vice versa. Thus, the complete NMHV amplitude is expressed as

$$A_6(\mathcal{H}_3) = \frac{1}{s_{l12}} \frac{\langle l|1+2|p\rangle\langle l|1+2|q\rangle^2}{\langle l1 \rangle \langle 12 \rangle [qp][pk]\langle 2l+1|k\rangle} + \frac{1}{s_{kl1}} \frac{[1|l+k|q][l|l+k|p]^2}{[1l][lk]\langle pq \rangle \langle q2 \rangle [k|1+l|2]}. \quad (4.2.56)$$

The above expression looks rather messy. However, one can use the little group scaling to check that Eq. (4.2.56) is indeed consistent. Recall that scaling an external leg labeled by i with helicity h_i will give rise to a weight t^{-2h_i} . One can for instance choose to scale the gluon l with helicity (-1) . With a fair amount of algebra, one can show that we indeed end up with a factor of t^2 . Notice that the terms s_{ijk} are invariant under scaling of i, j and k . Let us now consider the limit where the radiative gluons are collinear to the outgoing quark. If we represent by x the spinor products $\langle 12 \rangle, \langle 1q \rangle, \langle 2q \rangle, [12], [1q]$ and $[2q]$, thus, we see that the A_6^{MHV} amplitudes are of order of $\sim 1/x^2$ while the A_6^{NMHV} are of the order

of $\sim 1/x$. In the limit where $x \rightarrow 0$, the NLMV amplitudes are small compared to the MHV ones and therefore can be neglected. This tells us that in the soft-collinear limit, the radiative process is dominated by the MHV amplitudes.

The final expression of the emission current for the case of two gluon emission is then given by Eq.(4.2.51). We can now write down the expression of the momentum distribution for emitting two radiative gluons. Notice that we can factorize out the Poisson term in Eq. (4.2.51), so that the momentum distribution now writes as

$$dN_g^{(2)} = \frac{1}{2!} \left(1 + \frac{C_A}{C_F} \frac{\text{Tr}(p_1^\not{x} q_2^\not{x})}{4(pq)(s_1 s_2)} \right) \prod_{i=1,2} dN_g^{(1)}(i). \quad (4.2.57)$$

This expression shows that the emission of multiple radiative gluons (in the present case $n = 2$ radiative gluons) cannot be taken to be independent. In fact, a gluon can emerge from a gluon line as cartooned in Fig. 4.5. Requiring the gauge field of QCD to commute is equivalent to take the limit where the Casimir factor C_A tends to zero. Therefore, when taking the limit $C_A \rightarrow 0$ we should recover the QED result. Intuitively, this limit makes sense because (i) C_A is the Casimir factor in the adjoint representation of $SU(N)$ and since the theory of QED does not have an adjoint representation it is then natural to take $C_A = 0$ (ii) in the standard computation of quark-gluon amplitudes, the factor C_A appears when a gluon is emitted from another gluon line. As we can notice, if we take the limit C_A tends to zero in Eq. (4.2.51) the correction term from non-Abelian behavior vanishes and only remains the term which has been resummed in QED.

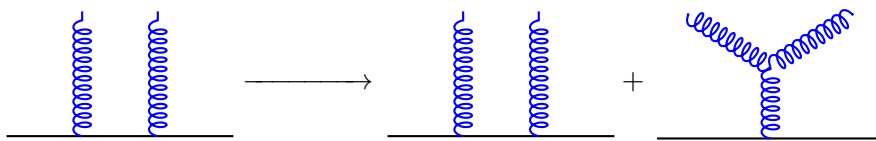


Figure 4.5: Independent emission of the two radiative gluons versus the case where the two radiative gluons can interact.

4.2.3 Three radiative gluon emission

The previous section showed that the non-Abelian nature of QCD affects the way two radiative gluons are emitted from a quark line. The evaluation of the momentum distribution for higher number of Bremsstrahlung gluons is important not only for the understanding of the radiative energy loss formalism in QGP but also for the study of the many body

problems in QCD. In this section, we aim to compute the probability distribution for emitting three radiative gluons (see Fig. 4.6). The amplitude for the process is given by the following expression

$$\mathcal{A}_7(\{p_i, h_i, a_i\}) = g_s^5 \sum_{\mathcal{P}_5} (T^{a_k} T^{a_l} T^{a_1} T^{a_2} T^{a_3}) A_7(p, k, l, 1, 2, 3, q). \quad (4.2.58)$$

By taking a similar approach as in Section 4.2.2, we compute separately the MHV and the N^k MHV ($k = 1, 2$) amplitudes. Again, using the BCFW on-shell recursion relations to compute the N^k MHV amplitudes, we show that the N^k MHV amplitudes are dominated by the MHV ones and therefore can be neglected.

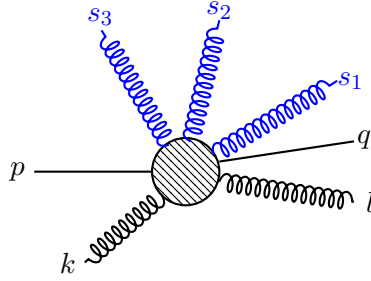


Figure 4.6: MHV diagrammatic representation of the three gluon emission in the $qgg\bar{q}$ -process. The soft radiative gluons s_1 , s_2 and s_3 ($s_1, s_2, s_3 \sim 0$) are assumed to be collinear to the high energetic quark passing through the QGP medium.

MHV amplitudes

For the MHV calculation, let us consider the case where all the gluons have positive helicities except the gluon labeled by k and let us denote such configuration by \mathcal{H}_4 . With this choice of helicity, the correspondent MHV amplitude is given by

$$\mathcal{A}_7(\mathcal{H}_4) = g_s^5 \frac{\langle pk \rangle^3 \langle qk \rangle}{\langle qp \rangle} \sum_{\mathcal{P}_5} \frac{(T^{a_k} T^{a_l} T^{a_1} T^{a_2} T^{a_3})}{\langle pk \rangle \langle kl \rangle \langle l1 \rangle \langle 12 \rangle \langle 23 \rangle \langle 3q \rangle}, \quad (4.2.59)$$

where the summation is performed over the permutation of the five gluons. One can notice that the expansion of this summation will give rise to 120 terms. Expanding directly this summation and taking the square of the given result will be a complete mess. As it was shown in the previous calculation (for $n = 1, 2$), one can always express all partial amplitudes in Eq. (4.2.59) in terms of the partial amplitudes of the parent process $A_4(k, l)$ and $A_4(l, k)$. In addition, one can always rearrange the color terms in such a way that we can factorize out the color terms of the hard gluons. As a result, we can write the

amplitude for \mathcal{H}_4 as $\mathcal{A}_7(\mathcal{H}_4) = \mathcal{A}_7(\text{parent}) + \mathcal{A}_7(\text{extra})$. In the collinear limit region we are interested in, $\mathcal{A}_7(\text{parent})$ dominates over $\mathcal{A}_7(\text{extra})$, thus the amplitude now becomes

$$\mathcal{A}_7(\mathcal{H}_4) \approx \mathcal{A}_4(-, +) \times \mathcal{J}_g^{(3)}(1, 2, 3), \quad (4.2.60)$$

where the three gluon current is given by Eq. (4.2.61). The details about these calculations can be found in the Appendix D.2. The emission current is given by

$$\mathcal{J}_g^{(3)}(1, 2, 3) = g_s^3 \langle pq \rangle \sum_{\mathcal{P}'_3} \frac{(T^{a_1} T^{a_2} T^{a_3})}{\langle p1 \rangle \langle 12 \rangle \langle 23 \rangle \langle 3q \rangle}. \quad (4.2.61)$$

The main task is now to compute the square of this expression and trace over the colors. As it was proved during the calculation of the emission current for the two gluon case, the computations become much easier when using the color factors as a basis. In addition, in order to simplify the notation let us denote $Tr(T^i \dots T^m) = Tr(i \dots m)$. Thus, we get

$$|\bar{\mathcal{J}}_g^{(3)}(1, 2, 3)|^2 = \mathcal{C}_s(1, 2, 3)K_s(1, 2, 3) + \mathcal{C}_a(1, 2, 3)K_a(1, 2, 3) + \mathcal{C}_1(1, 2, 3)K_1(1, 2, 3) + \\ \mathcal{C}_2(1, 2, 3)K_2(1, 2, 3) + \mathcal{C}_3(1, 2, 3)K_3(1, 2, 3) + \mathcal{C}_4(1, 2, 3)K_4(1, 2, 3). \quad (4.2.62)$$

In the above expression, \mathcal{C}_* is a function that contains the color factors of the radiative gluons while K_* contains the information on the kinematics. We shall emphasize that each K_* in Eq. (4.2.62) has 6 terms due to the sum over the permutation \mathcal{P}'_2 . Thus, the emission current $|\bar{\mathcal{J}}_g^{(3)}(1, 2, 3)|^2$ has in total 36 terms. The color factors in Eq. (4.2.62) are given by the following traces

$$\mathcal{C}_s(1, 2, 3) = Tr(123321), \quad \mathcal{C}_a(1, 2, 3) = Tr(123123), \quad \mathcal{C}_1(1, 2, 3) = Tr(123231), \\ \mathcal{C}_2(1, 2, 3) = Tr(123312), \quad \mathcal{C}_3(1, 2, 3) = Tr(123213), \quad \mathcal{C}_4(1, 2, 3) = Tr(123132),$$

which after evaluation gives the following result

$$\mathcal{C}_s(1, 2, 3) = C_A C_F^3, \quad \mathcal{C}_a(1, 2, 3) = C_A C_F^3 + 2C_A^3 C_F - 3C_A^2 C_F^2, \quad (4.2.63)$$

$$\mathcal{C}_{1/2}(1, 2, 3) = C_A C_F^3 - C_A^2 C_F^2, \quad \mathcal{C}_{3/4}(1, 2, 3) = C_A C_F^3 + C_A^3 C_F - 2C_A^2 C_F^2. \quad (4.2.64)$$

Notice that all the color factors contain the expression $C_A C_F^3$ and by combining the associated kinematic terms we recover the QED term for the emission of three radiative gluons. Therefore, the expression of the emission current squared in Eq. (4.2.62) simplifies as

$$|\bar{\mathcal{J}}_g^{(3)}(1, 2, 3)|^2 = C_A C_F^3 J_{\text{QED}}^{(3)}(1, 2, 3) + (2C_A^3 C_F - 3C_A^2 C_F^2) K_a(1, 2, 3) \\ - C_A^2 C_F^2 \sum_{i=\{1,2\}} K_i(1, 2, 3) + (C_A^3 C_F - C_A^2 C_F^2) \sum_{i=\{3,4\}} K_i(1, 2, 3). \quad (4.2.65)$$

We are now left with the computation of the expression of kinematics in Eq. (4.2.65). Let us first start by computing the kinematic with an asymmetric configuration,

$$K_a(1, 2, 3) = \sum_{\mathcal{P}'_3} \frac{\langle pq \rangle}{\langle p1 \rangle \langle 12 \rangle \langle 23 \rangle \langle 3q \rangle} \frac{[pq]}{[p3][32][21][1q]}, \quad (4.2.66)$$

$$= \frac{(pq)}{2} \sum_{\mathcal{P}'_3} \frac{1}{(s_1 s_2)(s_2 s_3)} \frac{1}{\langle p1q3p \rangle}. \quad (4.2.67)$$

From the first to the second line, we used the Lorentz invariant product and the shorthand notation to represent the product of angle and square spinors. Notice that the factor $1/((s_1 s_2)(s_2 s_3))$ is invariant under interchange of 1 and 3. On the other hand, we know that $\langle p1q3p \rangle^*$ and $\langle p3q1p \rangle$ are complex conjugate of each other. Thus, we can write K_s entirely in terms of traces and scalar products

$$K_a(1, 2, 3) = \frac{(pq)}{4} \sum_{\mathcal{P}'_3} \frac{1}{(s_1 s_2)(s_2 s_3)} \frac{Tr(\not{p}\not{s}_1\not{q}\not{s}_3)}{2^4(p s_1)(s_1 q)(p s_3)(s_3 q)}. \quad (4.2.68)$$

While looking at this expression we can see that we have an extra factor of $1/2$, this is because swapping i and j in $Tr(\not{p}\not{s}_i\not{q}\not{s}_j)$ will give the same result.

Let us now move to the computation of $K_1(1, 2, 3) + K_2(1, 2, 3)$,

$$\sum_{i=\{1,2\}} K_i(1, 2, 3) = \sum_{\mathcal{P}'_3} \frac{\langle pq \rangle}{\langle p1 \rangle \langle 12 \rangle \langle 23 \rangle \langle 3q \rangle} \frac{[pq]}{[p1][13][32][2q]} + \quad (4.2.69)$$

$$\sum_{\mathcal{P}'_3} \frac{\langle pq \rangle}{\langle p1 \rangle \langle 12 \rangle \langle 23 \rangle \langle 3q \rangle} \frac{[pq]}{[p2][21][13][3q]}. \quad (4.2.70)$$

By rewriting the expression in terms of the Lorentz invariant products and using our shorthand notation, we can show that this expression can be written as

$$\sum_{i=\{1,2\}} K_i(1, 2, 3) = -\frac{(pq)}{2} \sum_{\mathcal{P}_2} \sum_{\mathcal{P}'_3} \frac{1}{(p s_1)(s_2 s_3)} \frac{1}{\langle q213q \rangle}. \quad (4.2.71)$$

Applying the same argument as above and by noticing that $(s_2 s_3)$ is invariant under interchange of 2 and 3, and that $\langle r213r \rangle^* = \langle r312r \rangle$, we get

$$\sum_{i=\{1,2\}} K_i(1, 2, 3) = -\frac{(pq)}{4} \sum_{\mathcal{P}_2} \sum_{\mathcal{P}'_3} \frac{1}{(p s_2)(s_2 s_3)} \frac{Tr(\not{q}\not{s}_2\not{p}_1\not{s}_3)}{2^4(q s_2)(s_2 s_1)(q s_3)(s_3 s_1)}. \quad (4.2.72)$$

Here, $\mathcal{P}_2(p, q)$ permutes the label p and q . We are now left with the computation of the last kinematic term in Eq. (4.2.44), which is given by the following expression

$$\sum_{i=\{3,4\}} K_i(1, 2, 3) = \sum_{\mathcal{P}'_3} \frac{\langle pq \rangle}{\langle p1 \rangle \langle 12 \rangle \langle 23 \rangle \langle 3q \rangle} \frac{[pq]}{[p3][31][12][2q]} + \quad (4.2.73)$$

$$\sum_{\mathcal{P}'_3} \frac{\langle pq \rangle}{\langle p1 \rangle \langle 12 \rangle \langle 23 \rangle \langle 3q \rangle} \frac{[pq]}{[p2][23][31][1q]}. \quad (4.2.74)$$

With some simplifications, one can straightforwardly show that the above expression can now be expressed as follows

$$\sum_{i=\{3,4\}} K_i(1, 2, 3) = (pq) \sum_{\mathcal{P}'_3} \frac{1}{(s_1 s_2)} \left(\frac{1}{\langle p3q231p \rangle} - \frac{1}{\langle p13q23p \rangle} \right). \quad (4.2.75)$$

The above expression is slightly different from any other expressions we have encountered. In order to simplify this relation, let us first write down the explicit form of $\langle p3q231p \rangle$ and the complex conjugate of $\langle p13q23p \rangle$.

$$\begin{aligned} \langle p3q231p \rangle &= \langle p3 \rangle [3q] \langle q2 \rangle [23] \langle 31 \rangle [1p], \\ \langle p13q23p \rangle^* &= [p1] \langle 13 \rangle [3q] \langle q2 \rangle [23] \langle 3p \rangle. \end{aligned} \quad (4.2.76)$$

From these expressions, we can conclude that $\langle p3q231p \rangle$ and $(-\langle p13q23p \rangle)$ are complex conjugate of each other. Thus, we get

$$\sum_{i=\{3,4\}} K_i(1, 2, 3) = (pq) \sum_{\mathcal{P}'_3} \frac{1}{(s_1 s_2)} \frac{\text{Tr}(\not{p}\not{s}_1\not{s}_3\not{q}\not{s}_2\not{s}_3)}{64(p s_1)(p s_3)(s_1 s_3)(s_2 s_3)(s_2 q)(s_3 q)}. \quad (4.2.77)$$

Recall that the term in the denominator comes from expanding $|\langle p3q231p \rangle|^2$. One can remark in this expression that the kinematic is function of a trace of six components, in contrast to the previous results. Combining all these results, we can write down the explicit expression of the three-emission current in Eq. (4.2.65) as

$$\begin{aligned} |\bar{\mathcal{J}}_g^{(3)}(1, 2, 3)|^2 &= \frac{\mathcal{C}_s}{2^3} \prod_{i=1}^3 \frac{(pq)}{(ps_i)(s_i q)} + \frac{\mathcal{C}_a}{4} \sum_{\mathcal{P}'_3} \frac{(pq)}{(s_1 s_2)(s_2 s_3)} \frac{\text{Tr}(\not{p}\not{s}_1\not{q}\not{s}_3)}{2^4(p s_1)(s_1 q)(p s_3)(s_3 q)} + \\ &\frac{\mathcal{C}_{1/2}}{4} \sum_{\mathcal{P}_2} \sum_{\mathcal{P}'_3} \frac{(pq)}{(ps_2)(s_2 s_3)} \frac{\text{Tr}(\not{q}\not{s}_2\not{s}_1\not{s}_3)}{2^4(q s_2)(s_2 s_1)(q s_3)(s_3 s_1)} + \frac{\mathcal{C}_{3/4}}{s} \sum_{\mathcal{P}'_3} \frac{\text{Tr}(\not{p}\not{s}_1\not{s}_3\not{q}\not{s}_2\not{s}_3)}{64(p s_1)(p_1 s_3)(s_2 q)(s_3 q)}. \end{aligned} \quad (4.2.78)$$

The permutation invariant quantity s is given by the product $(s_1 s_2)(s_1 s_3)(s_2 s_3)$. Recall that the above result represents the emission current squared for our particular MHV helicity configuration. In addition, for the case of the three-gluon emission we have to compute the N^k MHV amplitudes for $k=1,2$. In the next section, we compute the N^2 MHV amplitudes. We see that the NMHV and the N^2 MHV amplitudes are related by symmetry.

N^2 MHV amplitudes

This section aims to compute the N^2 MHV amplitudes for the case of three radiative gluon emission. In our particular process, N^2 MHV refers to the class of amplitudes with four

negative helicity particles (1 quark and 3 gluons), one positive helicity gluons and one positive helicity antiquark (see Fig. 4.7). Let us denote such configuration of helicity as $\mathcal{H}_5 = (-, -, -, +, +)$. Recall that in this notation, the helicity of the quark and the antiquark are not taken into account. For the specific case of a 7-point amplitude, the NMHV amplitudes are related to the N^2 MHV by interchange of labels. To see that, let us consider an NMHV amplitude with three negative helicity particles (say one quark and two gluons) and four positive helicity gluons (say one antiquark and three gluons). The latter is related to the above N^2 MHV amplitude with all the square brackets becoming angle brackets and interchange of gluons. That is to say, computing an NMHV amplitude is equivalent to computing an $N^2\overline{\text{MHV}}$ amplitude.

As illustrated in the previous sections, the most efficient way to compute amplitudes beyond MHV is to use the BCFW on-shell recursion relations. Indeed, the BCFW formalism allows us to construct amplitudes recursively from fewer number of extra-legs. This is very useful for the computation of the N^2 MHV amplitude since we have already computed both the MHV and the NMHV amplitudes for 6 external state particles.

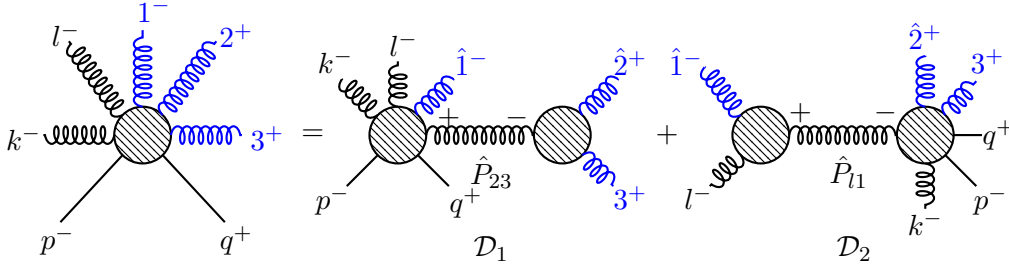


Figure 4.7: Diagrammatic representation of the BCFW recursion for the computation of N^2 MHV amplitude with $[1, 2]$ -shift. The two hard gluons and one soft gluon have negative helicity, where the remaining soft gluons have positive helicity.

Let us choose the gluons labeled by 1 and 2 to be our reference line. This is equivalent to consider a $[1, 2]$ -shift. Using the BCFW on-shell formalism, one can show that only two diagrams contribute to the full N^2 MHV amplitude as shown in Fig. 4.7. The shift equations are shown in Eq. (4.2.79). Recall that these are the only shift transformations that we can have and all the remaining momentum remain unshifted.

$$|\hat{1}\rangle = |1\rangle + z|2\rangle, \quad \text{and} \quad |\hat{2}\rangle = |2\rangle - z|1\rangle. \quad (4.2.79)$$

One can see in Fig. 4.7 that the first diagram \mathcal{D}_1 is composed of two $\overline{\text{MHV}}$ subdiagrams. On the other hand, the second diagram \mathcal{D}_2 is composed of one MHV and one $\overline{\text{MHV}}$ subdi-

agrams. Let us first evaluate the first diagram in the Fig. 4.7. Both the two subdiagrams of \mathcal{D}_1 are anti-MHV and written in its mathematical form, we get the following expression

$$\mathcal{D}_1 = \frac{[q\hat{P}_{23}]^3[p\hat{P}_{23}]}{[pk][kl][l\hat{1}][\hat{1}\hat{P}_{23}][\hat{P}_{23}q]} \frac{1}{\langle 12 \rangle [12]} \frac{[\hat{2}3]^4}{[\hat{P}_{23}\hat{2}][\hat{2}3][3\hat{P}_{23}]}. \quad (4.2.80)$$

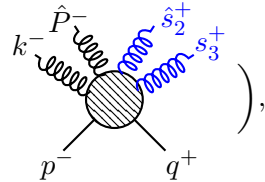
With the on-shell condition of \hat{P}_{23} , the momentum conservation and the shift equation we can express the shifted momenta in terms of the normal spinor vectors (Eq. 4.2.81). The details of this computation is found in the Appendix D.2.

$$|\hat{1}\rangle = |1\rangle + \frac{\langle 23 \rangle}{\langle 13 \rangle} |2\rangle, \quad |\hat{P}_{23}\rangle = |3\rangle, \quad \text{and} \quad |\hat{P}_{23}] = \frac{\langle 12 \rangle}{\langle 13 \rangle} |2] + |3]. \quad (4.2.81)$$

Combining all these results, putting them back into the expression of \mathcal{D}_1 , recalling that $|\hat{2}\rangle = |2\rangle$, rearranging the terms and performing some simplification we get the final expression of the first diagram in the N²MHV amplitude:

$$\mathcal{D}_1 = \frac{1}{s_{123}} \frac{\langle 1|2+3|q|^2 \langle 1|2+3|p]}{\langle 12 \rangle \langle 23 \rangle [pk][kl] \langle 3|1+2|l]}. \quad (4.2.82)$$

On the other hand, the diagram \mathcal{D}_2 is composed of one MHV subdiagram (left) and one NMHV subdiagram (right). Rewriting the MHV part and the internal line in terms of their mathematical expressions, this can be interpreted as

$$\mathcal{D}_2 = \frac{\langle l\hat{1} \rangle^4}{\langle l\hat{1} \rangle \langle \hat{1}\hat{P}_{l1} \rangle \langle \hat{P}_{l1}l \rangle} \frac{1}{\langle l1 \rangle [l1]} \times \left(\text{Diagram} \right), \quad (4.2.83)$$


$$= \frac{\langle l\hat{1} \rangle^4}{\langle l\hat{1} \rangle \langle \hat{1}\hat{P}_{l1} \rangle \langle \hat{P}_{l1}l \rangle} \frac{1}{\langle l1 \rangle [l1]} \times \mathcal{M}. \quad (4.2.84)$$

Here, the NMHV diagram is represented by \mathcal{M} . Using the expression that we derived for the computation of two radiative gluon emission, the NMHV part is given by the following expression

$$\mathcal{M} = \frac{1}{\hat{s}_{12P}} \frac{\langle \hat{P}_{l1}|\hat{2}+3|q|^2 \langle \hat{P}_{l1}|\hat{2}+3|p]}{\langle \hat{P}_{l1}\hat{2} \rangle \langle \hat{2}3 \rangle [qp][pk] \langle 3|\hat{P}_{l1}+\hat{2}|k]} + \frac{1}{\hat{s}_{k2P}} \frac{[\hat{2}|k+\hat{P}_{l1}|p]^2 [\hat{2}|k+\hat{P}_{l1}|q]}{[k\hat{P}_{l1}][\hat{P}_{l1}\hat{2}] \langle pq \rangle \langle q3 \rangle [k|\hat{P}_{l1}+\hat{2}|3]}. \quad (4.2.85)$$

Similarly to the previous calculations, the shifted momentum can be suppressed using the on-shell condition of \hat{P}_{l1} , the momentum conservation and the shift equations. As a consequence, we have the following expressions

$$|\hat{1}\rangle = |3\rangle - \frac{[l1]}{[l2]} |2\rangle, \quad |\hat{2}\rangle = |4\rangle + \frac{[l1]}{[l4]} |3\rangle, \quad |\hat{P}_{l1}\rangle = |l\rangle + \frac{[12]}{[l2]} |1\rangle, \quad \text{and} \quad |\hat{P}_{l1}] = |l]. \quad (4.2.86)$$

Putting back these expression in Eq. (4.2.84) and simplifying terms, the final expression for the N²MHV amplitude is given by

$$\mathcal{D}_2 = \left(\frac{\mathbf{S}_{l_2}^1[l_2]}{\langle 3|l+1|2\rangle[lk] + \langle 3|1+2|l\rangle[k2]} \right) \left\{ \frac{[l_2](s_{l12} - \langle 3|l+1|2\rangle[3q])^2}{s_{l12}[l_2] + \langle 3|1+2|l\rangle[23] + \langle 3|l+1|2\rangle[2l]} \times \right. \\ \left. \frac{s_{l12}[2p] - \langle 3|l+1|2\rangle[3p]}{s_{l12}[qp][pk][l|1+2|3]} + \frac{1}{[kl]\langle pq\rangle\langle q3\rangle} \frac{([2|k+l+1|p])^2[2|k+l+1|q]}{s_{l12}[l_2] + \langle k|1+2|l\rangle[2k] + \langle k|l+1|2\rangle[kl]} \right\}, \quad (4.2.87)$$

where $\mathbf{S}_{l_2}^1 = [l_2]/([l_1][12])$. Indeed, this is because Eq. (4.2.84) simplifies as $\mathcal{D}_2 = \mathbf{S}_{l_2}^1 \times \mathcal{M}$. Combining the two diagrams, we get the total expression for the N^kMHV ($k = 1, 2$) amplitudes. Using similar approach as for the study of the gluon emission, let us study the behavior of the N^kMHV amplitudes under the soft and collinear limit. In the limit where the radiative gluons are soft and collinear to the outgoing quark, the following spinor products tend to zero: $\langle 12\rangle, \langle 23\rangle, \langle 13\rangle, [12], [23], [13], \langle iq\rangle$ and $[iq]$ (for $i = 1, 2, 3$). If we represent by x these spinor products, thus, one can check that the A_7^{MHV} amplitudes are of the order $\sim 1/x^3$ while the A_7^{NMHV} amplitudes are of order $\sim 1/x$. Thus, for $x \rightarrow 0$, the N^kMHV amplitudes are negligible compared to the MHV amplitudes. Therefore, at leading-order, the process is dominated by the MHV helicity configuration.

Adding the appropriate normalization—which means dividing the color of the emission current by C_{A^-} —we can write down the final expression of the total emission current squared for the three-gluon case from Eq. (4.2.78). Written in a more compact form—in terms of traces and square-angle brackets—we have the following expression

$$|\bar{\mathcal{J}}_g^{(3)}(1, 2, 3)|^2 = \frac{C_F^3}{2^3} \prod_{i=1}^3 \frac{(pq)}{(ps_i)(s_iq)} + (2C_A^2 C_F - 3C_A C_F^2) \sum_{\mathcal{P}'_3} \frac{(pq)}{4(s_1 s_2)(s_2 s_3)} \frac{\text{Tr}(p\not{s}_1 q\not{s}_3)}{|\langle ps_1 q s_3 \rangle|^2} + \\ (C_A^2 C_F - 2C_A C_F^2) \sum_{\mathcal{P}'_3} \frac{(pq)}{(s_1 s_2)} \frac{\text{Tr}(p\not{s}_1 \not{s}_3 q\not{s}_2 \not{s}_3)}{|\langle p3q231p \rangle|^2} + C_A C_F^2 \sum_{\mathcal{P}_2, \mathcal{P}'_3} \frac{(pq)}{4(p s_1)(s_2 s_3)} \frac{\text{Tr}(q\not{s}_2 \not{s}_1 \not{s}_3)}{|\langle q213q \rangle|^2}. \quad (4.2.88)$$

The above expression represent the total emission current squared for the case of three gluon emission from which one can compute the multiplicity distribution. One can notice that Eq. (4.2.88) exhibits soft and collinear divergences. The soft divergences appear when the momentum of the radiative gluons tend to zero, namely $s_i \rightarrow 0$ (where i runs from 1 to 3). On the other hand, the collinear divergences occur when the radiative gluons and the outgoing quarks are collinear. In terms of the scalar products, the later can be expressed as $(s_i s_j) \rightarrow 0$ and $(s_i q) \rightarrow 0$ where $i, j = 1, 2, 3$. A quick check of the result shows that

if we require the theory to be Abelian, namely taking $C_A \rightarrow 0$, we can directly see from Eq. Eq. (4.2.88) that the correction/non-Abelian terms vanish and we are only left with the Poisson term. This quick check demonstrates that our result is consistent. However, in order to quantify qualitatively the contribution from the non-Abelian terms, we have to study the behavior of Eq. (4.2.88) under the strong angular limit.

4.3 Summary

In this Chapter, we focused on the study of the in-medium induced radiation. In particular, we analyzed the case for up to three radiative gluon emission. We started by re-deriving the multiplicity distribution for emitting n number of Bremsstrahlung photons using the MHV techniques. We then moved to the computation of the emission current (for the case of one, two and three gluon emission) which holds the information on the radiative process. In particular, for the case of multiple gluon emission (two and three emission), we found that some correction terms have to be added to the standard Poisson result. These correction terms reflect the non-Abelian nature of the strong force that is responsible for the interaction of gluons. In the next section, we evaluate these correction terms and compare the results to the standard Poisson approximation.

Chapter 5

Radiative Emission

Phenomenology

In the previous section, we analytically computed the expression of the momentum distribution for emitting multiple radiative gluons (up to three) beyond the usual Poisson approximation. We showed that radiative gluon emission cannot be treated as independent. At the leading-order calculation, we derived the analytic expression of the correction/non-Abelian terms. In this section, we are going to numerically evaluate the results derived in Chapter 4 and show how to tame the soft and collinear divergences exhibited by the MHV results. We first start the chapter by introducing our parametrization of the kinematics. Then, we study the energy spectrum for emitting radiative gluons as a function of the fractional energy carried on by the gluons. Then, the strong angular ordering will be then investigated afterwards to see if our results are consistent. At the end the chapter, we analyze the convoluted probability density as a function of the total fractional energy ϵ .

5.1 Parametrization of the kinematics and approximations

Recall that throughout our analytic calculations, we used the approximation that the soft gluons ($s_i \sim 0$) are emitted with a very small angles ($\theta_i \sim 0$) with respect to the outgoing quark, and the incoming quark is significantly deflected by the scattering with a hard gluon coming from the medium such that direction of the outgoing quark is perpendicular to the direction of the primordial quark, so we have $\vec{p} \cdot \vec{q} = 0$.

Let us define the z axis to be the spatial direction of the primordial quark and (x, z) to be the plane spanned by the spatial momenta of the incoming and the outgoing

quark. Therefore, in Minkowski space, using the notation (p_0, p_z, p_x, p_y) , the kinematics are parametrized as follows

$$p = (E, E, 0, 0), \quad (5.1.1)$$

$$q = \left((1 - \sum_{i=1}^3 x_i)E, 0, (1 - \sum_{i=1}^3 x_i)E, 0 \right), \quad (5.1.2)$$

$$s_i = (x_i E, s_{i\perp} \cos \phi_i, \sqrt{(x_i E)^2 - s_{i\perp}^2}, s_{i\perp} \sin \phi_i). \quad (5.1.3)$$

In the above expression, $x_i = \omega_i/E$ is the fraction of energy carried out by the i -th radiative gluon with a transverse momentum $s_{i\perp}$. Notice that these momenta satisfy the on-shell condition $p^2 = s_i^2 = q^2 = 0$. In addition, we consider the following approximation for our radiative energy loss model

- *Eikonal trajectory*: the energy of the initial quark is considered to be larger than the transverse momentum of the radiative gluons ($E \gg s_{i\perp}$).
- *Small angle/collinear emission*: the energy of an emitted gluon $\omega_i = x_i E$ is sufficiently high compared to its transverse momentum ($\omega_i \gg s_{i\perp}$).
- *Soft approximation*: the energy of the leading quark is much higher than the energy of the radiative gluons ($E \gg \omega_i$).

The expression of the momentum distributions are functions of dot products. Using the above parametrization, the dot products of the momenta can now be straightforwardly evaluated. In particular, $(pq) \approx E^2$ and $(ps_i) \approx x_i E$. In order to compute the scalar product $(s_i q)$ and $(s_1 s_2)$, one has to Taylor expand the term $\sqrt{(x_i E)^2 - s_{i\perp}^2}$ to obtain

$$\sqrt{(x_i E)^2 - s_{i\perp}^2} = x_i E \left(1 - \frac{s_{i\perp}^2}{2(x_i E)^2} \right) + \mathcal{O} \left(\frac{s_{i\perp}^4}{(x_i E)^4} \right). \quad (5.1.4)$$

Thus, we have

$$(s_i q) = x_i \left(1 - \sum_{i=1}^3 x_i \right) E^2 - x_i \left(1 - \sum_{i=1}^3 x_i \right) E \left(1 - \frac{s_{i\perp}^2}{2(x_i E)^2} \right) \approx \frac{s_{i\perp}^2}{2x_i}, \quad (5.1.5)$$

and

$$(s_i s_j) = \frac{s_{i\perp}^2 x_j}{2x_i} + \frac{s_{j\perp}^2 x_i}{2x_j} - \frac{s_{i\perp}^2 s_{j\perp}^2}{4x_i x_j E^2} - s_{i\perp} s_{j\perp} \cos \Delta\phi_{i,j} \quad (5.1.6)$$

$$\approx \frac{s_{i\perp}^2 x_j}{2x_i} + \frac{s_{j\perp}^2 x_i}{2x_j} - s_{i\perp} s_{j\perp} \cos \Delta\phi_{i,j}, \quad (5.1.7)$$

where $\Delta\phi_{ij} = (\phi_i - \phi_j)$ is the difference in angle between the two radiative gluons on the (z, y) -plane. On the other hand, from Eq. (5.1.3) we have

$$s_{i_z} = s_{i_\perp} \cos \phi_i, \quad (5.1.8)$$

$$s_{i_y} = s_{i_\perp} \sin \phi_i, \quad (5.1.9)$$

$$s_{i_x} = \sqrt{s_i^2 - s_{i_\perp}^2} \approx s_i. \quad (5.1.10)$$

Therefore, by computing the Jacobian one can straightforwardly find that the measure $d^3s_i = ds_{i_x} ds_{i_y} ds_{i_z}$ is given by $d^3s_i = s_{i_\perp} d\omega_i ds_{i_\perp} d\phi_i$ or $2d^3s_i = E dx_i ds_{i_\perp}^2 d\phi_i$. We are going to use these results to compute the energy spectrum as a function of the fractional energy $x = \sum_{i=1}^3 x_i$ which involves an integration over the Lorentz Invariant Phase Space or in short LIPS.

5.2 One gluon emission case

Let us first focus on the case of the single gluon emission. Using our parametrization, the expression of the multiplicity distribution is given by the following

$$\frac{dN_g^{(1)}}{dx} = \frac{\alpha_s}{(2\pi)^2} \frac{C_F}{x} \int d\phi_1 \int ds_{1_\perp}^2 \frac{1}{s_{1_\perp}^2} \quad (5.2.11)$$

$$= \frac{\alpha_s}{2\pi} \frac{C_F}{x} \log \left(\frac{s_{1_\perp}^2{}_{max}}{s_{1_\perp}^2{}_{min}} \right), \quad (5.2.12)$$

where the fractional energy x varies from x_{min} to 1. In our numerical evaluation, the minimal value of s_{1_\perp} is taken to be the mass of a pion ($m_\pi \sim 0.1$ GeV) while the maximum value is taken to be the minimum of xE and $(1-x)E$. We can therefore define a function $\rho^{(1)}(x)$ which represents the energy spectrum for a single radiated gluon

$$\rho^{(1)}(x) = \frac{dN_g^{(1)}}{dx} = \frac{\alpha_s}{2\pi} \frac{C_F}{x} \log \left(\frac{\min(x^2 E^2, (1-x)^2 E^2)}{m_\pi^2} \right). \quad (5.2.13)$$

In order to enhance the fact that the fraction of energy carried out by the radiative gluon is greater than a value x_{min} —which is defined by the energy of the primordial quark—let us define a new function $\tilde{\rho}^{(1)}(x)$,

$$\tilde{\rho}^{(1)}(x) = \rho^{(1)}(x) \Theta(1-x) \Theta(x-x_{min}). \quad (5.2.14)$$

We see in Fig. 5.1 the comparison of the energy spectrum of a single radiated gluon for different values of fraction of energy x_{min} and energy E of the primordial quark. Since

our analytic expression formally diverges for $x = 0$, we allow x to have as minimal values x_{min} . Notice that the values of α_s and x_{min} are defined by the energy E of the initial quark. One can notice that an increase of x with a decrease of E implies a decrease of the spectra and therefore a decrease of the number of radiated gluon $\langle N_g \rangle$.

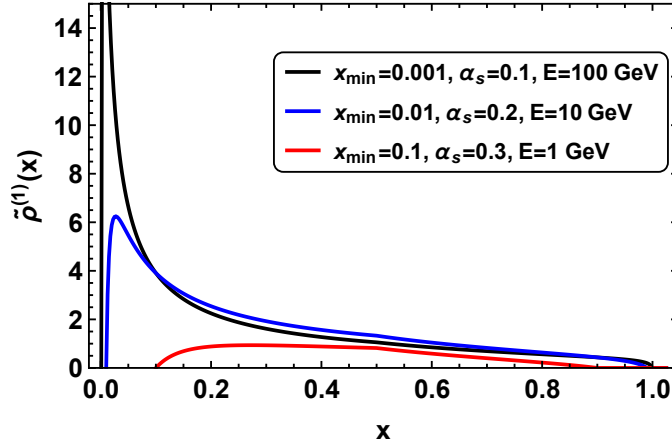


Figure 5.1: Energy spectrum for a single radiated gluon using Eq. (5.2.12) for different values of x_{min} , α_s and energy E which are represented by the different colors. As the energy of the initial quark increases, the probability of emitting a single radiated gluon decreases.

5.3 Two gluon emission case

Let us now move to the phenomenological study of the case of two gluon emission. For the two gluon case, we found that the MHV expression differs from the Poisson by a correction term which is a consequence of the non-Abelian nature of QCD. In this section, we quantitatively compare the MHV and Poisson results for the case of two gluon emission, again for different values of energy.

The energy spectrum of the Poisson result can be straightforwardly computed via two methods. The first method consists of directly integrating Eq. (4.2.51) using the parametrization in Section 5.1. After evaluating the scalar products and simplifying, we have the following result

$$\frac{dN_g^{(2)}}{dx} = \left(\frac{\alpha_s}{2\pi}\right)^2 C_F \int \left(\prod_{i=1}^2 dx_i ds_{i\perp} \right) \delta(x - x_1 - x_2) \frac{1}{x_1 x_2} \frac{1}{s_{1\perp}^2 s_{2\perp}^2}. \quad (5.3.15)$$

The above expression can be numerically challenging to evaluate. An alternative way to compute the two gluon Poisson case is to start from Eq. (5.2.14). Therefore, the expression

of the energy spectrum can be expressed as follows

$$\tilde{\rho}^{(2)}(x) = \frac{1}{2} \int dy \tilde{\rho}^{(1)}(x) \tilde{\rho}^{(1)}(x-y). \quad (5.3.16)$$

Both in Eq. (5.3.15) and Eq. (5.3.16), $x = x_1 + x_2$ denotes the total fraction of energy carried out by both the first and the second radiative gluon. Similarly to the case of the single gluon emission, the value of x is constrained within x_{min} and 1. This implies that y has to be integrated from x_{min} to $(x - x_{min})$ in Eq. (5.3.16). The evolution of the energy spectrum as a function of the fractional energy x for the Poisson case is shown in Fig. 5.2.

On the other hand, the numerical computation of the energy spectrum for the two gluon MHV result is much more complicated not only due to the multidimensional integration but also due to some divergences. Indeed, the soft divergence occurs when $x \rightarrow 0$ while the collinear divergence occurs when $(s_1 s_2) = 0$. Since we do not consider the case in which the first and the second gluon are collinear to be a radiation, we would like the scalar product $(s_1 s_2)$ to be greater than m_π^2 where as mentioned before m_π is the mass of a pion. This requirement sets a restriction on the minimal value that $\Delta\phi_{1,2}$ can take. Thus, the angle $\Delta\phi_{1,2}$ has to be greater than a $(\Delta\phi_{1,2})_{min}$ which is a function of m_π . It follows from Eq. (5.1.7) that requiring $(s_1 s_2) \geq m_\pi^2$ we can derive the expression of $(\Delta\phi_{1,2})_{min}$ which is given by

$$(\Delta\phi_{1,2})_{min} = \frac{1}{s_{1\perp} s_{2\perp}} \left(\frac{x_1 s_{2\perp}^2}{2x_2} + \frac{x_2 s_{1\perp}^2}{2x_1} - m_\pi^2 \right). \quad (5.3.17)$$

By the virtue of our parametrization of the kinematics, we can develop the trace term in Eq. (4.2.51) and simplify further the expression,

$$\begin{aligned} |\bar{\mathcal{J}}_g^{(2)}(1,2)|^2 &= g_s^4 \frac{C_F^2}{4} \prod_{i=1}^2 \frac{(pq)}{(ps_i)(s_iq)} + g_s^4 \frac{C_A C_F}{4} \frac{(pq)}{(s_1 s_2)} \left(\sum_{\mathcal{P}_2(1,2)} \frac{1}{(ps_1)(s_2q)} - \frac{(pq)(s_1 s_2)}{\prod_i (ps_i)(s_iq)} \right) \\ &= g_s^4 \frac{C_F^2}{4C_A} \prod_{i=1}^2 \frac{(pq)}{(ps_i)(s_iq)} + g_s^4 \frac{C_A C_F}{4} \frac{(pq)}{(s_1 s_2)} \sum_{\mathcal{P}_2(1,2)} \frac{1}{(ps_1)(s_2q)}. \end{aligned} \quad (5.3.18)$$

From the first to the second line, we expanded the term in parentheses, combined the Poisson terms and finally simplified the color terms. We can now numerically integrate the above expression in order to get the energy spectrum. Eq. (5.3.18) can be decomposed into the sum of two functions: a function $dN_{g/1}^{(2)}$ which exhibits the Poisson behavior and a function $dN_{g/2}^{(2)}$ which contains the remaining terms. Using the expression of the scalar products in Section 5.1, it is straightforward to show that the first term is given by the

following expression

$$dN_{g/1}^{(2)} = \frac{\alpha_s^2}{(2\pi)^4} \frac{C_F}{C_A} \int \left(\prod_{i=1}^2 dx_i ds_{i\perp}^2 d\phi_i \right) \frac{1}{x_1 x_2} \frac{1}{s_{1\perp}^2 s_{2\perp}^2}. \quad (5.3.19)$$

On the other hand, the second term for the MHV result is given by

$$dN_{g/1}^{(2)} = \frac{\alpha_s^2}{(2\pi)^4} C_A C_F \int \left(\prod_{i=1}^2 dx_i ds_{i\perp}^2 d\phi_i \right) \frac{1}{x_1 x_2} \left(\frac{x_1^2}{s_{1\perp}^2} + \frac{x_2^2}{s_{2\perp}^2} \right) \times \frac{\delta(x - x_1 - x_2)}{(x_1^2 s_{2\perp}^2 + x_2^2 s_{1\perp}^2) - 2x_1 x_2 s_{1\perp} s_{2\perp} \cos(\phi_1 - \phi_2)}. \quad (5.3.20)$$

These integrations are both performed by integrating over x_2 first, then integrated over x_1 from x_{min} to $(x - x_{min})$. One ends up with a function which only depends on the fraction of energy x . The results are numerically computed using our definition of the Casimir factors $C_A = 3$ and $C_F = 8/3$. The lower bound of $s_{i\perp}$ is m_π while the upper bound is taken to be the minimum of $(x_i E, (1 - x_i) E)$. Combining the results from Eq. (5.3.19) and Eq. (5.3.20), we can have the total energy spectrum for the two gluon emission case.

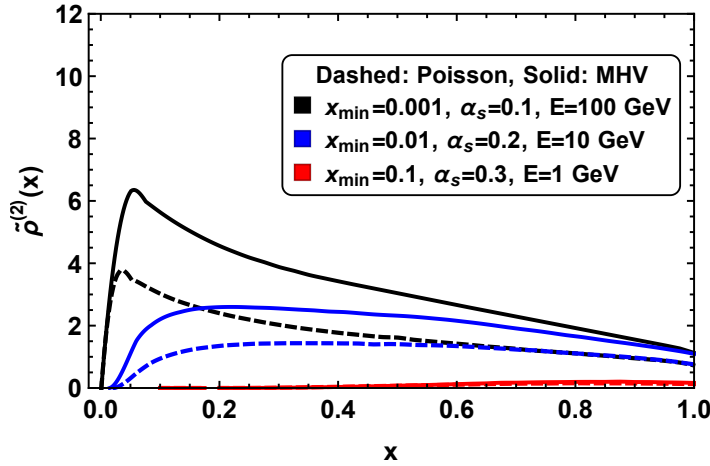


Figure 5.2: Energy spectrum for two gluon emission for different values of x_{min} , α_s and E . The dashed lines represent the Poisson Approximation and the solid lines represent the MHV result expressed by Eq. (5.3.19) and Eq. (5.3.20). The black, blue and red lines correspond respectively to $E = 100$ GeV (with $x_{min} = 0.001$, $\alpha_s = 0.1$), $E = 10$ GeV (with $x_{min} = 0.01$, $\alpha_s = 0.2$) and $E = 1$ GeV (with $x_{min} = 0.1$, $\alpha_s = 0.3$). In the calculation, m_π is taken to be 0.1 GeV/ c^2 .

Fig. 5.2 shows the energy spectrum for different values of x_{min} , coupling constant α_s , and energy E . One can notice that there is a significant difference between the usual Poisson approximation (represented by the dashed lines) and the new MHV result (represented by the solid lines). Indeed, the probability of emitting two radiative gluons from

the MHV result is larger compared to the Poisson result. In addition, one can notice that the energy spectrum does not converge to zero as the total fractional energy increases, namely approaching $x = 1$. This is due to the small x approximation from which we managed to simplify some expressions of the scalar products.

In order to check that our results are consistent, we will study in Section 5.5 the MHV behavior under the strong angular ordering limit. When the radiative gluons are strongly ordered ($\theta_1 \ll \theta_2 \ll \dots \ll \theta_n$), the MHV result should converge to the Poisson result.

5.4 Three gluon emission case

Compared to the one and two gluon case, the numerical evaluation of the three-gluon case is tedious and complicated. This is mainly due to multidimensional integration that we have to perform over all the allowed phase space. On the one hand, integrating directly the Poisson term is numerically heavy. However, the energy spectrum for the Poisson result can be computed in a very simple way following Eq. (5.2.14) and Eq. (5.3.16),

$$\tilde{\rho}^{(3)}(x) = \frac{1}{3} \int dy \tilde{\rho}^{(1)}(x) \tilde{\rho}^{(2)}(x - y). \quad (5.4.21)$$

Therein, y has to be integrated from x_{min} to $(x - x_{min})$ where $x = (x_1 + x_2 + x_3)$ is total fraction of energy carried on by the three gluons. On the other hand, in order to simplify the computation of the full MHV energy spectrum, let us decompose the expression of the emission current (represented by Eq. 4.2.88) into four terms. The first term is the Poisson term which can be computed from the above equation while the three remaining terms represent the non-Abelian correction.

It has already been shown that the scalar product of two radiative gluons is given by the following expression

$$(s_i s_j) \approx \frac{1}{2} \left(\frac{x_j s_{i\perp}^2}{x_i} + \frac{x_i s_{j\perp}^2}{x_j} \right) - s_{i\perp} s_{j\perp} \cos \Delta\phi_{i,j}. \quad (5.4.22)$$

Let us define an expression which is invariant under scaling of $s_i \rightarrow w s_i$ and $s_j \rightarrow v s_j$

$$\mathcal{S}_{i,j}^k = \frac{(s_i s_j)}{(s_i s_k)(s_k s_j)}. \quad (5.4.23)$$

Thus, using our parametrization of kinematics and with a fair amount of algebra the

correction terms are expressed as follows

$$\mathcal{K}_{g/1}^{(3)} = g_s^6 \mathcal{C}_1 \sum_{\mathcal{P}_3} \frac{1}{2(s_1 s_2)(s_2 s_3)} \left(\frac{1}{s_{1\perp}^2} + \frac{1}{s_{3\perp}^2} \right) - \frac{\mathcal{S}_{1,3}^2}{s_{1\perp}^2 s_{3\perp}^2}, \quad (5.4.24)$$

$$\mathcal{K}_{g/2}^{(3)} = g_s^6 \mathcal{C}_2 \sum_{\mathcal{P}_3} \frac{1}{(s_1 s_2)} \left(\frac{2x_2}{x_1 s_{2\perp}^2 s_{3\perp}^2} - \frac{x_2^2}{x_1 x_3 s_{2\perp}^2 (s_2 s_3)} + \frac{x_2 \mathcal{S}_{1,2}^3}{x_1 s_{2\perp}^2} - \frac{x_2 x_3}{x_1^2 (s_1 s_3)} \frac{s_{1\perp}^2}{s_{2\perp}^2 s_{3\perp}^2} \right), \quad (5.4.25)$$

and finally the last expression is given by

$$\begin{aligned} \mathcal{K}_{g/3}^{(3)} = g_s^6 \mathcal{C}_3 \sum_{\mathcal{P}_3} \frac{1}{x_1 (s_2 s_3)} & \left(\frac{x_2}{s_{2\perp}^2 (s_1 s_3)} + \frac{x_3}{s_{3\perp}^2 (s_1 s_2)} - \mathcal{S}_{2,3}^1 \frac{x_2 x_3}{s_{2\perp}^2 s_{3\perp}^2} \right) \\ & + g_s^6 \mathcal{C}_3 \sum_{\mathcal{P}_3} \frac{1}{2s_{1\perp}^2 (s_2 s_3)} \left(\frac{1}{x_2 (s_1 s_3)} + \frac{1}{x_3 (s_1 s_2)} - \mathcal{S}_{2,3}^1 \frac{x_1}{x_2 x_3} \right). \end{aligned} \quad (5.4.26)$$

In these expression, \mathcal{C}_i denotes the appropriate color factors which are respectively given by $\mathcal{C}_1 = (2C_A^2 C_F - 3C_A C_F^2)/4$ and $\mathcal{C}_2 = 2\mathcal{C}_3 = (C_A C_F^2)/4$. Combining these expressions with the Poisson term, the total momentum distribution can be written as

$$\frac{dN_{\text{MHV}}^{(3)}}{dx} = \frac{dN_{g/P}^{(3)}}{dx} + \frac{dN_{g/1}^{(3)}}{dx} + \frac{dN_{g/2}^{(3)}}{dx} + \frac{dN_{g/3}^{(3)}}{dx}, \quad (5.4.27)$$

where each term in the expression above is given by

$$\begin{aligned} \frac{dN_{g/1}^{(3)}}{dx} = \frac{\alpha_s^3}{3!(2\pi)^6} \mathcal{C}_1 \int \left(\prod_{i=1}^3 dx_i ds_{i\perp}^2 d\phi_i \right) & \frac{\delta(x - \sum_i x_i)}{x_1 x_2 x_3} \\ & \sum_{\mathcal{P}_3} \frac{1}{2(s_1 s_2)(s_2 s_3)} \left(\frac{1}{s_{1\perp}^2} + \frac{1}{s_{3\perp}^2} \right) - \frac{\mathcal{S}_{1,3}^2}{s_{1\perp}^2 s_{3\perp}^2}, \end{aligned} \quad (5.4.28)$$

$$\begin{aligned} \frac{dN_{g/2}^{(3)}}{dx} = \frac{\alpha_s^3}{3!(2\pi)^6} \mathcal{C}_2 \int \left(\prod_{i=1}^3 dx_i ds_{i\perp}^2 d\phi_i \right) & \frac{\delta(x - \sum_i x_i)}{x_1 x_2 x_3} \sum_{\mathcal{P}_3} \frac{1}{(s_1 s_2)} \times \\ & \left(\frac{2x_2}{x_1 s_{2\perp}^2 s_{3\perp}^2} - \frac{x_2^2}{x_1 x_3 s_{2\perp}^2 (s_2 s_3)} + \frac{x_2 \mathcal{S}_{1,2}^3}{x_1 s_{2\perp}^2} - \frac{x_2 x_3}{x_1^2 (s_1 s_3)} \frac{s_{1\perp}^2}{s_{2\perp}^2 s_{3\perp}^2} \right), \end{aligned} \quad (5.4.29)$$

and

$$\begin{aligned} \frac{dN_{g/3}^{(3)}}{dx} = \frac{\alpha_s^3}{3!(2\pi)^6} \frac{\mathcal{C}_3}{8} \int \left(\prod_{i=1}^3 dx_i ds_{i\perp}^2 d\phi_i \right) & \frac{\delta(x - \sum_i x_i)}{x_1 x_2 x_3} \sum_{\mathcal{P}_3} \frac{1}{x_1 (s_2 s_3)} \left\{ \frac{x_2}{s_{2\perp}^2 (s_1 s_3)} + \right. \\ & \left. \frac{x_3}{s_{3\perp}^2 (s_1 s_2)} - \mathcal{S}_{2,3}^1 \frac{x_2 x_3}{s_{2\perp}^2 s_{3\perp}^2} \right\} + \frac{1}{2} \sum_{\mathcal{P}_3} \frac{1}{s_{1\perp}^2 (s_2 s_3)} \left\{ \frac{1}{x_2 (s_1 s_3)} + \frac{1}{x_3 (s_1 s_2)} - \mathcal{S}_{2,3}^1 \frac{x_1}{x_2 x_3} \right\}. \end{aligned} \quad (5.4.30)$$

With all these expressions, we can plot the energy spectrum for the three-gluon MHV case. Fig. 5.3 shows the energy spectrum for different values of x_{min} , coupling constant

α_s , and energy E . Again, the MHV results are represented by the solid lines while the Poisson results are represented by the dashed lines. We see that the MHV results exhibit larger energy loss compared to the Poisson results. On the other hand, Fig. 5.4 shows the different energy spectrum for $n = 1, 2, 3$ using the two different methods (MHV and Poisson) for a quark jet with an initial energy $E = 100$ GeV. One can notice that as the number of emitted gluons increases, the energy spectrum decreases.

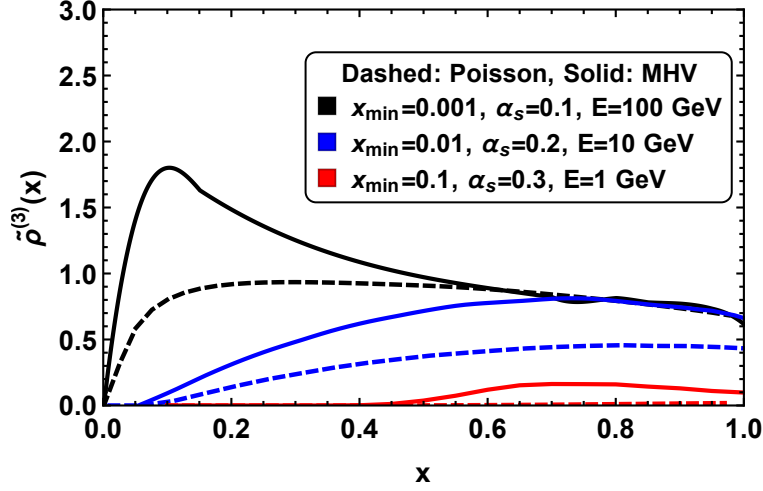


Figure 5.3: Energy spectrum for three gluon emission for different values of x, α_s and E . The dashed lines represent the Poisson Approximation and the solid lines represent the MHV result expressed by Eq. (5.4.27). The black, blue and red lines correspond respectively to $E = 100$ GeV (with $x_{min} = 0.001, \alpha_s = 0.1$), $E = 10$ GeV (with $x_{min} = 0.01, \alpha_s = 0.2$) and $E = 1$ GeV (with $x_{min} = 0.1, \alpha_s = 0.3$). In the calculation, m_π is taken to be 0.1 GeV/ c^2 .

5.5 Strong angular ordering

In the previous section, we studied the energy spectrum for emitting multiple radiative gluons by taking into account the contribution from the non-Abelian behavior of QCD. In order to check the consistency of our result, one can study the behavior of the MHV expressions in the strong angular ordering limit. When the emitted gluons are strongly ordered, interference between radiative gluons becomes negligible and the distribution tends to converge to the Poisson. Consider the case for the two gluon emission, we can study the ratio between the MHV and Poisson using Eq. (4.2.57). Thus, we have $f^{(2)}(\{p, q, s_i\})$

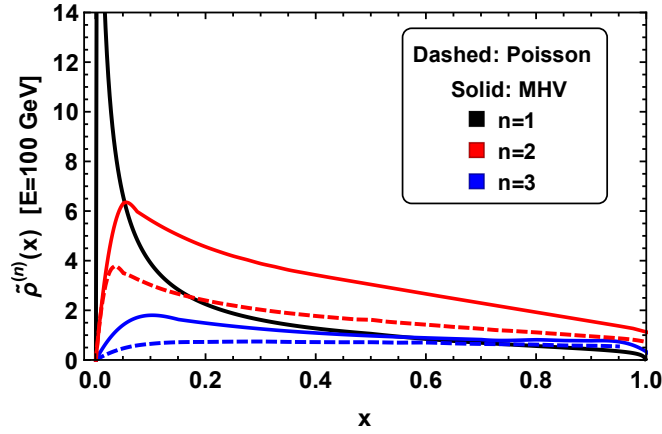


Figure 5.4: Comparison of the energy spectrum for emitting $n = 1, 2$ and 3 radiative gluons for an initial quark of energy $E = 100$ GeV, $x_{min} = 0.001$ and $\alpha_s = 0.1$. The different colors represent the number n of emitted radiative gluon. The solid lines represent the MHV results while the dashed lines represent the usual Poisson result for uncorrelated emission. The solid blue line correspond to the MHV results for three gluon emission represented by Eq.(5.4.27). In the calculation, the mass of the pion is taken to be $m_\pi = 0.1$ GeV/ c^2 .

which is given by

$$\frac{dN_{\text{MHV}}^{(2)}}{dN_{\text{P}}^{(2)}} = \frac{C_A}{C_F} \sum_{\mathcal{P}_2(1,2)} \frac{(ps_1)(s_2q)}{(pq)(s_1s_2)} + C_N, \quad (5.5.31)$$

where $C_N = (C_F - C_A)/C_F = 1/(1 - N^2)$. Using our parametrization and introducing θ_i which is defined to be the angle between the outgoing quark q and the radiative gluon i , Eq. (5.5.31) can be rewritten as

$$f^{(2)}(\{\theta_i, \phi_i\}) = C_N + \frac{C_A}{C_F} \sum_{\mathcal{P}_2(1,2)} \tilde{f}^{(2)}(1, 2), \quad (5.5.32)$$

with

$$\tilde{f}^{(2)}(1, 2) = \frac{(1 - \cos \theta_1)(1 - \sin \theta_2 \cos \phi_2)}{(1 - \cos \theta_1 \cos \theta_2 - \sin \theta_1 \sin \theta_2 \cos \Delta \phi_{1,2})}.$$

By virtue of these equations, one can plot the ratio $f^{(2)}$ as a function of the angle θ_2 of the second radiative gluon. Fig. 5.5 shows the ratio function for different values of $\Delta \phi_{1,2}$. By fixing the value of θ_1 and ϕ_1 , we see that as $\theta_2 \gg \theta_1$ the MHV results converge into the Poisson. The function converges quickly as the value of $\Delta \phi_{1,2}$ gets bigger. In particular, one can notice that for $\Delta \phi_{1,2} = \pi/2$ the MHV behaves exactly like the Poisson.

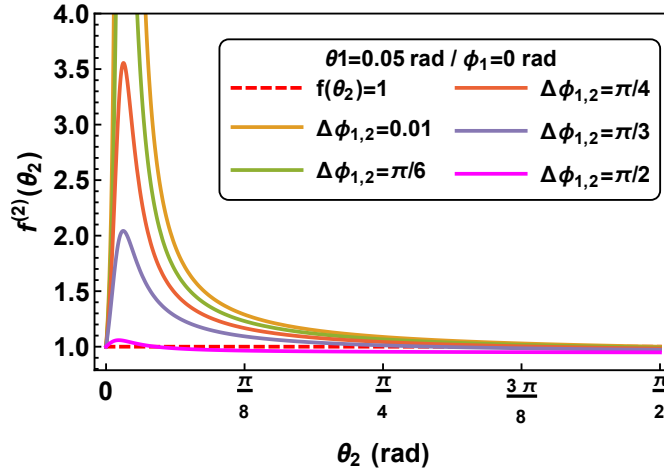


Figure 5.5: Ratio between the MHV momentum distribution and the Poisson given by Eq. (5.5.31) and Eq. (5.5.32). The values of the angles θ_1 and ϕ_1 are fixed and taken to be respectively 0.05 rad and 0 rad. The solid lines represent the ratio function $f^{(2)}(\{\theta_i, \phi_i\})$ for different values of $\Delta\phi_{1,2}$. The red dashed line (horizontal line) represents the case where the MHV results is exactly similar to the Poisson. As the difference in angles between gets bigger, the MHV result converges into the Poisson.

A similar approach can be taken to study the three gluon MHV case in the strong angular ordering limit. The ratio is now given by $f^{(3)}(\{\theta_i, \phi_i\})$ where i runs from 1 to 3. For the numerical calculation, we fixed $\theta_1 = 0.05$ rad and $\phi_1 = 0$ rad. Fig. 5.6 hews the variation of $f^{(3)}$ as a function of the angle θ_3 of the third gluon. We see that when $\theta_1 \ll \theta_2 \ll \theta_3$ and $\phi_2 \neq \phi_3$, the gluons seem uncorrelated and the results tend to the Poisson. This can be clearly seen for $\phi_3 = \pi/2$ where the MHV results, represented by the dashed lines, behave more like a Poisson. The peaks at $\theta_3 \sim 0.05$ and $\theta_3 \sim 0.25$ indicates the interference between the third and the first gluon and/or the third and the second gluon. The large peak at $\theta_3 \sim 0.25$ for the green solid curve is due to the fact that $\phi_1 \approx \phi_2$.

5.6 Probability density

In addition, one can compute the probability density of the total fractional energy loss $\epsilon = \sum_i \omega_i/E$ for a quark jet with an initial energy E . For the emission of up to three radiated gluons, the total probability distribution is given by $P_{1+2+3}(\epsilon) = \sum_{n=0}^3 p_n(\epsilon)$,

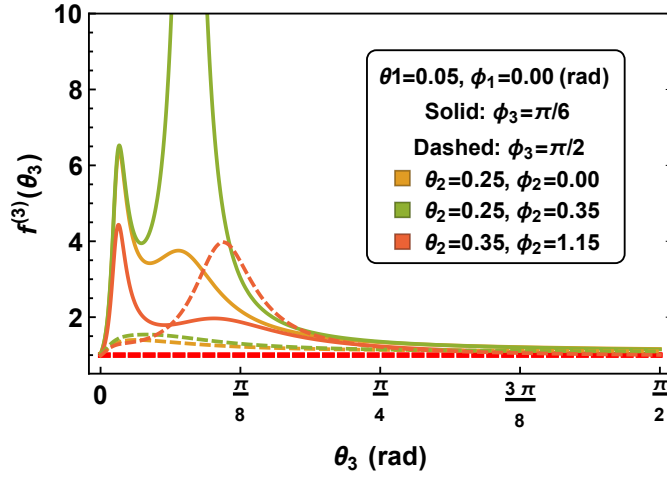


Figure 5.6: Ratio between the MHV momentum distribution and the Poisson for the case of three radiated gluons. We fixed $\theta_1 = 0.05$ rad and $\phi_1 = 0$ rad. The different lines represent the ratio $f^{(3)}(\{\theta_i, \phi_i\})$. The solid lines represent the ratio for $\phi_3 = \pi/6$ while the dashed lines represent the ratio for $\phi_3 = \pi/2$. Similarly, the red dashed line represents the case where the MHV result is exactly similar to the Poisson, which is the case where the angles are strongly ordered. The peaks show the region where $\theta_3 \approx \theta_1$ and/or $\theta_3 \approx \theta_2$.

where for the Poisson case each probability is given by

$$p_0(\epsilon) = e^{-\langle N_g \rangle} \delta(\epsilon), \quad (5.6.33)$$

$$p_1(\epsilon) = e^{-\langle N_g \rangle} \tilde{\rho}^{(1)}(\epsilon), \quad (5.6.34)$$

$$p_2(\epsilon) = \frac{1}{2} \int dx \tilde{\rho}^{(1)}(x) p_1(x - \epsilon), \quad (5.6.35)$$

$$p_3(\epsilon) = \frac{1}{3} \int dx \tilde{\rho}^{(1)}(x) p_2(x - \epsilon). \quad (5.6.36)$$

In the above expressions, the mean number of radiated gluons is defined to be $\langle N_g \rangle = \int dx \tilde{\rho}^{(1)}(x)$. On the other hand, for the MHV case, p_2 and p_3 are given by

$$p_2(\epsilon) = e^{-\langle N_g \rangle} \frac{dN_{\text{MHV}}^{(2)}}{d\epsilon}, \quad (5.6.37)$$

$$p_3(\epsilon) = e^{-\langle N_g \rangle} \frac{dN_{\text{MHV}}^{(3)}}{d\epsilon}. \quad (5.6.38)$$

Fig. 5.7 shows the numerical evaluation of the total probability for a quark jet with an energy $E = 100$ GeV. In addition, the first, second, and third order probability are individually shown. It is noticed that the MHV results exhibit larger probability for emitting radiative gluons compared to the Poisson. The results indicate that both $P_{1+2+3}(\epsilon)$ and $p_n(\epsilon)$ increase dramatically from $\epsilon = 0.001$ up to a scale $\epsilon \sim m_\pi/E$ before decreasing

quickly. For $\epsilon > 0.2$, it appears that the curves do not change much and remain approximately constant, especially for the case of three gluon emission. In addition, one can notice that after some value of ϵ , the Poisson results for one, two, and three gluon emission look the same while the difference is significant for the MHV results. Given the fact that α_s are the same for all the curves, the enhancement might be due to the extra emission possibilities allowed by the non-Abelian coupling of gluons to themselves. From these results, one can also compute the mean fractional energy $\langle \epsilon \rangle$ which is given by $\langle \epsilon \rangle_{P/M} = \int_{x_{min}}^1 d\epsilon \epsilon P(\epsilon)_{P/M}$. The numerical evaluation of the mean fractional of energy loss gives $\langle \epsilon \rangle_P = 0.201$ and $\langle \epsilon \rangle_M = 0.272$ for the Poisson and MHV result respectively.

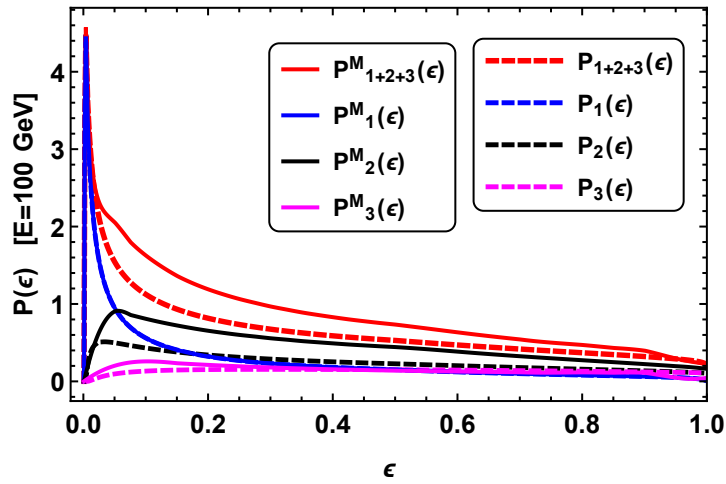


Figure 5.7: Probability density of total fractional energy given by $\epsilon = \sum_i \omega_i/E$ for a quark jet with an initial energy $E = 100$ GeV up to a third order. We restricted ϵ to belong in the interval $[0, 1]$. The solid lines represent the probability density for the MHV case where the dashed lines represent the probability density for the usual Poisson. The red lines (both solid and dashed) represent the total probability density at third order (respectively for MHV and Poisson). The individual probability are shown in different colors. The probability for no radiation $p_0(\epsilon)$ (for the case $n = 0$) is not shown above.

5.7 Summary

In this chapter we wanted to numerically evaluate the MHV results computed in Chapter 4. We started by parameterizing the kinematics taking into account the soft and collinear approximation. The first section was focused on the study of the energy spectrum for emitting radiative gluons. The results were compared to the Poisson results in order to

understand the non-Abelian effect. In particular, for multiple gluon emission (See Fig. 5.2 and Fig. 5.4) the probability for emitting two and three gluons from the MHV approach is significantly larger compared to the standard Poisson results. We then analyzed the strong angular ordering, in which we found that as expected our results converge to the Poisson. This demonstrates that when the radiative gluons are strongly ordered, their interactions become negligible and the theory becomes Abelian. At the end of the chapter, we studied the convoluted probability density. Again, the results indicated that exhibit larger probability.

Chapter 6

Conclusions and discussions

Cross sections are one of the most fundamental observables in modern high energy particle physics. They lie directly in the intersection between theoretical predictions and experimental data. From the experimental point of view, cross sections represent the objects that can be tested using collider experiments (such as LHC and RHIC). From the theoretical point of view, computing scattering amplitudes efficiently is absolutely crucial in order to get results to a precision matching that from modern experiments. In high energy heavy-ion collisions—in which multi-jet processes often occur—scattering amplitudes likely play a vital role in the understanding of the formation and the dynamics of the quark-gluon plasma.

In this thesis we focused on the computation of scattering amplitudes within the multi-jet QCD framework. In particular, we studied the radiative energy loss phenomena by computing multiple radiative gluon emission (for up to three-gluon emission). We presented computations which represent progress in the comprehension of multiple induced radiative emission in QGP using MHV techniques. We demonstrated that the MHV techniques can be potentially applied to the study of the hot QCD matter formed during an ultrarelativistic heavy-ion collisions. One of the chief outputs from this thesis was the quantitative assessment of the non-Abelian contribution to the multiplicity distribution as shown in Chapter 4 and Chapter 5.

The MHV formalism was introduced in Chapter 2. We showed that the MHV techniques exploit the power of the spinor helicity formalism. In addition, we showed in Section 2.1 that spinor variables are very simple mathematical objects. They reveal the simple structure and the hidden symmetry of the scattering amplitudes. As an illustration, we used the spinor helicity formalism to compute the four-point pure gluon process,

$2g \rightarrow 2g$. It was shown that while expressed in terms of the spinor variables, computation of two-to-two processes in QCD become trivial. Further simplification can be made by stripping off the color factors. We demonstrated in Section 2.2 that the color-kinematic decomposition provides a good description of the color-kinematic degrees of freedom. It turns out that the resultant color-stripped partial amplitudes are much easier to compute than computing directly the full amplitude. In Section 2.4, we studied the gauge invariant partial amplitudes in a complex plane by defining complex spinors. This complexification of momenta allowed us to construct a recursion relation. We devoted a particular look at the BCFW on-shell recursion relation—which as opposed the CSW (Cachazo-Svrcek-Witten) expansion only shift two of the external legs. The BCFW recursion relation was an important tool and has been used several times throughout this thesis to compute higher order scattering amplitudes.

The first section of Chapter 3 reviewed the computation of the full cross section of the parent process—which was the building block of the study of the in-medium radiative energy loss. In order to perform such computation, we used all the mathematical tools introduced in Chapter 2. In section 3.2, we constructed via induction the general formula for any higher order scattering amplitudes with a presence of a fermion line. Eq. (3.4.45) and Eq. (3.4.46) represent the general formula for the MHV and $\overline{\text{MHV}}$ respectively for a physical process which involves n arbitrary number of gluons and a pair of quark-antiquark. With these expressions, one can write down the expression of any $N^k\text{MHV}$ amplitude by relying on the BCFW on-shell recursion.

After gaining insights from the computation of the parent process and the generalization formula, we then moved to the main core of the thesis, which is the study of radiative energy loss phenomena. We started by reviewing photon Bremsstrahlung emission in the theory of electrodynamics. The change in momentum and the emission of the Bremsstrahlung photons are induced by a tickling photon. We managed to show with the Eq.(4.1.11) that for the MHV helicity configuration, the total emission current is given by the independent current of each emitted photon. One can square Eq. (4.1.11) and write down the expression of the multiplicity distribution

$$dN_\gamma^{(n)}(\{s_i\}) = \prod_{i=1}^n \frac{d^3 s_i}{(2\pi)^3 2\omega_i} \overline{|J_\gamma^{(n)}(i)|^2} = \frac{1}{n!} \prod_{i=1}^n dN_\gamma^{(1)}(\{s_i\}). \quad (6.0.1)$$

Eq.(6.0.1) shows that for the MHV helicity configuration the distribution follows the Poisson distribution—meaning that the emission of each Bremsstrahlung photon is independent.

For the case of multiple radiative gluon emission, however, things can get extremely complicated. The presence of the generator matrices T^a —which represent the color charges in QCD—makes the computation cumbersome. In order to simplify the computations, we applied the soft-collinear approximation. We assumed that the radiative gluons are soft ($s_i \sim 0$) and emitted with a very small angle ($\theta_i \sim 0$) with respect to the outgoing quark. In addition, the incoming particles are assumed to scatter by a large angle ($\pi/2$). We first found that for the single gluon emission case, our result is comparable to the expression derived by Gunion and Bertsch in [70]. Then, in Section 4.2.2, we computed the two gluon emission off a massless quark. There, we computed the next-to-leading correction term to the Poisson distribution. The second term in Eq. (4.2.51) represents the correction term, which also reflects the non-Abelian behavior of the strong force. The ratio between the MHV result and the Poisson result $\left(dN_g^{(2)}/(dN_g^{(1)}(1)dN_g^{(1)}(2))\right)$ for the two gluon case is represented by Eq. (4.2.57). If we require the theory to be Abelian, this ratio should be 1. We found that the ratio is exactly 1 when $C_A \rightarrow 0$. Thus, the correlation term holds the information on how the two emitted gluons interact with each other. Similarly, we derived the three-gluon emission current using the soft and collinear approximation. Eq. (4.2.88) represents the emission current for the three gluon case from which we can compute the multiplicity distribution. Again, in order to check that our result is consistent, if we require $C_A \rightarrow 0$ Eq. (4.2.88) tends to the standard Poisson result. Notice that our MHV expressions—both for the two and three gluon case—exhibit two types of divergences: (i) *soft divergences* when the momentum of the radiative gluons tend to zero ($s_i \rightarrow 0$), and (ii) *collinear divergences* which appear when the radiative gluons and/or the outgoing quark are collinear ($(s_i s_j) \sim 0, (s_i q) \sim 0$).

In Chapter 5, we investigated the phenomenological implications of our results. We first started by parameterizing our kinematic in Section 5.1. We also adopted the soft and collinear approximation, which are consistent with the radiative energy loss picture in QGP. We began by studying the energy spectrum for emitting radiative gluons and compared the results for MHV and Poisson. The plot of the energy spectrum as a function of the fractional energy x carried by the single radiated gluon for different values of energy E of the initial quark jet is shown in Fig. 5.1. We made a similar plot of the energy spectrum for the two gluon emission case. In order to tame the collinear divergences, we required the scalar product $(s_i s_j)$ of two radiative gluons to be greater than the mass of a pion, $(s_i s_j) \geq m_\pi^2$. As a result, this requirement imposes a constraint on the azimuthal

difference $\Delta\phi$ —which has to be greater than a $(\Delta\phi)_{min}$ defined by Eq. (5.3.17). Fig. 5.2 shows the comparison between the energy spectrum computed from the MHV and Poisson results. As expected, both results decrease as the value of the fraction of energy x increases and the energy E decreases. We see that there is a significant difference between the two results. Interestingly, the MHV results seem to exhibit larger energy spectrum compared to the Poisson result. The same analysis was performed for the three-gluon case. In particular, we computed the energy spectrum for the three-gluon emission case for an initial quark jet with energy $E = 100$ GeV and compared the results to the results from one and two gluon emission. The MHV and the Poisson results are both shown in Fig. 5.4. The fact that the results do not converge to zero as the value of x approaches 1 is due to the small x approximation. Indeed, due to the soft and collinear approximations, the MHV results does not capture the large- x behavior. In Section 5.5, we studied the two and three gluon emission MHV results under the strong angular limit. Fig. 5.5 and Fig. 5.6 clearly shows that the MHV results converge into the Poisson distribution as the radiative gluons become strongly ordered. A more physical quantity that one may study is the convoluted probability density as a function of the total fractional energy $\epsilon = \sum_i \omega_i/E$. The results of such an analysis is plotted in Fig. 5.7. The figure shows that both the total and the individual probability densities are larger for the MHV results.

Some comments are, however, in order: (i) for higher accuracy, the subleading terms in the soft-collinear approximation need to be taken into account. In addition, the N^k MHV results also need to be evaluated carefully for better precision and understanding of the fully complete radiative processes in QCD. (ii) In spite of the collinear assumption, wide angle emissions are important. Generally speaking, the soft and collinear approximations are made for the sake of analytic simplicity, but they are not inherently required. The consequences of the collinear approximation for the GLV energy loss model have been quantified in [71]. It was found that the GLV formalism requires a far more careful treatment of wide angle radiation in order to reduce the systematic uncertainty in the calculation; this is true for other energy loss models such as AMY and ASW [71]. (iii) The MHV calculations presented here do not capture explicitly the exchanged momentum between the propagating parton (here considered to be a quark) and the highly energetic gluon coming from the medium. (iv) The results presented in this thesis do not take into account the Landau-Pomeranchuk-Migdal (LPM) effect which describe the mean free path of the partons between each scattering with the medium [72].

Trying to improve the current work by taking into account the above comments would be a reasonable extension as a future work. More ambitiously, it would be interesting to include masses in the calculations. Including mass in the description of the MHV techniques now seems feasible. In fact, further generalization of the spinor helicity formalism includes massive particles [44–46]. In addition, the on-shell techniques introduced in this thesis are restricted to their applications to tree-level amplitudes. However, significant development has been done toward the formulation of MHV techniques to include loops [73–79]. The exploration of these techniques might lead to important insights into a better understanding of multiple radiative processes in QCD and therefore shed light on the radiative energy loss phenomena in QGP.

Appendix A

Spinor Helicity Formalism

A.1 Conventions for 4D Spinor Helicity Formalism

For our conventions, let us consider a mostly minus metric $g_{\mu\nu} = (+, -, -, -)$. The four-momentum vector is given by $p_\mu = (p_0, p_i)_{i=1,2,3}$ so that the contraction of two four-momentum vectors is given by

$$p_\mu p^\mu = p_0^2 - \vec{p}^2. \quad (\text{A.1.1})$$

In terms of the spinor representation, the Pauli matrices are given by

$$(\sigma^\mu)_{\dot{a}b} = (\mathbf{1}, \sigma_i)_{\dot{a}b}, \quad \text{and} \quad (\bar{\sigma}^\mu)^{\dot{a}b} = (\mathbf{1}, -\sigma_i)^{\dot{a}b}, \quad (\text{A.1.2})$$

where the σ_i are given by

$$\sigma_1 = \begin{pmatrix} 0 & 1 \\ 1 & 0 \end{pmatrix}, \quad \sigma_2 = \begin{pmatrix} 0 & -i \\ i & 0 \end{pmatrix}, \quad \sigma_3 = \begin{pmatrix} 1 & 0 \\ 0 & -1 \end{pmatrix}. \quad (\text{A.1.3})$$

Spinor indices are raised and lower using the tensor

$$\varepsilon^{ab} = \varepsilon^{\dot{a}\dot{b}} = \begin{pmatrix} 0 & 1 \\ -1 & 0 \end{pmatrix} = -\varepsilon_{ab} = -\varepsilon_{\dot{a}\dot{b}}. \quad (\text{A.1.4})$$

For instance, we have

$$\xi^a = \varepsilon^{ab} \xi_b, \quad \tilde{\xi}^{\dot{a}} = \varepsilon^{\dot{a}\dot{b}} \tilde{\xi}_{\dot{b}}, \quad \text{where} \quad (\xi_a)^* = \tilde{\xi}_{\dot{a}}. \quad (\text{A.1.5})$$

In addition, the antisymmetric tensors satisfy $\varepsilon_{ab} \varepsilon^{bc} = \delta_a^c$. Moreover, the spinor representation of the Pauli matrices also satisfy

$$(\sigma^\mu)_{\dot{a}\dot{a}} = \varepsilon_{ab} \varepsilon_{\dot{a}\dot{b}} (\bar{\sigma}^\mu)^{\dot{b}b} \quad (\text{A.1.6})$$

$$(\bar{\sigma}^\mu)^{\dot{a}a} = \varepsilon^{ab} \varepsilon^{\dot{a}\dot{b}} (\sigma^\mu)_{\dot{b}b} \quad (\text{A.1.7})$$

$$(\bar{\sigma}^\mu)^{\dot{a}a} (\bar{\sigma}_\nu)_{\dot{b}b} g_{\mu\nu} = 2\varepsilon^{\dot{a}\dot{b}} \varepsilon_{ab}. \quad (\text{A.1.8})$$

A.2 Spinor variables

In the spinor representation, the momentum of a particle can be expressed as follows

$$p_{a\dot{a}} = \lambda_a \tilde{\lambda}_{\dot{a}}. \quad (\text{A.2.9})$$

We can raise and lower the indice of the left and right handed spinor λ_a and $\tilde{\lambda}_{\dot{a}}$ using the antisymmetric tensors ε_{ab} and $\varepsilon_{\dot{a}\dot{b}}$ as

$$\lambda_a = \varepsilon_{ab} \lambda^b \quad \text{and} \quad \tilde{\lambda}_{\dot{a}} = \varepsilon_{\dot{a}\dot{b}} \tilde{\lambda}^{\dot{b}}. \quad (\text{A.2.10})$$

Thus, in addition, we also have

$$p^{\dot{a}a} = \varepsilon^{ab} \varepsilon^{\dot{a}\dot{b}} p_{\dot{b}b} = p_{\mu} (\bar{\sigma}^{\mu})^{\dot{a}a}. \quad (\text{A.2.11})$$

One can also construct the expression of the slashed momentum \not{p} as

$$\not{p} = p_{\mu} \gamma^{\mu} = \begin{pmatrix} 0 & p_{a\dot{a}} \\ p^{\dot{a}a} & 0 \end{pmatrix} \quad \text{with} \quad \gamma^{\mu} = \begin{pmatrix} 0 & (\sigma^{\mu})_{a\dot{a}} \\ (\bar{\sigma}^{\mu})^{\dot{a}a} & 0 \end{pmatrix}. \quad (\text{A.2.12})$$

The relation between the solutions of the massless Dirac equation $u_{\pm}(p) = v_{\mp}(p)$ and the helicity spinors λ_a and $\tilde{\lambda}_{\dot{a}}$ are given below

$$\begin{aligned} u_+(p) = v_-(p) &= \begin{pmatrix} \lambda_a \\ 0 \end{pmatrix} \equiv |p\rangle, & u_-(p) = v_+(p) &= \begin{pmatrix} 0 \\ \tilde{\lambda}_{\dot{a}} \end{pmatrix} \equiv |p] \\ \bar{u}_+(p) = \bar{v}_+(p) &= \begin{pmatrix} 0 & \tilde{\lambda}_{\dot{a}} \end{pmatrix} \equiv [p|, & \bar{u}_-(p) = \bar{v}_-(p) &= \begin{pmatrix} \lambda^a & 0 \end{pmatrix} \equiv \langle p|. \end{aligned}$$

From these expressions, we can write

$$p_{a\dot{a}} \equiv |p\rangle [p|, \quad \text{and} \quad p^{\dot{a}a} \equiv [p| \langle p|, \quad (\text{A.2.13})$$

and the closed product of the square and angle brackets are given by

$$\langle p_i | p_j \rangle \equiv \langle ij \rangle = \lambda_i^a (\lambda_j)_a \quad \text{and} \quad [p_i | p_j] \equiv [ij] = (\tilde{\lambda}_i)_{\dot{a}} (\tilde{\lambda}_j)^{\dot{a}}. \quad (\text{A.2.14})$$

Appendix B

Spinor Identities

B.1 Momentum Conservation

Let us now see how the momentum conservation can be written in terms of the spinor variables. For n momenta, considering all the momentum to be incoming (or outgoing), the momentum conservation in the spinor representation writes as

$$\sum_{j=1}^n (p_j)_{a\dot{a}} = 0 \iff \sum_{j=1}^n |j\rangle[j] = 0 \quad (\text{B.1.1})$$

We can add to this expression two momenta p_i and p_j different from p_i to get

$$\sum_{j=1}^n \langle ij\rangle[jk] = 0. \quad (\text{B.1.2})$$

Indeed, if $i = j = k$, then the spinor products are trivially zero.

B.2 Fierz rearrangement

Here, let us now prove the Fierz rearrangement. We have

$$[i|\gamma^\mu|j\rangle[k|\gamma_\mu|l] = (\tilde{\lambda}_i)_{\dot{a}}(\lambda_j)_a(\tilde{\lambda}_k)_{\dot{b}}(\lambda_l)_b(\bar{\sigma}^\mu)^{\dot{a}a}(\bar{\sigma}_\nu)^{\dot{b}b}g_{\mu\nu} \quad (\text{B.2.3})$$

$$= 2\varepsilon^{\dot{a}\dot{b}}\varepsilon_{ab}(\tilde{\lambda}_i)_{\dot{a}}(\lambda_j)_a(\tilde{\lambda}_k)_{\dot{b}}(\lambda_l)_b \quad (\text{B.2.4})$$

$$= 2\langle jl\rangle[k i]. \quad (\text{B.2.5})$$

On the first line, we expanded the matrix products on the left-hand side and translated the variables into the left and right-handed spinors λ . From the first to the second line, we used the Eq. (A.1.8). Finally, from the second to the third line we contracted the correspondent indices and translated the final expression into the square and angle brackets notation.

B.3 Schouten identity

The Schouten identity states that:

$$\langle ij \rangle \langle kl \rangle + \langle ki \rangle \langle jl \rangle + \langle kj \rangle \langle li \rangle = 0 \quad (\text{B.3.6})$$

We know that three vectors in 2-dimensional vector space cannot be linearly independent. Therefore, if we have three two-component vectors $|i\rangle, |j\rangle$ and $|k\rangle$, we can write one of them (say $|k\rangle$) as a linear combination of the two others

$$|k\rangle = a|i\rangle + b|j\rangle, \quad (\text{for some } a \text{ and } b). \quad (\text{B.3.7})$$

To find the value of a and b , one can multiply the above expression either by $\langle i|$ or $\langle j|$. Thus, we find

$$a = \frac{\langle jk \rangle}{\langle ji \rangle} \quad \text{and} \quad b = \frac{\langle ik \rangle}{\langle ij \rangle}. \quad (\text{B.3.8})$$

Using these results in the expression [B.3.7](#), we have the following result

$$|k\rangle - \frac{\langle jk \rangle}{\langle ji \rangle} |i\rangle - \frac{\langle ik \rangle}{\langle ij \rangle} |j\rangle = 0 \iff \langle ij \rangle |k\rangle - \langle jk \rangle |i\rangle - \langle ik \rangle |j\rangle = 0. \quad (\text{B.3.9})$$

The Schouten identity is often written with a fourth vector $\langle l|$,

$$\langle ij \rangle \langle lk \rangle + \langle jk \rangle \langle il \rangle + \langle ik \rangle \langle jl \rangle = 0. \quad (\text{B.3.10})$$

With the same computations, the Schouten identity also applies for square brackets

$$[ij][lk] + [jk][il] + [ik][jl] = 0. \quad (\text{B.3.11})$$

B.4 From spinors to Dirac Traces

Consider two momenta $(p_i)_{a\dot{a}} = \lambda_a \tilde{\lambda}_{\dot{a}}$ and $(p_j)_{a\dot{a}} = \mu_a \tilde{\mu}_{\dot{a}}$. If we take the sum of $\langle iji \rangle$ and its complex conjugate $[iji]$, we have the following expression

$$\langle iji \rangle + [iji] = \langle ij \rangle [ji] + [ij] \langle ji \rangle \quad (\text{B.4.12})$$

Translated into the original lambda spinors, we have the following

$$\langle iji \rangle + [iji] = -\lambda_a \tilde{\lambda}_{\dot{a}} \tilde{\mu}^{\dot{a}} \mu^a - \tilde{\lambda}^{\dot{a}} \lambda^a \mu_a \tilde{\mu}_{\dot{a}} \quad (\text{B.4.13})$$

One can straightforwardly check that Eq. [\(A.2.12\)](#) is equivalent to taking the trace of the sum of \not{p}_i and \not{p}_j as $\langle iji \rangle + [iji] = -Tr(\not{p}_i \not{p}_j)$. One can also take similar approach to show that we have the following

$$\langle ijkli \rangle + [ijkli] = Tr(\not{p}_i \not{p}_j \not{p}_k \not{p}_l). \quad (\text{B.4.14})$$

Appendix C

Color Structures

C.1 Definition and normalization

The theory of chromodynamics is defined by the non-Abelian gauge invariance $SU(3)$. For the sake of generality, let us generalize it to $SU(N)$. Throughout the calculations, the generator matrices are normalized such that:

$$\text{Tr}(T^a T^b) = \delta^{ab}, \quad \text{and} \quad [T^a, T^b] = i\tilde{f}^{abc}T^c, \quad (\text{C.1.1})$$

where the structure constant is defined as $\tilde{f}^{abc} = \sqrt{2}f^{abc}$. The structure constant can be expressed in terms of traces as follows

$$i\tilde{f}^{abc} = \text{Tr}(T^a T^b T^c) - \text{Tr}(T^a T^c T^b). \quad (\text{C.1.2})$$

The Fierz identity is defined as:

$$(T^a)_{ij}(T^a)_{kl} = \delta_{il}\delta_{kj} - \frac{1}{N}\delta_{ij}\delta_{kl}. \quad (\text{C.1.3})$$

C.2 Color computation

In this section, we compute the color factors for the QCD process, $qg \rightarrow qg$, in Chapter 3. In matrix notation, the color factors for the pure-matrix squared and the crossed terms are respectively given by

$$\mathcal{C}_s(k, l) = \text{Tr}(T^{a_k} T^{a_l} T^{a_l} T^{a_k}) = (T^{a_k})_{ij}(T^{a_k})_{jk}(T^{a_l})_{kl}(T^{a_l})_{li}, \quad (\text{C.2.4})$$

$$\mathcal{C}_a(k, l) = \text{Tr}(T^{a_k} T^{a_l} T^{a_k} T^{a_l}) = (T^{a_k})_{ij}(T^{a_k})_{kl}(T^{a_l})_{jk}(T^{a_l})_{li}. \quad (\text{C.2.5})$$

Using the relation given in Eq. (C.1.3) and taking into account the property of the Kronecker delta, for instance $\delta_{ii} = N$, the symmetric configuration is given by

$$\mathcal{C}_s(k, l) = \left(\delta_{ik} \delta_{jj} - \frac{1}{N} \delta_{ij} \delta_{jk} \right) \left(\delta_{ki} \delta_{ll} - \frac{1}{N} \delta_{kl} \delta_{li} \right) \quad (\text{C.2.6})$$

$$= \delta_{ik} \delta_{ki} \left(\frac{N^2 - 1}{N} \right)^2 \quad (\text{C.2.7})$$

$$= N \left(\frac{N^2 - 1}{N} \right)^2. \quad (\text{C.2.8})$$

By taking similar approach, the antisymmetric color is given by

$$\mathcal{C}_a(k, l) = (T^{a_l})_{jk} (T^{a_l})_{li} \left[\delta_{il} \delta_{jk} - \frac{1}{N} \delta_{ij} \delta_{kl} \right] \quad (\text{C.2.9})$$

$$= - \left(\frac{N^2 - 1}{N} \right). \quad (\text{C.2.10})$$

Let us define the following factors,

$$C_A = N \quad \text{and} \quad C_F = \frac{N^2 - 1}{N}. \quad (\text{C.2.11})$$

With these definitions, we can write down the final expression of the color factors as

$$\mathcal{C}_s(k, l) = \text{Tr}(T^{a_k} T^{a_l} T^{a_l} T^{a_k}) = C_A C_F^2 \quad (\text{C.2.12})$$

$$\mathcal{C}_a(k, l) = \text{Tr}(T^{a_k} T^{a_l} T^{a_k} T^{a_l}) = -C_F. \quad (\text{C.2.13})$$

C.3 Decomposition of product of T^a

The non-Abelian nature of the $SU(N)$ group makes the calculation of scattering amplitudes complicated. However, as a way of simplifying computations, one can written the product of the generator matrices T^a as a function of commutator. For instance,

$$T^{a_1} T^{a_k} T^{a_l} = T^{a_k} T^{a_l} T^{a_1} + [T^{a_1}, T^{a_k} T^{a_l}] \quad (\text{C.3.14})$$

$$T^{a_k} T^{a_1} T^{a_l} = T^{a_k} T^{a_l} T^{a_1} + T^{a_k} [T^{a_1}, T^{a_l}]. \quad (\text{C.3.15})$$

The other configurations can be derived from the above expressions by interchange of k and l . One can perform similar calculations to simplify the color factors for the two gluon case. The idea is to separate the color factors of the hard scattering so that one can

separate the contribution from the radiative process. So, we have:

$$T^{a_1} T^{a_k} T^{a_l} T^{a_2} = T^{a_k} T^{a_l} T^{a_2} T^{a_1} + [T^{a_1}, T^{a_k} T^{a_l}] T^{a_2} \quad (\text{C.3.16})$$

$$T^{a_1} T^{a_k} T^{a_2} T^{a_l} = T^{a_k} T^{a_l} T^{a_2} T^{a_1} + T^{a_1} [T^{a_k}, T^{a_2}] T^{a_l} \quad (\text{C.3.17})$$

$$T^{a_k} T^{a_1} T^{a_l} T^{a_2} = T^{a_k} T^{a_l} T^{a_2} T^{a_1} + T^{a_k} [T^{a_1}, T^{a_l}] T^{a_2} \quad (\text{C.3.18})$$

$$T^{a_1} T^{a_2} T^{a_k} T^{a_l} = T^{a_k} T^{a_l} T^{a_1} T^{a_2} + [T^{a_1} T^{a_2}, T^{a_k} T^{a_l}] \quad (\text{C.3.19})$$

$$T^{a_k} T^{a_1} T^{a_2} T^{a_l} = T^{a_k} T^{a_l} T^{a_2} T^{a_1} + T^{a_k} [T^{a_1} T^{a_2}, T^{a_l}] \quad (\text{C.3.20})$$

Similarly, the remaining configurations can be derived from the above equations by interchange of k and l plus interchange of 1 and 2. Finally, similar decompositions can be done for the case of three gluon emission where we have in this case five gluons.

$$T^{a_k} T^{a_1} T^{a_l} T^{a_2} T^{a_3} = T^{a_k} T^{a_l} T^{a_1} T^{a_2} T^{a_3} + T^{a_k} [T^{a_1}, T^{a_l}] T^{a_2} T^{a_3} \quad (\text{C.3.21})$$

$$T^{a_k} T^{a_1} T^{a_2} T^{a_l} T^{a_3} = T^{a_k} T^{a_l} T^{a_1} T^{a_2} T^{a_3} + T^{a_k} [T^{a_1} T^{a_2}, T^{a_l}] T^{a_3} \quad (\text{C.3.22})$$

$$T^{a_k} T^{a_1} T^{a_2} T^{a_3} T^{a_l} = T^{a_k} T^{a_l} T^{a_1} T^{a_2} T^{a_3} + T^{a_k} [T^{a_1} T^{a_2} T^{a_3}, T^{a_l}] \quad (\text{C.3.23})$$

$$T^{a_1} T^{a_k} T^{a_l} T^{a_2} T^{a_3} = T^{a_k} T^{a_l} T^{a_1} T^{a_2} T^{a_3} + [T^{a_1}, T^{a_k} T^{a_l}] T^{a_2} T^{a_3} \quad (\text{C.3.24})$$

$$T^{a_1} T^{a_2} T^{a_3} T^{a_k} T^{a_l} = T^{a_k} T^{a_l} T^{a_1} T^{a_2} T^{a_3} + [T^{a_1} T^{a_2} T^{a_3}, T^{a_k} T^{a_l}] \quad (\text{C.3.25})$$

$$T^{a_1} T^{a_2} T^{a_k} T^{a_l} T^{a_3} = T^{a_k} T^{a_l} T^{a_1} T^{a_2} T^{a_3} + [T^{a_1} T^{a_2}, T^{a_k} T^{a_l}] T^{a_3} \quad (\text{C.3.26})$$

$$T^{a_1} T^{a_2} T^{a_k} T^{a_3} T^{a_l} = T^{a_k} T^{a_l} T^{a_1} T^{a_2} T^{a_3} + [T^{a_1} T^{a_2}, T^{a_k} T^{a_l}] T^{a_3} + T^{a_1} T^{a_2} T^{a_k} [T^{a_3}, T^{a_l}]$$

$$T^{a_1} T^{a_k} T^{a_2} T^{a_l} T^{a_3} = T^{a_k} T^{a_l} T^{a_1} T^{a_2} T^{a_3} + T^{a_1} T^{a_k} [T^{a_2}, T^{a_l}] T^{a_3} + [T^{a_1}, T^{a_k} T^{a_l}] T^{a_2} T^{a_3}$$

$$T^{a_1} T^{a_k} T^{a_2} T^{a_3} T^{a_l} = T^{a_k} T^{a_l} T^{a_1} T^{a_2} T^{a_3} + T^{a_1} T^{a_k} [T^{a_2} T^{a_3}, T^{a_l}] + [T^{a_1}, T^{a_k} T^{a_l}] T^{a_2} T^{a_3}.$$

Appendix D

MHV/ N^k MHV Amplitude Calculations

D.1 Two gluon emission

MHV amplitudes

From the general formula represented by the Eq. (3.4.45), the MHV helicity configuration for the two gluon case is given by

$$\mathcal{A}_6(\mathcal{H}_1) = g_s^4 \frac{\langle pk \rangle^3 \langle qk \rangle}{\langle qp \rangle} \sum_{\mathcal{P}_4} \frac{(T^{a_k} T^{a_l} T^{a_1} T^{a_2})}{\langle pk \rangle \langle kl \rangle \langle l1 \rangle \langle 12 \rangle \langle 2q \rangle}. \quad (\text{D.1.1})$$

The above amplitude can be factorized such that we can recover the expression of the partial amplitudes for the parent process. This can be done using the above decomposition of the product of T^a 's and by breaking the sum over the permutation so we can write Eq. (D.1.1) as follows

$$\mathcal{A}_6(\mathcal{H}_1) = \mathcal{A}_6(\text{parent}) + \mathcal{A}_6(\text{extra}), \quad (\text{D.1.2})$$

where each amplitude written above is given by

$$\begin{aligned} \mathcal{A}_6(\text{parent}) = g_s^4 (T^{a_k} T^{a_l}) A_4(k, l) & \left\{ (T^{a_1} T^{a_2}) \left(\frac{\langle l2 \rangle}{\langle l1 \rangle \langle 12 \rangle} \frac{\langle lq \rangle}{\langle l2 \rangle \langle 2q \rangle} + \frac{\langle k2 \rangle}{\langle k1 \rangle \langle 12 \rangle} \frac{\langle kl \rangle}{\langle k2 \rangle \langle 2l \rangle} + \frac{\langle kl \rangle}{\langle k1 \rangle \langle 1l \rangle} \right. \right. \\ & \left. \left. + \frac{\langle lq \rangle}{\langle l2 \rangle \langle 2q \rangle} + \frac{\langle pk \rangle}{\langle p1 \rangle \langle 1k \rangle} \frac{\langle lq \rangle}{\langle l2 \rangle \langle 2q \rangle} + \frac{\langle pk \rangle}{\langle p1 \rangle \langle 1k \rangle} \frac{\langle kl \rangle}{\langle k2 \rangle \langle 2l \rangle} + \frac{\langle pk \rangle}{\langle p1 \rangle \langle 1k \rangle} \frac{\langle 1k \rangle}{\langle 12 \rangle \langle 2k \rangle} \right) + (1 \leftrightarrow 2) \right\} + (k \leftrightarrow l), \end{aligned} \quad (\text{D.1.3})$$

and for the extra-term

$$\begin{aligned} \mathcal{A}_6(\text{extra}) = & g_s^4 A_4(k, l) \left\{ T^{a_k} [T^{a_1} T^{a_2}, T^{a_l}] \frac{\langle k2 \rangle}{\langle k1 \rangle \langle 12 \rangle} \frac{\langle kl \rangle}{\langle k2 \rangle \langle 2l \rangle} + T^{a_k} [T^{a_1}, T^{a_l}] T^{a_2} \frac{\langle kl \rangle}{\langle k1 \rangle \langle 1l \rangle} \frac{\langle lq \rangle}{\langle 12 \rangle \langle 2q \rangle} \right. \\ & + [T^{a_1}, T^{a_k} T^{a_l}] T^{a_2} \frac{\langle pk \rangle}{\langle p1 \rangle \langle 1k \rangle} \frac{\langle lq \rangle}{\langle 12 \rangle \langle 2q \rangle} + T^{a_1} [T^{a_k}, T^{a_2}] T^{a_l} \frac{\langle pk \rangle}{\langle p1 \rangle \langle 1k \rangle} \frac{\langle kl \rangle}{\langle k2 \rangle \langle 2l \rangle} + [T^{a_1} T^{a_2}, T^{a_k} T^{a_l}] \\ & \left. \frac{\langle pk \rangle}{\langle p1 \rangle \langle 1k \rangle} \frac{\langle 1k \rangle}{\langle 12 \rangle \langle 2k \rangle} + (1 \longleftrightarrow 2) \right\} + (k \longleftrightarrow l). \end{aligned} \quad (\text{D.1.4})$$

The partial amplitudes $A_4(k, l)$ and $A_4(l, k)$ are expressed as

$$A_4(k, l) = \frac{\langle pk \rangle^3 \langle qk \rangle}{\langle pk \rangle \langle kl \rangle \langle lq \rangle \langle qp \rangle} \quad \text{and} \quad A_4(l, k) = \frac{\langle pk \rangle^3 \langle qk \rangle}{\langle pl \rangle \langle lk \rangle \langle kq \rangle \langle qp \rangle}. \quad (\text{D.1.5})$$

The amplitude which is explicitly expressed in terms of the born amplitude in Eq. (D.1.3) can be further simplified using the *Schouten identity*. With a fair amount of algebra, one can arrive at the following result

$$\mathcal{A}_6(\text{parent}) = g_s^4 (T^{a_k} T^{a_l}) A_4(k, l) \left\{ (T^{a_1} T^{a_2}) \frac{\langle pq \rangle}{\langle p1 \rangle \langle 12 \rangle \langle 2q \rangle} + (1 \leftrightarrow 2) \right\} + (k \leftrightarrow l) \quad (\text{D.1.6})$$

We notice that the terms inside the braces are independent of k and l . Thus, the above equation can be written nicely as

$$\mathcal{A}_6(\text{parent}) = g_s^4 \left(\sum_{\mathcal{P}_2} (T^{a_k} T^{a_l}) A_4(k, l) \right) \left(\sum_{\mathcal{P}'_2} (T^{a_1} T^{a_2}) \frac{\langle pq \rangle}{\langle p1 \rangle \langle 12 \rangle \langle 2q \rangle} \right). \quad (\text{D.1.7})$$

Rewriting the above equation, we have

$$\mathcal{A}_6(\text{parent}) = \mathcal{A}_4(\text{parent}) \mathcal{J}_g^{(2)}(1, 2), \quad \mathcal{J}_g^{(2)}(1, 2) = g_s^2 \langle pq \rangle \sum_{\mathcal{P}'_2} \frac{(T^{a_1} T^{a_2})}{\langle p1 \rangle \langle 12 \rangle \langle 2q \rangle}. \quad (\text{D.1.8})$$

One can clearly see by comparing Eq. (D.1.8) and Eq. (D.1.4) that for the case where the two radiative gluons are collinear with respect to the outgoing quark—equivalent to say that the cross products $\langle 12 \rangle, \langle 1q \rangle$ and $\langle 2q \rangle$ vanish—the full amplitude in Eq. (D.1.2) is dominated by $\mathcal{A}_4(\text{parent})$. Putting back the helicity sign, the two MHV helicity configurations represented by \mathcal{H}_1 and \mathcal{H}_2 are given by

$$\mathcal{A}_6(\mathcal{H}_1) \approx \mathcal{A}_4(-, +) \times \mathcal{J}_g^{(2)}(1, 2), \quad (\text{D.1.9})$$

$$\mathcal{A}_6(\mathcal{H}_2) \approx \mathcal{A}_4(+, -) \times \mathcal{J}_g^{(2)}(1, 2). \quad (\text{D.1.10})$$

When summing over the possible MHV helicity configuration, we only have to consider \mathcal{H}_1 and \mathcal{H}_2 and by symmetry interchange the labels in order to derive the final answer shown in Eq. (4.2.38).

NMHV/BCFW Calculations

Here, we are going to compute the NMHV amplitude for the case of the two gluon emission and which is diagrammatically represented in Fig. 4.4. The mathematical expression is given by Eq. (4.2.53). The on-shell condition tells us that

$$\hat{P}_{12}^2 = \langle \hat{1}2 \rangle [12] = 0 \iff \langle \hat{1}2 \rangle = 0. \quad (\text{D.1.11})$$

This implies that the spinors $|\hat{1}\rangle$ and $|2\rangle$ are proportional so we can write $|\hat{1}\rangle = |2\rangle$. Using the shift equations (4.2.52), we can find the value of the complex parameter z

$$\langle \hat{1}2 \rangle = \langle 12 \rangle - z \langle l2 \rangle = 0 \implies z = \frac{\langle 12 \rangle}{\langle l2 \rangle}, \quad (\text{D.1.12})$$

so the shift-equations now become:

$$|\hat{l}\rangle = |l\rangle + \frac{\langle 12 \rangle}{\langle l2 \rangle} |1\rangle, \quad \text{and} \quad |\hat{1}\rangle = |1\rangle - z |l\rangle. \quad (\text{D.1.13})$$

In addition, we can derive the value of the factor x from

$$|\hat{1}\rangle = |1\rangle - \frac{\langle 12 \rangle}{\langle l2 \rangle} |l\rangle = x |2\rangle \implies x = \frac{\langle l1 \rangle}{\langle l2 \rangle}. \quad (\text{D.1.14})$$

Finally, the internal momentum $\hat{P}_{12} = \hat{p}_1 + p_2$. In terms of spinor representation, this expression can be rewritten as

$$\hat{P}_{12} = |\hat{1}\rangle [1 + |2\rangle = |2\rangle \left(\frac{\langle l1 \rangle}{\langle l2 \rangle} [1 + |2] \right) \quad (\text{D.1.15})$$

$$\text{Thus, } |\hat{P}_{12}\rangle = |2\rangle, \quad \text{and} \quad |\hat{P}_{12}] = \left(\frac{\langle l1 \rangle}{\langle l2 \rangle} [1 + |2] \right). \quad (\text{D.1.16})$$

D.2 Three gluon emission

MHV amplitudes

In this section, we are going to show that the MHV amplitude for the emission of three gluons are given by Eq. (4.2.60) and Eq. (4.2.61). From the general formula, the full amplitude can be written as

$$\mathcal{A}_7(\mathcal{H}_4) = g_s^5 \frac{\langle pk \rangle^3 \langle qk \rangle}{\langle qp \rangle} \sum_{\mathcal{P}_5} \frac{(T^{a_k} T^{a_l} T^{a_1} T^{a_2} T^{a_3})}{\langle pk \rangle \langle kl \rangle \langle l1 \rangle \langle 12 \rangle \langle 23 \rangle \langle 3q \rangle}, \quad (\text{D.2.17})$$

for the helicity configuration \mathcal{H}_4 . Similarly to what we have done for the case of two gluon emission, we can factorize some terms in order to isolate the expression of the partial amplitude of the parent process so we can have

$$\mathcal{A}_7(\mathcal{H}_4) = \mathcal{A}_7(\text{parent}) + \mathcal{A}_7(\text{extra}). \quad (\text{D.2.18})$$

First, in order to simplify notation, let us define the following quantity:

$$\mathcal{S}_{i,j}^k = \frac{\langle ij \rangle}{\langle ik \rangle \langle jk \rangle}. \quad (\text{D.2.19})$$

Thus, the amplitude $\mathcal{A}_7(\text{parent})$ which can be explicitly expressed in terms of the partial amplitude of the parent process writes as

$$\begin{aligned} \mathcal{A}_7(\text{parent}) = g_s^5 (T^{a_k} T^{a_l}) A_4(k, l) & \left\{ (T^{a_1} T^{a_2} T^{a_3}) \left(\mathcal{S}_{p,k}^1 \mathcal{S}_{k,l}^2 \mathcal{S}_{l,q}^3 + \mathcal{S}_{k,l}^1 \mathcal{S}_{1,l}^2 \mathcal{S}_{l,q}^3 + \mathcal{S}_{k,l}^1 \mathcal{S}_{l,q}^2 \mathcal{S}_{2,q}^3 + \right. \right. \\ & \mathcal{S}_{p,k}^1 \mathcal{S}_{l,q}^2 \mathcal{S}_{2,q}^3 + \mathcal{S}_{p,k}^1 \mathcal{S}_{k,l}^2 \mathcal{S}_{2,l}^3 + \mathcal{S}_{p,k}^1 \mathcal{S}_{1,k}^2 \mathcal{S}_{l,q}^3 + \mathcal{S}_{p,k}^1 \mathcal{S}_{1,k}^2 \mathcal{S}_{k,l}^3 + \mathcal{S}_{l,q}^1 \mathcal{S}_{1,q}^2 \mathcal{S}_{2,q}^3 + \\ & \left. \left. \mathcal{S}_{k,l}^1 \mathcal{S}_{1,l}^2 \mathcal{S}_{2,q}^3 + \mathcal{S}_{p,k}^1 \mathcal{S}_{1,k}^2 \mathcal{S}_{2,k}^3 \right) + \text{perm}(1, 2, 3) \right\} + (k \longleftrightarrow l). \quad (\text{D.2.20}) \end{aligned}$$

The above expression can be written in a more compact and simple form. Indeed, we have

$$\mathcal{A}_7(\text{parent}) = g_s^5 (T^{a_k} T^{a_l}) A_4(k, l) \mathcal{J}_{k,l}(1, 2, 3) + g_s^5 (T^{a_l} T^{a_k}) A_4(l, k) \mathcal{J}_{l,k}(1, 2, 3), \quad (\text{D.2.21})$$

where the partial amplitudes A_4 are defined as in Eq. (D.1.5) and the \mathcal{J} are color-dependent partial amplitudes. One can, fortunately, simplify further the expression of \mathcal{J} by pairing up terms using the Schouten identity. For instance, we have

$$\mathcal{S}_{p,k}^1 \mathcal{S}_{k,l}^2 \mathcal{S}_{l,q}^3 + \mathcal{S}_{p,k}^1 \mathcal{S}_{k,l}^2 \mathcal{S}_{2,l}^3 = \mathcal{S}_{p,k}^1 \mathcal{S}_{k,l}^2 (\mathcal{S}_{2,l}^3 + \mathcal{S}_{l,q}^3) = \mathcal{S}_{p,k}^1 \mathcal{S}_{k,l}^2 \mathcal{S}_{2,q}^3. \quad (\text{D.2.22})$$

By doing repeatedly such procedure, one will end up with

$$\mathcal{J}_{k,l}(1, 2, 3) = \sum_{\mathcal{P}'_3} (T^{a_1} T^{a_2} T^{a_3}) \mathcal{S}_{p,q}^1 \mathcal{S}_{1,q}^2 \mathcal{S}_{2,q}^3 \quad (\text{D.2.23})$$

$$= \sum_{\mathcal{P}'_3} (T^{a_1} T^{a_2} T^{a_3}) \frac{\langle pq \rangle}{\langle p1 \rangle \langle 1q \rangle} \frac{\langle 1q \rangle}{\langle 12 \rangle \langle 2q \rangle} \frac{\langle 2q \rangle}{\langle 22 \rangle \langle 2q \rangle} \quad (\text{D.2.24})$$

$$= \langle pq \rangle \sum_{\mathcal{P}'_3} \frac{(T^{a_1} T^{a_2} T^{a_3})}{\langle p1 \rangle \langle 12 \rangle \langle 23 \rangle \langle 3q \rangle}. \quad (\text{D.2.25})$$

One can straightforwardly check that the computation of $\mathcal{J}_{l,k}(1, 2, 3)$ gives exactly the same result. So, finally, one can write the amplitude $\mathcal{A}_4(\text{parent})$ as

$$\mathcal{A}_7(\text{parent}) = g_s^3 \langle pq \rangle \mathcal{A}_4(\text{parent}) \sum_{\mathcal{P}'_3} \frac{(T^{a_1} T^{a_2} T^{a_3})}{\langle p1 \rangle \langle 12 \rangle \langle 23 \rangle \langle 3q \rangle}. \quad (\text{D.2.26})$$

On the other hand, according to the color decomposition in Section C.3 of the Appendix

C, the extra-terms is given by the following expression

$$\begin{aligned}
\mathcal{A}_7(\text{extra}) = g_s^5 (T^{a_k} T^{a_l}) A_4(k, l) & \left\{ (T^{a_k} [T^{a_1}, T^{a_l}] T^{a_2} T^{a_3}) \mathcal{S}_{p,k}^1 \mathcal{S}_{k,l}^2 \mathcal{S}_{l,q}^3 + (T^{a_k} [T^{a_1} T^{a_2}, T^{a_l}] T^{a_3}) \right. \\
& \mathcal{S}_{k,l}^1 \mathcal{S}_{1,l}^2 \mathcal{S}_{l,q}^3 + (T^{a_k} [T^{a_1} T^{a_2} T^{a_3}, T^{a_l}]) \mathcal{S}_{k,l}^1 \mathcal{S}_{l,q}^2 \mathcal{S}_{2,q}^3 + ([T^{a_1}, T^{a_k} T^{a_l}] T^{a_2} T^{a_3}) \mathcal{S}_{p,k}^1 \mathcal{S}_{l,q}^2 \mathcal{S}_{2,q}^3 + \\
& (T^{a_1} T^{a_k} [T^{a_2}, T^{a_l}] T^{a_3} + [T^{a_1}, T^{a_k} T^{a_l}] T^{a_2} T^{a_3}) \mathcal{S}_{p,k}^1 \mathcal{S}_{k,l}^2 \mathcal{S}_{2,l}^3 + (T^{a_1} T^{a_k} [T^{a_2} T^{a_3}, T^{a_l}] + \\
& [T^{a_1}, T^{a_k} T^{a_l}] T^{a_2} T^{a_3}) \mathcal{S}_{p,k}^1 \mathcal{S}_{1,k}^2 \mathcal{S}_{l,q}^3 + \mathcal{S}_{p,k}^1 \mathcal{S}_{1,k}^2 \mathcal{S}_{k,l}^3 + ([T^{a_1} T^{a_2}, T^{a_k} T^{a_l}] T^{a_3}) \mathcal{S}_{l,q}^1 \mathcal{S}_{1,q}^2 \mathcal{S}_{2,q}^3 + \\
& \left. ([T^{a_1} T^{a_2}, T^{a_k} T^{a_l}] T^{a_3} + T^{a_1} T^{a_2} T^{a_k} [T^{a_3}, T^{a_l}]) \mathcal{S}_{k,l}^1 \mathcal{S}_{1,l}^2 \mathcal{S}_{2,q}^3 + ([T^{a_1} T^{a_2} T^{a_3}, T^{a_k} T^{a_l}]) \mathcal{S}_{p,k}^1 \mathcal{S}_{1,k}^2 \mathcal{S}_{2,k}^3 \right\}
\end{aligned} \tag{D.2.27}$$

one can expand this relation and found that, similarly to the case of two gluon emission, this expression is dominated by the MHV results for the case where the spinor products $\langle 12 \rangle$, $\langle 13 \rangle$, $\langle 23 \rangle$ and $\langle iq \rangle$ (for $i = 1, 2, 3$) are zero. Thus, the full amplitude is given by the MHV helicity configurations.

N²MHV/BCFW Calculations

(a) From the BCFW diagrammatic representation of the N²MHV amplitude for the case of two gluon emission, one can remark that both the two subdiagrams \mathcal{D}_1 are $\overline{\text{MHV}}$. Using the general formula for the $\overline{\text{MHV}}$ amplitudes, one can write down the mathematical expression of the first diagram \mathcal{D}_1

$$\mathcal{D}^{(1)} = \frac{[q \hat{P}_{23}]^3 [p \hat{P}_{23}]}{[pk][kl][l\hat{1}][\hat{1}\hat{P}_{23}][\hat{P}_{23}q]} \frac{1}{\langle 12 \rangle [12]} \frac{[\hat{23}]^4}{[\hat{P}_{23}\hat{2}][\hat{23}][3\hat{P}_{23}]} . \tag{D.2.28}$$

The above expression is still a function of the shifted momentum. However, we would like to have an expression which only depends on the real spinors. In order to get rid of the complex momentum, one can use the properties of the on-shell conditions. The *on-shell condition* tells us that $\hat{P}_{23}^2 = 0$. This implies that

$$(\hat{p}_2 + p_3)^2 = \langle \hat{23} \rangle [\hat{23}] = 0. \tag{D.2.29}$$

For real valued momenta, the spinor product $[\hat{23}]$ is equal to $[23]$ and is non-zero, $\langle \hat{23} \rangle$ must vanish. We can use such condition to find the expression of the complex paramter z as follows

$$\langle \hat{23} \rangle = \langle 23 \rangle - z \langle 13 \rangle = 0 \implies z = \frac{\langle 23 \rangle}{\langle 13 \rangle}. \tag{D.2.30}$$

Using the above equation, the shift-equations can now be written as

$$|\hat{1}\rangle = |1\rangle + \frac{\langle 23 \rangle}{\langle 13 \rangle} |2\rangle, \quad \text{and} \quad |\hat{2}\rangle = |2\rangle - \frac{\langle 23 \rangle}{\langle 13 \rangle} |1\rangle. \tag{D.2.31}$$

Furthermore, the fact that $\langle \hat{2}3 \rangle = 0$ suggests that the two spinors $|\hat{2}\rangle$ and $|3\rangle$ are *collinear* and we have the relation $|\hat{2}\rangle = x|3\rangle$ which leads to the expression,

$$|2\rangle - \frac{\langle 23 \rangle}{\langle 13 \rangle} |1\rangle = x|3\rangle. \quad (\text{D.2.32})$$

Again we can multiply each side of this equation by any spinor we want. Note that we would like get the simplest expression of x . If we multiply each side of the equation by the vector $\langle 1|$ we cancel one term. Therefore, we have

$$\langle 12 \rangle = x\langle 13 \rangle \implies x = \frac{\langle 12 \rangle}{\langle 13 \rangle}. \quad (\text{D.2.33})$$

By virtue of the *on-shell condition*, the shifted momenta, we can now get rid of the shifted momenta in the expression of the internal momentum \hat{P}_{23} . Indeed, in terms of the square and angle brackets \hat{P}_{23} can be written as $\hat{P}_{23} = |\hat{2}\rangle\langle \hat{2}| + |3\rangle\langle 3|$ and by developing this expression, we get

$$\hat{P}_{23} = |3\rangle \left(\frac{\langle 12 \rangle}{\langle 13 \rangle} [2] + [3] \right). \quad (\text{D.2.34})$$

Thus we have,

$$|\hat{P}_{23}\rangle = |3\rangle \quad \text{and} \quad |\hat{P}_{23}] = \frac{\langle 12 \rangle}{\langle 13 \rangle} [2] + [3]. \quad (\text{D.2.35})$$

From the above expressions, we see that the shifted spinors can be expressed in terms of the unshifted spinors. Now, using these expressions, let us get rid of the shifted momenta in \mathcal{D}_1 . First of all, we have

$$\begin{aligned} [q\hat{P}_{23}] &= [q| \left(\frac{\langle 13 \rangle}{\langle 13 \rangle} [2] + [3] \right), \\ &= \frac{\langle 12 \rangle}{\langle 13 \rangle} [q2] + [q3], \\ &= \frac{\langle 12 \rangle [q2] + \langle 13 \rangle [q3]}{\langle 35 \rangle}. \end{aligned} \quad (\text{D.2.36})$$

The numerator in the last line can be rewritten as $(\langle 12 \rangle [q2] + \langle 13 \rangle [q3])$ which is also equivalent to $-(\langle 1|2[q] + \langle 1|3[q])$. Thus, it follows that

$$[q\hat{P}_{23}] = -\frac{\langle 1|2 + 3|q]}{\langle 13 \rangle}. \quad (\text{D.2.37})$$

By symmetry, we can get the expression of $[p\hat{P}_{23}]$ without doing any computation,

$$[p\hat{P}_{23}] = -\frac{\langle 1|2 + 3|p]}{\langle 13 \rangle}. \quad (\text{D.2.38})$$

Doing the exact same computation as for $[q\hat{P}_{23}]$, we can straightforwardly derive the following expressions:

$$[l\hat{1}] = \frac{\langle 3|1 + 2|l]}{\langle 13 \rangle}, \quad [\hat{P}_{23}\hat{2}] = [32] \quad \text{and} \quad [3\hat{P}_{23}] = \frac{\langle 12 \rangle}{\langle 13 \rangle} [32]. \quad (\text{D.2.39})$$

The remaining form that we have to compute is

$$[\hat{1}\hat{P}_{23}] = \left([1] + \frac{\langle 23 \rangle}{\langle 13 \rangle} [2] \right) \left(\frac{\langle 12 \rangle}{\langle 13 \rangle} [2] + [3] \right), \quad (\text{D.2.40})$$

$$= \frac{\langle 12 \rangle [12] + \langle 13 \rangle [13] + \langle 23 \rangle [23]}{\langle 13 \rangle}. \quad (\text{D.2.41})$$

From the first to the second line, we just expanded the equation (D.2.40) by taking into account that $[22] = 0$. In a more compact form, the equation (D.2.41) becomes

$$[\hat{1}\hat{P}_{23}] = \frac{s_{123}}{\langle 13 \rangle}, \quad \text{where} \quad s_{123} = \langle 12 \rangle [12] + \langle 13 \rangle [13] + \langle 13 \rangle [13]. \quad (\text{D.2.42})$$

Finally, after combining all these result, rearranging some terms and performing some simplification we get the final mathematical expression of the diagram represented by \mathcal{D}_1 , given by the following expression

$$\mathcal{D}_1 = \frac{1}{s_{123}} \frac{\langle 1|2+3|q|^2 \langle 1|2+3|p \rangle}{\langle 12 \rangle \langle 23 \rangle [pk] [kl] \langle 3|1+2|l \rangle}. \quad (\text{D.2.43})$$

(b) We can now move to the computation of the second diagram \mathcal{D}_2 in Fig. 4.7. The left subdiagram of \mathcal{D}_2 is a MHV-diagram while the right subdiagram is a NMHV-diagram.

The NMHV part, that we are going to call \mathcal{M} , is given by

$$\mathcal{M} = \frac{1}{\hat{s}_{12P}} \frac{\langle \hat{P}_{l1} | \hat{2} + 3|q|^2 \langle \hat{P}_{l1} | \hat{2} + 3|p \rangle}{\langle \hat{P}_{l1} \hat{2} \rangle \langle \hat{2} 3 \rangle [qp] [pk] \langle 3 | \hat{P}_{l1} + \hat{2} | k \rangle} + \frac{1}{\hat{s}_{k2P}} \frac{[\hat{2} | k + \hat{P}_{l1} | p]^2 [\hat{2} | k + \hat{P}_{l1} | q]}{[k \hat{P}_{l1}] [\hat{P}_{l1} \hat{2}] \langle pq \rangle \langle q 3 \rangle [k | \hat{P}_{l1} + \hat{2} | 3]}. \quad (\text{D.2.44})$$

As for the previous calculations, we first need to get rid of the shifted momentum. The *on-shell condition*, $\hat{P}_{l1} = (l + \hat{p}_1) = \langle l1 \rangle [l\hat{1}] = 0$, implies that $[l\hat{1}] = 0$ which also shows the two spinors $|l\rangle$ and $|\hat{1}\rangle$ are collinear. By exploiting these properties, we can derive the expression of the complex parameter z ,

$$[l\hat{1}] = [l1] + z[l2] = 0 \implies z = -\frac{[l1]}{[l2]}. \quad (\text{D.2.45})$$

We can use the above expression to re-write the shift-equations. The shifted momentum \hat{p}_1 and \hat{p}_2 can now be expressed in terms of the real spinors

$$|\hat{1}\rangle = |1\rangle - \frac{[l1]}{[l2]} |2\rangle \quad \text{and} \quad |\hat{2}\rangle = |2\rangle + \frac{[l1]}{[l2]} |1\rangle. \quad (\text{D.2.46})$$

On the other hand, the collinear restriction, $|\hat{1}\rangle = x|l\rangle$, induces that

$$|1\rangle - \frac{[l1]}{[l2]} |2\rangle = x|l\rangle, \quad (\text{D.2.47})$$

and by multiplying each side of this equation by $|2\rangle$, we get the value of the scalar factor x , which is given by

$$[21] = x[2l] \implies x = \frac{[12]}{[l2]}. \quad (\text{D.2.48})$$

Therefore, the internal momentum \widehat{P}_{l1} that can be written as a function of the square and angle brackets as follows $\widehat{P}_{l1} = |l\rangle[l] + |\hat{1}\rangle[\hat{1}]$ now writes as

$$\widehat{P}_{l1} = \left(|l\rangle + \frac{[12]}{[l2]} |1\rangle \right) [l], \quad (\text{D.2.49})$$

where the square and angle bracket are separately given by

$$|\widehat{P}_{l1}\rangle = |l\rangle + \frac{[12]}{[l2]} |1\rangle \quad \text{and} \quad [\widehat{P}_{l1}] = [l]. \quad (\text{D.2.50})$$

Let us now get rid of the terms that contain a shifted momentum in the Eq. (4.2.84).

First, using the shift-equation, one can straightforwardly show that

$$\langle \hat{1} \widehat{P}_{l1} \rangle = \langle 1 \widehat{P}_{l1} \rangle = \langle 1l \rangle \quad \text{and} \quad \langle \widehat{P}_{l1} l \rangle = \frac{[12]}{[l2]} \langle 1l \rangle, \quad (\text{D.2.51})$$

and therefore, the diagram \mathcal{D}_2 is given by

$$\mathcal{D}_2 = \mathbf{S}_{l2}^1 \times \mathcal{M}, \quad \text{where} \quad \mathbf{S}_{l2}^1 = \frac{[l2]}{[l1][l2]}. \quad (\text{D.2.52})$$

The main task is now to compute the NMHV partial amplitude \mathcal{M} . By virtue of the computation that we have done while computing the partial amplitude \mathcal{D}_1 , it is straightforward to show that

$$\langle \widehat{P}_{l1} \hat{2} \rangle = \frac{s_{l12}}{[l2]}, \quad \langle \hat{2} 3 \rangle = \frac{\langle 3|1+2|l \rangle}{[l2]} \quad \text{and} \quad [\widehat{P}_{l1} \hat{2}] = [l2]. \quad (\text{D.2.53})$$

Let us now turn ourselves into the computation of the difficult part of computing the partial amplitude \mathcal{M} . Such computation involve the square-angle bracket terms. They are given by $\langle \widehat{P}_{l1} | 2 + 3|q \rangle$, $\langle 3 | \widehat{P}_{l1} + \hat{2} | k \rangle$, $[\hat{2} | k + \widehat{P}_{l1} | p \rangle$, $[\hat{2} | k + \widehat{P}_{l2} | q \rangle$ and $[k | \widehat{P}_{l1} + \hat{2} | 3 \rangle$.

- First of all, we have

$$\langle \widehat{P}_{l1} | 2 + 3|q \rangle = \langle \widehat{P}_{l1} \hat{2} | 2q \rangle + \langle \widehat{P}_{l1} 3 | 3q \rangle, \quad (\text{D.2.54})$$

with

$$\langle \widehat{P}_{l1} 3 \rangle = -\frac{\langle 3|l+1|2 \rangle}{[l2]}. \quad (\text{D.2.55})$$

Thus,

$$\langle \widehat{P}_{l1} | 2 + 3|q \rangle = \frac{s_{l12}}{[l2]} [2q] - \frac{\langle 3|l+1|2 \rangle}{[l2]} [3q]. \quad (\text{D.2.56})$$

- In a similar way,

$$\langle 3 | \widehat{P}_{l1} + \hat{2} | k \rangle = \langle 3 \widehat{P}_{l1} | lk \rangle + \langle 3 \hat{2} | 2k \rangle, \quad (\text{D.2.57})$$

where we have,

$$\langle 3 \hat{2} \rangle = -\frac{\langle 3|l+2|l \rangle}{[l2]} \quad \text{and} \quad \langle 3 \widehat{P}_{l1} \rangle = -\langle \widehat{P}_{l1} 3 \rangle. \quad (\text{D.2.58})$$

So, we can get the following expression

$$\langle 3|\widehat{P}_{l1} + \widehat{2}|k\rangle = \frac{\langle 3|l+1|2\rangle}{[l2]}[lk] - \frac{\langle 3|l+2|l\rangle}{[l2]}[2k]. \quad (\text{D.2.59})$$

- Now, it can be easily seen that the last trace term has a form

$$\begin{aligned} [\widehat{2}|k + \widehat{P}_{l1}|p\rangle &= [2k]\langle kp\rangle + [2\widehat{P}_{l1}]\langle \widehat{P}_{l1}p\rangle, \\ &= [2k]\langle kp\rangle + [2l] \left(\langle lp\rangle + \frac{[12]}{[l2]}\langle 1p\rangle \right), \\ &= [2|k|p\rangle + [2|l|p\rangle + [2|1|p\rangle, \end{aligned} \quad (\text{D.2.60})$$

which gives as a result

$$[\widehat{2}|k + \widehat{P}_{l1}|p\rangle = [2|k+l+1|p\rangle. \quad (\text{D.2.61})$$

And we know that the two terms $[\widehat{2}|k + \widehat{P}_{l2}|p\rangle$ and $[\widehat{2}|k + \widehat{P}_{l2}|q\rangle$ are related by symmetry, thus

$$[\widehat{2}|k + \widehat{P}_{l1}|q\rangle = [2|k+l+1|q\rangle. \quad (\text{D.2.62})$$

Finally, we are now left with the computation of the terms \widehat{s}_{23P} and \widehat{s}_{k2P} . Recall that generally, \widehat{s}_{23P} is defined as

$$\widehat{s}_{23P} = \langle \widehat{23}\rangle[\widehat{23}] + \langle 3\widehat{P}_{l1}\rangle[3\widehat{P}_{l1}] + \langle \widehat{2}\widehat{P}_{l1}\rangle[\widehat{2}\widehat{P}_{l1}] \quad (\text{D.2.63})$$

which after a fair amount of calculations gives

$$\widehat{s}_{23P} = s_{l12} + \frac{\langle 3|1+2|l\rangle}{[l2]}[23] + \frac{\langle 3|l+1|2\rangle}{[l2]}[2l]. \quad (\text{D.2.64})$$

By doing a similar calculation, we get as a result

$$\widehat{s}_{14P} = s_{l12} + \frac{\langle k|1+2|l\rangle}{[l2]}[2k] + \frac{\langle k|l+1|2\rangle}{[l2]}[kl]. \quad (\text{D.2.65})$$

At this point, we have managed to cancel all the shifted momenta in the expression of \mathcal{M} . Combining all the result that we have derived previously, making some simplification and rearranging some terms we end up with the following expression

$$\begin{aligned} \mathcal{M} &= \frac{1}{s_{l12}} \frac{[l2](s_{l12}[2q] - \langle 3|l+1|2\rangle[3q])^2}{(s_{l12}[l2] + \langle 3|1+2|l\rangle[23] + \langle 3|l+1|2\rangle[2l])[l1+2|3]} \times \\ &\quad \frac{s_{l12}[2p] - \langle 3|l+1|2\rangle[3p]}{[qp][pk](\langle 3|l+1|2\rangle[lk] + \langle 3|1+2|l\rangle[k2])} + \frac{[l2]}{[kl]\langle pq\rangle\langle q3\rangle} \times \\ &\quad \frac{([2|k+l+1|p\rangle)^2[2|k+l+1|q]}{(s_{l12}[l2] + \langle k|1+2|l\rangle[2k] + \langle k|l+1|2\rangle[kl])(\langle 3|l+1|2\rangle[lk] + \langle 3|1+2|l\rangle[k2])} \end{aligned} \quad (\text{D.2.66})$$

Simplifying the above expression, combining all the results, and rearranging some terms, we can get the final expression of the second diagram represented by \mathcal{D}_2

$$\mathcal{D}_2 = \left(\frac{s_{l2}^1[l2]}{\langle 3|l+1|2\rangle[lk] + \langle 3|1+2|l\rangle[k2]} \right) \left\{ \frac{[l2](s_{l12} - \langle 3|l+1|2\rangle[3q])^2}{s_{l12}[l2] + \langle 3|1+2|l\rangle[23] + \langle 3|l+1|2\rangle[2l]} \right. \\ \left. \frac{s_{l12}[2p] - \langle 3|l+1|2\rangle[3p]}{s_{l12}[qp][pk][l1+2|3]} + \frac{1}{[kl]\langle pq\rangle\langle q3\rangle} \frac{([2|k+l+1|p])^2[2|k+l+1|q]}{s_{l12}[l2] + \langle k|1+2|l\rangle[2k] + \langle k|l+1|2\rangle[kl]} \right\}, \quad (\text{D.2.67})$$

Bibliography

- [1] W. J. Marciano and H. Pagels, “Quantum Chromodynamics: A Review,” *Phys. Rept.* **36** (1978) 137.
- [2] **Particle Data Group** Collaboration, J. Beringer *et al.*, “Review of Particle Physics (RPP),” *Phys. Rev.* **D86** (2012) 010001.
- [3] D. J. Gross and F. Wilczek, “Ultraviolet Behavior of Nonabelian Gauge Theories,” *Phys. Rev. Lett.* **30** (1973) 1343–1346. [,271(1973)].
- [4] H. D. Politzer, “Reliable Perturbative Results for Strong Interactions?,” *Phys. Rev. Lett.* **30** (1973) 1346–1349. [,274(1973)].
- [5] N. Cabibbo and G. Parisi, “Exponential Hadronic Spectrum and Quark Liberation,” *Phys. Lett.* **59B** (1975) 67–69.
- [6] J. C. Collins and M. J. Perry, “Superdense Matter: Neutrons Or Asymptotically Free Quarks?,” *Phys. Rev. Lett.* **34** (1975) 1353.
- [7] H. R. Schmidt and J. Schukraft, “The Physics of ultrarelativistic heavy ion collisions,” *J. Phys.* **G19** (1993) 1705–1796.
- [8] J. W. Harris and B. Muller, “The Search for the quark - gluon plasma,” *Ann. Rev. Nucl. Part. Sci.* **46** (1996) 71–107, [arXiv:hep-ph/9602235](#) [[hep-ph](#)].
- [9] M. Gyulassy and L. McLerran, “New forms of QCD matter discovered at RHIC,” *Nucl. Phys.* **A750** (2005) 30–63, [arXiv:nucl-th/0405013](#) [[nucl-th](#)].
- [10] **PHENIX** Collaboration, K. Adcox *et al.*, “Formation of dense partonic matter in relativistic nucleus-nucleus collisions at RHIC: Experimental evaluation by the PHENIX collaboration,” *Nucl. Phys.* **A757** (2005) 184–283, [arXiv:nucl-ex/0410003](#) [[nucl-ex](#)].

- [11] **BRAHMS** Collaboration, I. Arsene *et al.*, “Quark gluon plasma and color glass condensate at RHIC? The Perspective from the BRAHMS experiment,” *Nucl. Phys.* **A757** (2005) 1–27, [arXiv:nucl-ex/0410020 \[nucl-ex\]](#).
- [12] B. B. Back *et al.*, “The PHOBOS perspective on discoveries at RHIC,” *Nucl. Phys.* **A757** (2005) 28–101, [arXiv:nucl-ex/0410022 \[nucl-ex\]](#).
- [13] **STAR** Collaboration, J. Adams *et al.*, “Experimental and theoretical challenges in the search for the quark gluon plasma: The STAR Collaboration’s critical assessment of the evidence from RHIC collisions,” *Nucl. Phys.* **A757** (2005) 102–183, [arXiv:nucl-ex/0501009 \[nucl-ex\]](#).
- [14] U. W. Heinz and M. Jacob, “Evidence for a new state of matter: An Assessment of the results from the CERN lead beam program,” [arXiv:nucl-th/0002042 \[nucl-th\]](#).
- [15] **ATLAS** Collaboration, G. Aad *et al.*, “Observation of a Centrality-Dependent Dijet Asymmetry in Lead-Lead Collisions at $\sqrt{s_{NN}} = 2.77$ TeV with the ATLAS Detector at the LHC,” *Phys. Rev. Lett.* **105** (2010) 252303, [arXiv:1011.6182 \[hep-ex\]](#).
- [16] **CMS** Collaboration, S. Chatrchyan *et al.*, “Indications of suppression of excited Υ states in PbPb collisions at $\sqrt{s_{NN}} = 2.76$ TeV,” *Phys. Rev. Lett.* **107** (2011) 052302, [arXiv:1105.4894 \[nucl-ex\]](#).
- [17] **ALICE** Collaboration, K. Aamodt *et al.*, “Suppression of Charged Particle Production at Large Transverse Momentum in Central Pb-Pb Collisions at $\sqrt{s_{NN}} = 2.76$ TeV,” *Phys. Lett.* **B696** (2011) 30–39, [arXiv:1012.1004 \[nucl-ex\]](#).
- [18] **ALICE** Collaboration, K. Aamodt *et al.*, “Elliptic flow of charged particles in Pb-Pb collisions at 2.76 TeV,” *Phys. Rev. Lett.* **105** (2010) 252302, [arXiv:1011.3914 \[nucl-ex\]](#).
- [19] **ALICE** Collaboration, S. Aiola, “Measurement of jet p_T spectra and R_{AA} in pp and PbPb collisions at $\sqrt{s_{NN}} = 2.76$ TeV with the ALICE detector,” *Nucl. Phys.* **A931** (2014) 382–387, [arXiv:1408.0479 \[nucl-ex\]](#).
- [20] **CMS** Collaboration, S. Chatrchyan *et al.*, “Observation and studies of jet quenching in PbPb collisions at nucleon-nucleon center-of-mass energy = 2.76 TeV,” *Phys. Rev.* **C84** (2011) 024906, [arXiv:1102.1957 \[nucl-ex\]](#).

- [21] ALICE Collaboration, B. Abelev *et al.*, “Suppression of high transverse momentum D mesons in central Pb-Pb collisions at $\sqrt{s_{NN}} = 2.76$ TeV,” *JHEP* **09** (2012) 112, [arXiv:1203.2160 \[nucl-ex\]](#).
- [22] N. Armesto and E. Scapparini, “Heavy-ion collisions at the Large Hadron Collider: a review of the results from Run 1,” *Eur. Phys. J. Plus* **131** no. 3, (2016) 52, [arXiv:1511.02151 \[nucl-ex\]](#).
- [23] F. Antinori and E. V. Shuryak, “A Comment on conical flow induced by heavy-quark jets,” *J. Phys.* **G31** (2005) L19, [arXiv:nucl-th/0507046 \[nucl-th\]](#).
- [24] G.-Y. Qin and X.-N. Wang, “Jet quenching in high-energy heavy-ion collisions,” *Int. J. Mod. Phys.* **E24** no. 11, (2015) 1530014, [arXiv:1511.00790 \[hep-ph\]](#).
[309(2016)].
- [25] Y.-J. Lee, “Jet Quenching at RHIC and the LHC,” *J. Phys. Conf. Ser.* **446** (2013) 012001.
- [26] M. Gyulassy, I. Vitev, X.-N. Wang, and B.-W. Zhang, “Jet quenching and radiative energy loss in dense nuclear matter,” [arXiv:nucl-th/0302077 \[nucl-th\]](#).
- [27] N. Armesto *et al.*, “Comparison of Jet Quenching Formalisms for a Quark-Gluon Plasma ‘Brick’,” *Phys. Rev.* **C86** (2012) 064904, [arXiv:1106.1106 \[hep-ph\]](#).
- [28] R. Baier, D. Schiff, and B. G. Zakharov, “Energy loss in perturbative QCD,” *Ann. Rev. Nucl. Part. Sci.* **50** (2000) 37–69, [arXiv:hep-ph/0002198 \[hep-ph\]](#).
- [29] R. Pasechnik and M. Umbera, “Phenomenological Review on QuarkGluon Plasma: Concepts vs. Observations,” *Universe* **3** no. 1, (2017) 7, [arXiv:1611.01533 \[hep-ph\]](#).
- [30] H. Fritzsch, M. Gell-Mann, and H. Leutwyler, “Advantages of the Color Octet Gluon Picture,” *Phys. Lett.* **47B** (1973) 365–368.
- [31] W. A. Horowitz and M. Gyulassy, “Heavy quark jet tomography of Pb + Pb at LHC: AdS/CFT drag or pQCD energy loss?,” *Phys. Lett.* **B666** (2008) 320–323, [arXiv:0706.2336 \[nucl-th\]](#).

- [32] I. Bouras, O. Fochler, F. Reining, F. Senzel, J. Uphoff, C. Wesp, Z. Xu, and C. Greiner, “RHIC and LHC heavy ion collisions with pQCD Boltzmann transport,” *J. Phys. Conf. Ser.* **455** (2013) 012051.
- [33] E. V. Shuryak, “Non-perturbative phenomena in QCD vacuum, hadrons, and quark-gluon plasma,”.
- [34] J. D. Bjorken, “Energy Loss of Energetic Partons in Quark - Gluon Plasma: Possible Extinction of High p_{\perp} Jets in Hadron - Hadron Collisions,”.
- [35] M. Gyulassy and X.-n. Wang, “Multiple collisions and induced gluon Bremsstrahlung in QCD,” *Nucl. Phys.* **B420** (1994) 583–614, [arXiv:nuc1-th/9306003](https://arxiv.org/abs/nuc1-th/9306003) [nuc1-th].
- [36] X.-N. Wang, “High p(T) hadron spectra, azimuthal anisotropy and back to back correlations in high-energy heavy ion collisions,” *Phys. Lett.* **B595** (2004) 165–170, [arXiv:nuc1-th/0305010](https://arxiv.org/abs/nuc1-th/0305010) [nuc1-th].
- [37] X.-F. Chen, C. Greiner, E. Wang, X.-N. Wang, and Z. Xu, “Bulk matter evolution and extraction of jet transport parameter in heavy-ion collisions at RHIC,” *Phys. Rev.* **C81** (2010) 064908, [arXiv:1002.1165](https://arxiv.org/abs/1002.1165) [nuc1-th].
- [38] S. A. Bass *et al.*, “Hot and dense qcd matter unraveling the mysteries of the strongly interacting quark-gluon-plasma a community white paper on the future of relativistic heavy-ion physics in the us executive summary. us heavy-ion community.” https://www.bnl.gov/npp/docs/Bass_RHI_WP_final.pdf.
- [39] M. Gyulassy, P. Levai, and I. Vitev, “Jet quenching in thin quark gluon plasmas. 1. Formalism,” *Nucl. Phys.* **B571** (2000) 197–233, [arXiv:hep-ph/9907461](https://arxiv.org/abs/hep-ph/9907461) [hep-ph].
- [40] N. Armesto, C. A. Salgado, and U. A. Wiedemann, “Medium induced gluon radiation off massive quarks fills the dead cone,” *Phys. Rev.* **D69** (2004) 114003, [arXiv:hep-ph/0312106](https://arxiv.org/abs/hep-ph/0312106) [hep-ph].
- [41] M. E. Peskin and D. V. Schroeder, *An Introduction to quantum field theory*. Addison-Wesley, Reading, USA, 1995. <http://www.slac.stanford.edu/~mpeskin/QFT.html>.
- [42] M. Gyulassy, P. Levai, and I. Vitev, “NonAbelian energy loss at finite opacity,” *Phys. Rev. Lett.* **85** (2000) 5535–5538, [arXiv:nuc1-th/0005032](https://arxiv.org/abs/nuc1-th/0005032) [nuc1-th].

- [43] M. Gyulassy, P. Levai, and I. Vitev, “Reaction operator approach to multiple elastic scatterings,” *Phys. Rev.* **D66** (2002) 014005, [arXiv:nucl-th/0201078 \[nucl-th\]](#).
- [44] S. Dittmaier, “Weyl-van der Waerden formalism for helicity amplitudes of massive particles,” *Phys. Rev.* **D59** (1998) 016007, [arXiv:hep-ph/9805445 \[hep-ph\]](#).
- [45] C. Schwinn and S. Weinzierl, “SUSY ward identities for multi-gluon helicity amplitudes with massive quarks,” *JHEP* **03** (2006) 030, [arXiv:hep-th/0602012 \[hep-th\]](#).
- [46] R. Boels, “Covariant representation theory of the Poincare algebra and some of its extensions,” *JHEP* **01** (2010) 010, [arXiv:0908.0738 \[hep-th\]](#).
- [47] N. Arkani-Hamed, T.-C. Huang, and Y.-t. Huang, “Scattering Amplitudes For All Masses and Spins,” [arXiv:1709.04891 \[hep-th\]](#).
- [48] R. Britto, F. Cachazo, and B. Feng, “New recursion relations for tree amplitudes of gluons,” *Nucl. Phys.* **B715** (2005) 499–522, [arXiv:hep-th/0412308 \[hep-th\]](#).
- [49] R. Britto, F. Cachazo, B. Feng, and E. Witten, “Direct proof of tree-level recursion relation in Yang-Mills theory,” *Phys. Rev. Lett.* **94** (2005) 181602, [arXiv:hep-th/0501052 \[hep-th\]](#).
- [50] J. M. Henn and J. C. Plefka, “Scattering Amplitudes in Gauge Theories,” *Lect. Notes Phys.* **883** (2014) pp.1–195.
- [51] F. A. Berends and W. Giele, “The Six Gluon Process as an Example of Weyl-Van Der Waerden Spinor Calculus,” *Nucl. Phys.* **B294** (1987) 700–732.
- [52] F. Caravaglios, M. L. Mangano, M. Moretti, and R. Pittau, “A New approach to multijet calculations in hadron collisions,” *Nucl. Phys.* **B539** (1999) 215–232, [arXiv:hep-ph/9807570 \[hep-ph\]](#).
- [53] F. Cachazo and D. Skinner, “On the structure of scattering amplitudes in N=4 super Yang-Mills and N=8 supergravity,” [arXiv:0801.4574 \[hep-th\]](#).
- [54] V. P. Nair, “A Current Algebra for Some Gauge Theory Amplitudes,” *Phys. Lett.* **B214** (1988) 215–218.
- [55] C. Schwinn and S. Weinzierl, “On-shell recursion relations for all Born QCD amplitudes,” *JHEP* **04** (2007) 072, [arXiv:hep-ph/0703021 \[HEP-PH\]](#).

- [56] M. E. Peskin, “Simplifying Multi-Jet QCD Computation,” in *Proceedings, 13th Mexican School of Particles and Fields (MSPF 2008): San Carlos, Sonora, Mexico, October 2-11, 2008*. 2011. [arXiv:1101.2414 \[hep-ph\]](https://arxiv.org/abs/1101.2414). <http://www-public.slac.stanford.edu/sciDoc/docMeta.aspx?slacPubNumber=SLAC-PUB-14352>.
- [57] C. Cheung, “TASI Lectures on Scattering Amplitudes,” in *Theoretical Advanced Study Institute in Elementary Particle Physics: Anticipating the Next Discoveries in Particle Physics (TASI 2016) Boulder, CO, USA, June 6-July 1, 2016*, pp. 571–623. 2018. [arXiv:1708.03872 \[hep-ph\]](https://arxiv.org/abs/1708.03872).
- [58] P. Bhatt, H. P. Trivedi, A. Kumar, R. Kumar, L. K. Gupta, and J. P. Gupta, “An Analytical Study of Total Cross-section of Proton Proton And Proton Antiproton Interactions,” *DAE Symp. Nucl. Phys.* **59** (2014) 758–759.
- [59] L. J. Dixon, “Calculating scattering amplitudes efficiently,” in *QCD and beyond. Proceedings, Theoretical Advanced Study Institute in Elementary Particle Physics, TASI-95, Boulder, USA, June 4-30, 1995*, pp. 539–584. 1996. [arXiv:hep-ph/9601359 \[hep-ph\]](https://arxiv.org/abs/hep-ph/9601359). <http://www-public.slac.stanford.edu/sciDoc/docMeta.aspx?slacPubNumber=SLAC-PUB-7106>.
- [60] S. J. Bidder, *Efficient techniques for calculating scattering amplitudes in non-abelian gauge theories*. PhD thesis, Swansea U., 2006. <https://ifind.swan.ac.uk/discover/Record/529008>.
- [61] L. J. Dixon, “A brief introduction to modern amplitude methods,” in *Proceedings, 2012 European School of High-Energy Physics (ESHEP 2012): La Pommeraye, Anjou, France, June 06-19, 2012*, pp. 31–67. 2014. [arXiv:1310.5353 \[hep-ph\]](https://arxiv.org/abs/1310.5353). <https://inspirehep.net/record/1261436/files/arXiv:1310.5353.pdf>.
- [62] H. Johansson and A. Ochirov, “Color-Kinematics Duality for QCD Amplitudes,” *JHEP* **01** (2016) 170, [arXiv:1507.00332 \[hep-ph\]](https://arxiv.org/abs/1507.00332).
- [63] F. Maltoni, K. Paul, T. Stelzer, and S. Willenbrock, “Color flow decomposition of QCD amplitudes,” *Phys. Rev.* **D67** (2003) 014026, [arXiv:hep-ph/0209271 \[hep-ph\]](https://arxiv.org/abs/hep-ph/0209271).
- [64] H. Elvang and Y.-t. Huang, *Scattering Amplitudes in Gauge Theory and Gravity*. Cambridge University Press, 2015. <http://www.cambridge.org/mw/academic/>

[subjects/physics/theoretical-physics-and-mathematical-physics/scattering-amplitudes-gauge-theory-and-gravity?format=AR](#).

- [65] B. Feng and M. Luo, “An Introduction to On-shell Recursion Relations,” *Front. Phys.(Beijing)* **7** (2012) 533–575, [arXiv:1111.5759 \[hep-th\]](#).
- [66] F. Cachazo, P. Svrcek, and E. Witten, “MHV vertices and tree amplitudes in gauge theory,” *JHEP* **09** (2004) 006, [arXiv:hep-th/0403047 \[hep-th\]](#).
- [67] F. A. Berends and W. T. Giele, “Recursive Calculations for Processes with n Gluons,” *Nucl. Phys.* **B306** (1988) 759–808.
- [68] A. N. Rasoanaivo and W. A. Horowitz, “Gluon Radiation beyond Poisson using MHV Techniques, Ph.D. Thesis,”.
- [69] T. R. Rabemananjara and W. A. Horowitz, “Computing the $qg \rightarrow qg$ cross section using the BCFW recursion and introduction to jet tomography in heavy ion collisions via MHV techniques,” *J. Phys. Conf. Ser.* **889** no. 1, (2017) 012021.
- [70] J. F. Gunion and G. Bertsch, “HADRONIZATION BY COLOR BREMSSTRAHLUNG,” *Phys. Rev.* **D25** (1982) 746.
- [71] W. A. Horowitz and B. A. Cole, “Systematic theoretical uncertainties in jet quenching due to gluon kinematics,” *Phys. Rev.* **C81** (2010) 024909, [arXiv:0910.1823 \[hep-ph\]](#).
- [72] X.-N. Wang, M. Gyulassy, and M. Plumer, “The LPM effect in QCD and radiative energy loss in a quark gluon plasma,” *Phys. Rev.* **D51** (1995) 3436–3446, [arXiv:hep-ph/9408344 \[hep-ph\]](#).
- [73] J. J. M. Carrasco, M. Chiodaroli, M. Gnyaydin, and R. Roiban, “One-loop four-point amplitudes in pure and matter-coupled N=4 supergravity,” *JHEP* **03** (2013) 056, [arXiv:1212.1146 \[hep-th\]](#).
- [74] J. J. Carrasco and H. Johansson, “Five-Point Amplitudes in N=4 Super-Yang-Mills Theory and N=8 Supergravity,” *Phys. Rev.* **D85** (2012) 025006, [arXiv:1106.4711 \[hep-th\]](#).

- [75] N. E. J. Bjerrum-Bohr, T. Dennen, R. Monteiro, and D. O’Connell, “Integrand Oxidation and One-Loop Colour-Dual Numerators in N=4 Gauge Theory,” *JHEP* **07** (2013) 092, [arXiv:1303.2913 \[hep-th\]](#).
- [76] R. H. Boels, R. S. Isermann, R. Monteiro, and D. O’Connell, “Colour-Kinematics Duality for One-Loop Rational Amplitudes,” *JHEP* **04** (2013) 107, [arXiv:1301.4165 \[hep-th\]](#).
- [77] M. Chiodaroli, Q. Jin, and R. Roiban, “Color/kinematics duality for general abelian orbifolds of N=4 super Yang-Mills theory,” *JHEP* **01** (2014) 152, [arXiv:1311.3600 \[hep-th\]](#).
- [78] Z. Bern, S. Davies, T. Dennen, Y.-t. Huang, and J. Nohle, “Color-Kinematics Duality for Pure Yang-Mills and Gravity at One and Two Loops,” *Phys. Rev.* **D92** no. 4, (2015) 045041, [arXiv:1303.6605 \[hep-th\]](#).
- [79] J. Nohle, “Color-Kinematics Duality in One-Loop Four-Gluon Amplitudes with Matter,” *Phys. Rev.* **D90** no. 2, (2014) 025020, [arXiv:1309.7416 \[hep-th\]](#).